DIFFERENTIAL WEATHERING EFFECTS AND MECHANISMS

Thesis by

James Louis Conca

In Partial Fulfillment of the Requirements

for the Degree of

Doctor of Philosophy

1985

California Institute of Technology

Pasadena, California

April 21, 1985

ACKNOWLEDGEMENTS

The seemingly long and labyrinthine path that began in childhood and that led eventually to this thesis is punctuated at many turns by those few people who through their actions, brilliance, stubbornness or simply love, contributed to my development as a scientist and a person, and which has culminated in this work. I wish to acknowledge some of them here.

To have grown up in as wonderful a family as mine was the first good fortune. Nancy, MaryLou, Steve, Mike, Betty, Tom and I may have strained the patience of my parents, Louis and Marguerite, but the fertile and diverse environment of nine minds (all talking at once around the table) was to form the basis of my approach to viewing this universe.

I'd also like to thank Andrew Astor who has been the strong friend I needed in these years at Caltech and who put up with so much. Andy also produced several computer-generated figures for this thesis.

But the single, deepest influence in my life has been Mary Torregrossa, who gave such poignant meaning to love and friendship and without whom I could never have arrived at this point.

It has been my good fortune to have known Robert P. Sharp, who introduced me to this thesis topic on one of the Ge 136 field trips for which he will long be remembered, and who gave support and good humor throughout my tenure at Caltech. I am deeply indebted to him.

The thesis would not have crystallized without the support of Barclay Kamb and the trust he showed in my abilities.

However, George Rossman has been the rock upon whom this work was

done. His encouragement and help never waivered even when I seemed to.

I would also like to thank Don Burnett and Dotty Woolum for their support in the early years.

I give special thanks to Jim Head who was responsible for my first becoming interested in the geological sciences.

The friends I've had at Caltech deserve more than recognition. Rosemarie Cubba, Don Piepgras, Daniel Wenkert, Jim Friedson, Gerry Fine, Astrid Howard, Mary Stordal, Sally Rigden, and Peter Larson all have made my experience at Caltech more worthwhile.

Finally, I can never repay my father for those times he spent with me over that black 1936 Royale. This dissertation is dedicated to him and to my mother.

This work was supported by grants from the National Science Foundation (EAR-8212590 and DPP-8215121), the Sigma Xi Scientific Research Society, and the ARCS Foundation.

ABSTRACT

The physical and chemical characteristics of the two differential weathering effects, case hardening and core softening, are examined to determine their formation mechanisms by investigating several field areas exhibiting differential weathering effects. The terms differential weathering effects, factors, mechanisms, processes, morphologies and their cause and effect relationships are defined in the context of the overall problem.

Because differential weathering effects are defined on the basis of spatial variations in relative and absolute hardness, a portable field instrument has been developed to measure rock hardness as manifested in the abrasion resistance of the material.

The design and operation of the instrument as well as results from standard materials are discussed in light of abrasive wear theory. The way in which the instrument removes material appears dominated by abrasive wear mechanisms. However, the concept of hardness implied by such mechanisms is profoundly different for rock than for homogeneous materials, and the effective hardness calculated for rock material using this instrument is more insensitive to mineralogy than expected, and is sensitive to the character of the intergranular bond.

At the first locality, Valley of Fire, Nevada, cavernous weathering of the Aztec Sandstone results from the differential weathering effect of case hardening. The case-hardened crust is an induration phenomenon consisting primarily of host rock, calcite cement, kaolinite and fine-grained quartz. The calcite occurs in a wide range of concentrations (0.001 to 5.0 wt%). The hydrated calcium borate, colemanite, was also found as a non-cementing hardening agent on two outcrops and can be used

as a tracer constituent. In all cases kaolinite and quartz were the major constituents of the indurating materials by weight and are necessary components of the crust. Eolian deposition and interaction with meteoric water were determined to be the primary differential weathering mechanism within the Valley of Fire.

At Catavina, Baja California, tonalite exhibiting cavernous weathering is found to be core-softened. Soft cores are more chemically weathered than the exterior rock as indicated by higher kaolinite contents. Hematite formed from the leaching of biotite occurs in coatings on rock surfaces, but the hardening effect of the coating is insignificant compared to the core-softening of the interior. The hardness, measured by the abrasion resistance hardness tester, is inversely correlated with kaolinite content in the tonalite. A one-dimensional water flow model was developed for core-softened, cavernously weathered boulders, and indicates that during infiltration and dessication the moisture flux through a boulder's surface is greatest at the interior cavern wall because of changes in the hydraulic conductivities induced by core softening.

The differential weathering effects developed in the Ferrar dolerite within the Labyrinth of the Dry Valleys, Antarctica are caused by two different mechanisms. The primary mechanism is precipitation of a brown, iron-stained silica coating in the exterior rock of outcrops and joint blocks. This is also true for the case-hardened Beacon Sandstone. Precipitation can occur in the rock's outer few millimeters to centimeters, thereby decreasing the exterior rock's permeability, and consequently its susceptibility to chemical weathering. The coating's effect on a dolerite block's internal moisture regime is modeled for the

case of saturated flow, and shows that the contours of the pore water flow mimic subsequent morphology. Weathering of material underlying the coating results in core softening of the dolerite. In dolerite blocks of intermediate size, expansion of the interior owing to weathering can cause the less weathered outer zone to separate into an array of polyhedral cracks. Further weathering and removal of the underlying rock by the combined action of hydration, salt weathering and eolian processes leads to the development of cavernous weathering.

A less common differential mechanism occurs in the bottom of the Antarctic Labyrinth troughs in which an eolian polish develops on rock surfaces exposed to the austral winter winds. Development of the polish protects the underlying material with similar, but less dramatic effects, than accompanies the presence of the silica coating.

Exposures of the Bishop Tuff in the Mono Basin exhibit the differential weathering effect of case hardening. Early devitrification along joint planes to an average depth of 1 cm greatly increased the resistance of the joint faces to weathering over that of the joint block interiors. The absolute and relative hardnesses between interior and exterior change systematically with exposure age, and cavernous weathering results only on outcrops with long enough exposure ages, on the order of ten to twenty thousand years.

The Towel Creek Tuff in Cottonwood Basin, Arizona, weathers into peculiar forms: conical-shaped tepees which show cavernous weathering as a result of case-hardening by calcite precipitation in the exterior rock. Calcite contents of different materials are observed to vary directly with the abrasion hardness of the material. Basal surfaces are formed at the base of the tepees by heterogeneous fluvial erosion and

the cavernous hollows are initiated in these zones. Although infiltration of meteoric water into the tepees occurs through all surfaces, moisture flow during dessication of the tepees occurs primarily through the basal surfaces and the lower cavernous hollows. Equilibrium aqueous chemistry limits the interior rock's carbonate content, but calcite can accumulate at the rock exterior.

Because of the overall differences in the intergranular bonding character between crystalline materials such as granite and clastic materials such as sandstone, the results of this study indicate that crystalline rocks tend to core-soften whereas clastic materials case-harden. Clastic materials will be affected by redistribution of secondary cements and greater accumulation at an interface can result in case hardening. In clastic rocks therefore, the hardness of different areas can either increase or decrease with time. On the other hand, a crystalline rock in a weathering environment will have its intergranular and intragranular bonds disrupted by chemical alteration. Spatial variations in disruption can result in core softening or case softening, but the hardness of all areas will decrease with time. Accumulation of secondary cements can often enhance differential effects in crystalline rocks but without case hardening the rock.

CONTENTS

LIST OF ILLUSTRATIONS

LIST OF TABLES

Once I saw mountains angry,
And ranged in battle-front.
Against them stood a little man;
Aye, he was no bigger than my finger.
I laughed, and spoke to one near me:
"Will he prevail?"
"Surely," replied this other;
"His grandfathers beat them many times."
Then did I see much virtue in grandfathers,-
At least, for the little man
Who stood against the mountains.

- Stephen Crane

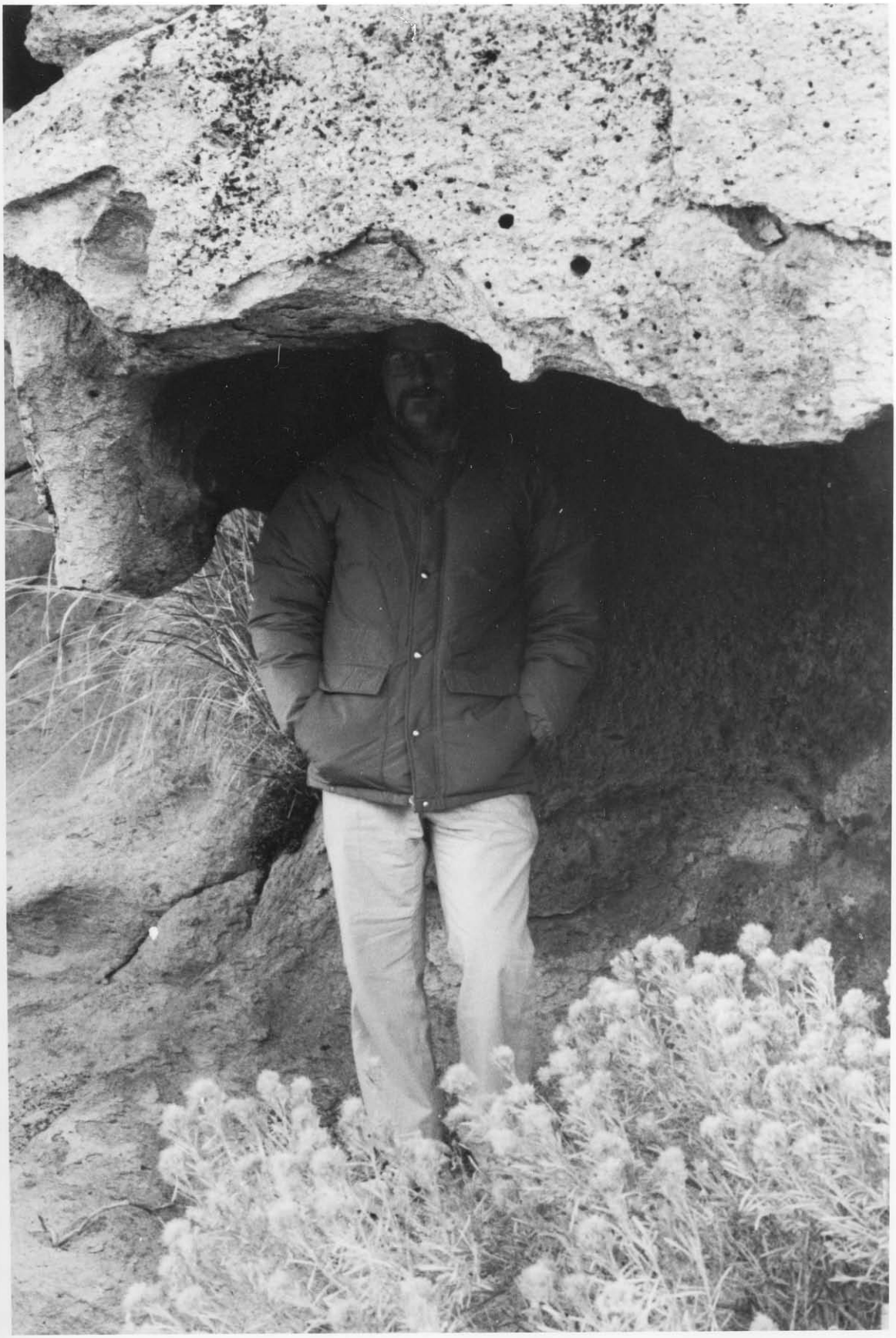

CHAPTER 1

INTRODUCTION

The many definitions of weathering proposed over the last century indicate the difficulty of describing precisely a complex subject as though it were a single process or a set of processes necessarily related in space and time. Simple terms such as rock breakdown, decomposition or degradation refer only to small portions of the weathering spectrum. More general definitions such as put forward by Reiche (1950) are based on a system viewpoint: "Weathering is the response of materials, which were in equilibrium within the lithosphere, to conditions at or near its contact with the atmosphere, the hydrosphere and the biosphere." But, as Keller (1957) points out, rocks are in equilibrium only momentarily while the environment in which they formed persists.

Since weathering is mostly envisioned within the framework of the earth, interaction with the atmosphere, hydrosphere and biosphere is usually implied. Yet thermal ablation of a silicate-ice layer to produce a lag deposit on the surface of an icy satellite such as Ganymede might be considered as weathering processes even in the absence of an atmosphere, hydrosphere or biosphere. Likewise, although relatively low temperatures and pressures are implied for weathering in order to distinguish it from diagenesis or metamorphism, the high transient temperature produced at the point of surface lightning strikes or the pressure produced at the crystal-rock interface of a Na_2SO_4 pore solution, will certainly contribute to the breakdown of the material. And should the weathering system include the entire mineral grain whose

outer surface is in contact with an aqueous solution, or the entire lithosphere whose outer surface is also in contact with an aqueous solution? One might think of weathering as the lithospheric interaction with the extralithospheric environment, but even this restricts the system to that which has been part of a lithosphere.

It is seen, then, that weathering is an arbitrary region chosen along the temperature, pressure, compositional, space and time axes which usually corresponds to geologic systems viewed by humans at or near the earth's surface, but can often be applied to situations with only the remotest similarities to these systems.

Thus we come to the present study of differential weathering effects. The variety of situations described in widely dispersed geographical locations has resulted in many terms with subtle differences in meaning. For the purpose of this study, a differential weathering effect refers to a spatial variation in some property of the material that affects its subsequent weathering behavior. A process or property which gives rise to a differential weathering effect is a differential weathering mechanism or factor, respectively. Peculiar morphologies such as cavernous weathering can result from these effects. Therefore, rock that has experienced one or more differential weathering mechanisms or factors may develop a differential weathering effect which, under the influence of one or more external processes, may eventually result in a particular morphology.

In the present study the property having spatial variations is the rock hardness, and its definition and method of measurement will be discussed in Chapter 2. The study centers on a particular set of differential weathering effects, i.e., those in which the exterior rock

is harder than the interior rock. The definition of exterior and interior in this case is somewhat arbitrary. Whatever parcel or volume of rock is being discussed, e.g., a boulder, block, or outcrop, has an outer boundary or zone seperating the parcel from the exterior environment, which can be air, water, sediment, other rock, etc. This boundary is called the exterior, and the zone of rock at or near the exterior that has a defined set of properties different from that of the underlying or interior rock is called the exterior rock. Since a boulder or outcrop can be bounded by more than one external environment at any time, such as a boulder half-buried in a soil, there may be more than one type of exterior rock.

The are four subsets of differential weathering effects based on a relative hardness difference between exterior rock and interior rock, and are given the names: 1) case hardening, 2) core softening, 3) case softening and 4) core hardening. The difference between these effects concerns the evolution of the absolute hardness with time. With case hardening, the absolute hardness of the exterior increases with time, while the absolute hardness of the interior usually remains the same or decreases. However, during core softening, the absolute hardness of the exterior actually decreases with time but to a lesser degree than the interior, resulting in a differential hardness similar to that developed during case hardening. A similar relationship exists between case softening and core hardening. Before the development of an abrasion resistance hardness tester core softening was not recognized as a differential weathering effect, and many ostensibly case-hardened rocks may, in fact, be core-softened.

Because of the variety of properties and processes, acting

separately or simultaneously, that can be involved in weathering situations, each situation must be examined individually in order to determine what mechanisms or factors may be involved. The ultimate aim of such a study is to understand the relationships among the different processes and properties of a system and its environment. The degree to which a morphology such as cavernous weathering will be developed is a complex function of differential weathering effects, weathering rates and exposure ages of the particular system.

The outline shown on the following page is a breakdown of the categories adopted for this study. The list is not complete, and includes only those processes, factors, mechanisms, effects and morphologies relating to this study.

Six field areas exhibiting differential weathering effects were selected for detailed investigation. They include the Aztec sandstone (Nevada), the Beacon sandstone (Antarctica), the Bishop tuff (California), the Towel Creek tuff (Arizona), the Ferrar dolerite (Antarctica) and a tonalite from Baja California. A variety of other areas were studied in lesser detail. Each area presents a different situation, and together they span the range of categories outlined below. The preferential occurrence of differential weathering effects and resulting morphologies in arid to semi-arid regions seems to reflect the greater variety of mechanisms, processes and weathering rates which accompany the decreased water budget of these regions.

A number of studies have been conducted concerning the differential weathering effects which cause cavernous weathering, tafoni, honeycomb or alveolar weathering (Mustoe 1982; Jennings 1968). Cavernous weathering itself has long been recognized as an important morphological

I. **EXTERNAL PROCESSES** - Processes which lead to the removal, addition or alteration of material (processes which can contribute to a change in the physical and/or chemical properties of the system at the present time)

A. Chemical Alteration of Existing Phases
   1) hydration
   2) oxidation
   3) carbonization
   4) leaching
   5) hydrothermal reactions
   6) metabolic reactions
   7) substitution reactions
   8) adsorption reactions
   9) other reactions

B. Dissolution
   1) congruent
   2) incongruent

C. Precipitation
   1) insoluble solids and gels (silicates and oxides)
   2) soluble salts (**salt weathering**)
   3) ice (**freeze-thaw**)

D. Insolation

E. Unloading of Overburden

F. Erosion
   1) fluvial
   2) eolian
   3) glacial
   4) mass wasting
   5) impact
   6) other fluids and forces

II. **DIFFERENTIAL WEATHERING FACTORS** - Properties of the system and its surroundings which influence the present system's response to external processes in a spatially variable manner

A. Variations in Initial (Pre-weathered) Properties
   1) structural variations
      a. jointing
      b. sedimentary and igneous structures
   2) grain-size and textural variations
   3) compositional variations
      a. chemical
      b. mineralogical

B. Variations in External Conditions
   microclimatic variations (moisture, temperature)

III. DIFFERENTIAL WEATHERING MECHANISMS - Processes which have produced a spatially variable response to external processes in the present system.

A. Variations in the Redistribution of Constituents
   1) variations in the precipitation or emplacement of secondary constituents
      a. calcite
      b. silica
      c. iron oxides
      d. clay minerals
      e. other
   2) variations in dissolution and alteration of existing constituents

B. Variations in External Conditions
   variations in pore water flow

IV. DIFFERENTIAL WEATHERING EFFECTS - Spatial variations in one or more material properties (rock hardness for the purpose of this study)

A. Case Hardening
   exterior hardness increases with time
   interior hardness remains less than exterior

B. Core Softening
   interior hardness decreases with time
   exterior hardness does not increase with time but remains greater than interior hardness

C. Case Softening
   exterior hardness decreases with time
   interior hardness does not increase with time but remains greater than exterior

D. Core Hardening
   interior hardness increases with time
   exterior hardness remains less than interior

V. RESULTING MORPHOLOGIES

A. Residual Core Stones and Spheroidal Weathering (case softening)

B. Cavernous Weathering (case hardening and core softening)
   1) tafoni (hollows formed secondarily in rock material, named for its Corsican type locality)
   2) honeycomb or alveolar weathering (small scale hollows)

C. Concretions (core hardening)

phenomenon, and many descriptive papers have been written concerning it (Anderson, 1931; Blackwelder, 1929; Bryan, 1922; Lattman, 1973; Ollier and Tuddenham, 1962; Sekyra, 1972, and White, 1944). Processes cited for the origin of cavernous weathering include case hardening (Dragovich, 1969; Charlesworth, 1959, and Grantz, 1976), core softening (Conca and Rossman, 1985 and this study), salt weathering (Evans, 1970; Goudie, 1974; Selby, 1971; Malin, 1974), hydration shattering (White, 1976), insolation (Rice, 1976), frost action (Fahey, 1973) and wind erosion. Whalley and McGreevy (1983) give a rather complete review of the recent weathering literature. Many of these weathering processes and effects are not mutually exclusive, and while a single process may dominate in many situations, it is by no means the rule. Several differential mechanisms and weathering processes can occur simultaneously or sequentially both in space and time, especially in arid regions.

Given the variety of situations encountered in weathering environments, it is not surprising that past studies often seem in contradiction to each other. Thus, Winkler (1980) disputed Bradley, Hutton and Twidale's (1978) claim that salt weathering was important in developing granitic tafoni in South Australia. Winkler asserted that case hardening is the primary cause of all tafoni and honeycomb morphologies, citing evidence from his work on the Cliff House sandstone in New Mexico. Bradley, et. al. (1980) correctly pointed out that tafonis may be convergent forms produced by differing mechanisms, and they reasserted their conclusion that salt weathering is important in their field area.

The above argument underscores the conclusion of this thesis, that

generalizations should not be made concerning differential weathering without some knowledge of the processes, effects and mechanisms involved. Winkler's sandstone exhibits the differential weathering **effect** of case hardening, whereas Bradley et. al.'s granite is most likely core-softened. Salt weathering is the dominant weathering **process** acting on the granite's interior wall, while dissolution of calcite cement is the dominant process implied for the sandstone. The only generalization that can be made concerning differential weathering effects (and even this should be accepted only in lieu of direct investigation) is that crystalline rocks, such as granites, diorites, gneisses, etc., will tend to core-soften, whereas clastic materials, such as sandstones, conglomerates, volcanic tuffs and limestones (chemical precipitates), will case-harden. This generalization is clearly demonstrated when crystalline rocks undergo brecciation as a result of faulting or sliding. This changes the rock's nature from crystalline to clastic. The character of the intergranular bonding in the original material is replaced by that of a clastic material and becomes susceptible to redistribution of cements and case hardening. Because of this, the deformed rock often exhibits cavernous weathering whereas the parent material does not exhibit cavernous weathering (some examples in California being Armagosa Chaos, Baker Hill, and Tin Mountain).

I have found no evidence for direct microbial mediation in this study. However, recent findings by Friedmann (1982) discussed in Chapter 5, Dorn and Oberlander (1981 and 1982) and Wilson and Jones (1983) show that the role of microorganisms must be investigated as possible mechanisms in differentially weathered materials, not only as

direct mechanisms, but indirectly such as changing the P_{CO_2} of different microclimates and the production of salts, chelating agents and other metabolic products which can have chemical or physical effects on subsequent weathering.

EXPERIMENTAL METHODS

Homogenized powders were made from kg-sized samples upon which whole rock chemistry was determined using X-ray fluorescence (Al_2O_3, SiO_2, total Fe as FeO, K_2O, TiO_2 and MnO) and atomic absorption spectroscopy (Na_2O and MgO). Specific mineral chemistries were obtained using an electron microprobe on polished mineral grain mounts. Ferrous iron was determined using a modified Wilson's method (Whipple 1974). Mineralogy was determined using X-ray diffraction on powders, thin section petrography, infrared spectroscopy on KBr pellets (Farmer 1974) and scanning electron microscopy (SEM). A DuPont moisture evolution analyzer was used for water analyses.

Scanning electron microscopy was performed on gold-coated, pristine rock fragments and individual mineral grains using an ISI Super-II Scanning Electron Microscope equipped for energy dispersive X-ray analysis.

Infrared spectra were obtained with a Perkin-Elmer model 180 spectrophotometer on between 0.5 and 1.5 mg of powdered sample dispersed in 200 mg KBr pellets. Spectra covered the 4000 cm^{-1} to 400 cm^{-1} region.

Fluorescence spectra were taken using incident laser light of 488 nm with a Spex Spectrophotometer model 14018 and a Spectra-Physics

170 argon-ion laser.

Thin sections of case-hardened rocks were irradiated with thermal neutrons at the U.C.L.A. Nuclear Energy Laboratory. Plastic track detectors (Kodak film CA80-15) were placed over polished, doubly-impregnated thin sections and the assemblage placed in the thermal column of the reactor. Irradiation causes alpha particles to be emitted from the $^{10}B(n,\alpha)^{7}Li$ reaction, producing radiation damage in the detector. Etching the detector for 70 minutes at 29° C in a 6 N NaOH solution enlarges the damaged areas to conical-shaped tracks, which may be counted with an optical microscope at 1000X magnification. Background track density for this method was found to be equivalent to only 0.3 ppm B and is well below concentrations determined for the case-hardened samples. Colemanite standards were from the Old Thompson Mine, Death Valley, California.

CHAPTER 2

ROCK HARDNESS AND ITS MEASUREMENT

A method of measuring the hardness of materials as manifested by the abrasion resistance was developed in order to compare the hardness of different materials as they evolve under changing conditions. A portable field instrument was designed and built to measure changes in the abrasion resistance hardness of geologic materials, especially those changes resulting from weathering.

In discussing rock hardness in its relation to weathering, the term hardness is usually applied to the rock as a whole and not to its constituent mineral grains. Rock hardness can be thought of as the friability, the resistance to erosion, the abrasion resistance, the durability, the cohesion, or other descriptions and combination of descriptions of physical properties that apply to rock material. Because of the variety of properties involved in rock hardness, it is difficult to choose and perform a suitable test for comparing hardness among different rocks, especially in the field.

Recently Day and Goudie (1977) have been successful in using a Schmidt Test Hammer to measure rock hardness and its relationship to landform development. The Schmidt Hammer measures the coefficient of restitution (the fractional rebound distance of a mass upon impact) which depends on the cohesion of the surface and subsurface material. The Schmidt Hammer is not applicable to the study of case hardening or core softening because 1) most exterior crusts are quite thin (mm to cm), 2) the hammer will be influenced by the underlying softer material and 3) the measurement will physically break the exterior

crust. Gillespie (1982) used acoustic wave speeds to measure the degree of weathering of glacial erratics in Sierra Nevada moraines and discovered that these measurements were affected by the development of case-hardened crusts. However, acoustic wave speeds measure a bulk property and, in practice, it is difficult to use them to investigate small areas within individual rocks.

In materials science, extensive hardness testing has been done on homogeneous materials such as metals and hard rubber. These tests consist of Vickers and Brinell indentation tests. These tests are inapplicable to heterogeneous materials such as rocks because the durability of rock in the face of erosive agents may depend only slightly on the indentation properties of the individual grains.

A useful test of rock hardness would measure a property or set of properties that influences the erosional behavior of a rock. Resistance to abrasion is such a set of properties which determines the behavior of the rock in response to the shear stresses and gouging action of abrasion.

THE ABRASION RESISTANCE HARDNESS TESTER

The abrasion resistance hardness tester (ARHT), a portable field instrument, was developed with the above ideas in mind (Fig. 1). ARHT abrades the material by means of a diamond coring bit, which is turned slowly by a constant-speed motor and which is driven into the rock by a constant normal force or load. The measured time required to abrade to a fixed depth is related to the material's abrasion resistance. During the operation of ARHT, the operator has control of the load, L, and the

depth of penetration, D. Convenient units obtained from the instrument, that discriminate hardness among different materials, are the abrasion resistance hardness value (H_a) and the coefficient of relative hardening for an exterior surface (C), defined as:

$$H_a = \frac{L \cdot t}{D} \times 10^{-5} \qquad (1)$$

$$C = \frac{H_a \text{ (exterior)}}{H_a \text{ (interior)}} \qquad (2)$$

where H_a is the abrasion resistance hardness value (10^5 N sec/m), C is the coefficient of relative hardening (dimensionless), L is the load, or normal force (Newtons), D is the depth of drill penetration (meters), and t is the time (seconds). The reason for defining H_a in terms of D, L and t as given in equation (1) will be dicussed below. For most geologic materials, H_a is found to lie in the range from about 1 to 100 (in units of 10^5 N sec/m) For example, H_a is about 10 for a well-cemented sandstone and about 50 for an unweathered granitic rock. Values of C greater than 1 indicate case hardening or core softening. H_a as defined in equation (1) is not the same as H_A used in Tabor's abrasion tests for plastics (ASTM, 1979).

H_a is dependent on a number of factors that combine to determine the resistance to abrasion, such as the kinetic coefficient of friction, average mineral hardness and the character of the intergranular bond. If L and D are kept constant then the changes in t will reflect changes

Figure 1 Photograph of the abrasion resistance hardness tester (ARHT) developed to measure the hardness of brittle, inhomogeneous material. The instrument stands 100 cm tall and weighs 15 kg.

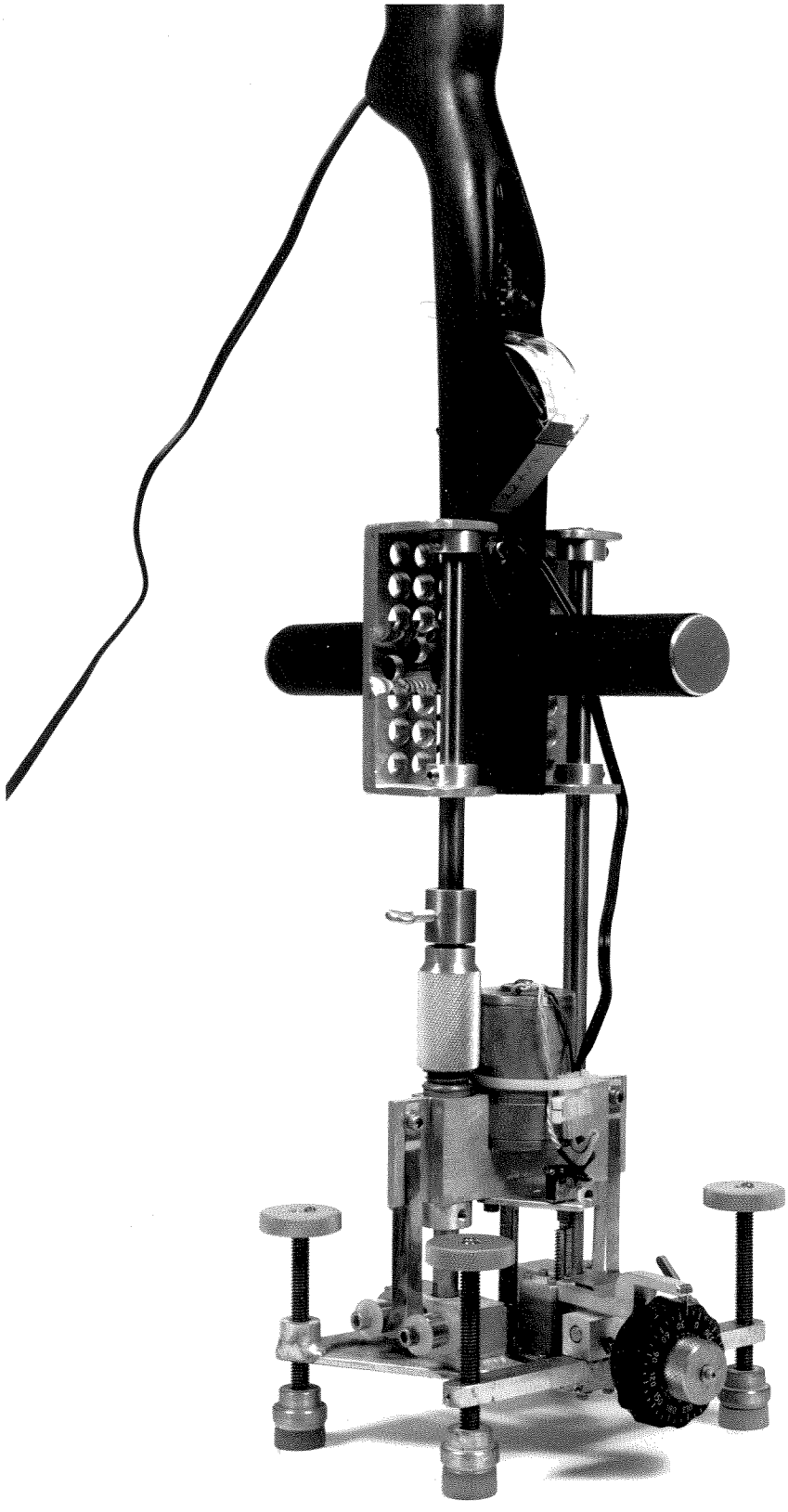

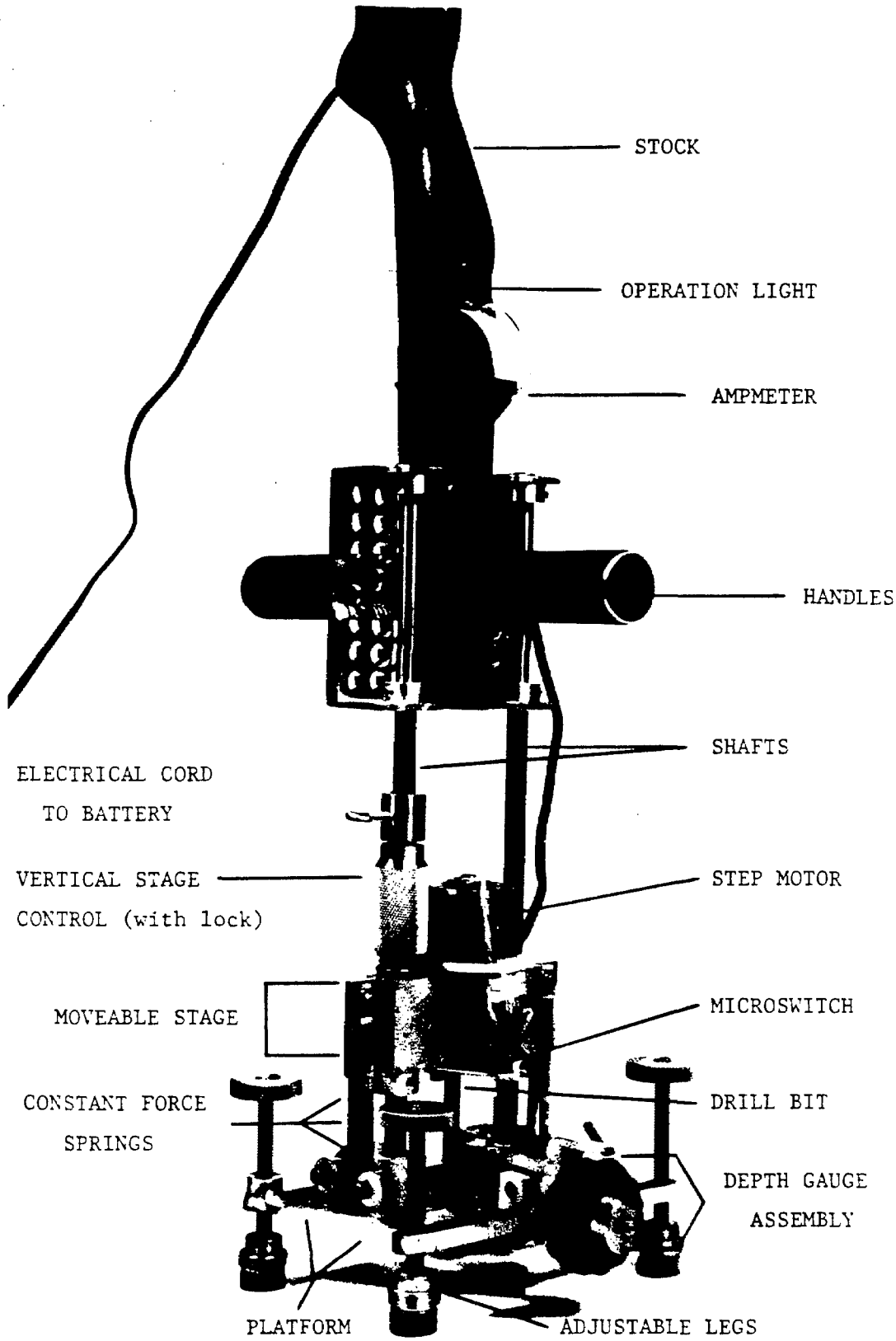
STOCK
OPERATION LIGHT
AMPMETER
HANDLES
SHAFTS
ELECTRICAL CORD
TO BATTERY
VERTICAL STAGE
CONTROL (with lock)
STEP MOTOR
MOVEABLE STAGE
MICROSWITCH
CONSTANT FORCE
SPRINGS
DRILL BIT
DEPTH GAUGE
ASSEMBLY
PLATFORM
ADJUSTABLE LEGS

FIGURE 1

in the abrasion resistance of the rock without actually describing the variables involved or their relationship to each other. The advantages of this method are that it measures a total effect of a group of factors that influence erosion, is portable and is relatively fast. This method is, in effect, a scratch test for the rock as a whole. The measurement of H_a involves a small volume of material (<0.5 cm^3) and is not influenced by the surrounding material, thus allowing investigation of a rock on the scale of centimeters. The disadvantage of this method is that little information is obtained concerning individual factors and mechanisms. On the other hand, the summation of the effects of all the factors into a single measured parameter (H_a) mimics the natural environment, and allows different rock types and different portions of the same rock to be compared under fixed conditions. If the resistance to abrasion is positively correlated with the resistance to weathering and erosion, then these measurements will provide a relative scale of rock hardness in relation to rock weathering.

Design

In order to perform reliably in harsh field environments (some of the field areas are in the Antarctic) ARHT was designed to be simple (Fig. 1). The abrasive agent is medium-grained diamond which is metal-bonded to a coring bit having an outside diameter of 12.0 mm and an inside diameter of 7.5 mm, producing an annular hole whose cross-sectional area is 78.5 mm^2. The diamond particle size (500 μm) is above the critical abrasive particle size (Rabinowicz, 1965) so that the wear rate is independant of the diamond particle size. The bit diameter is chosen large enough to average the surface's physical properties, i.e.,

larger than the average grain size of the minerals. The bit is chosen to be a coring bit in order to keep the linear speed of each contact point on the bit relatively constant over the area of the annular cross-section. A much larger bit diameter would require a larger motor and stage assembly, such that the instrument would become impractically heavy for field work. For coarse-grained materials, however, a small diameter head will introduce problems depending on where the bit was placed on the rock surface.

The bit is driven by a small electric stepmotor which is mounted on a stage. The stage is free to move vertically on two stainless steel shafts. The power supply for the motor is a 12 volt battery which has a capacity of approximately 7 ampere-hours under normal conditions (4 amphours under Antarctic conditions) which is sufficient for over 3000 hardness measurements. In practice, the battery is recharged after every thousand measurements. Drill rotation rate is 400 rpm. The current draw by the motor is monitored by an ammeter mounted on the stock.

The normal force or load on the rock surface is supplied by four constant-force springs (springs in which force is constant and not dependant upon displacement) attached at one end to the stage and at the other to the stationary platform. The force can be varied stepwise from 10 to 75 N by changing spring sets.

The operator holds the platform against the rock by means of a stock. The penetration depth is set by a depth gauge and microswitch which automatically shuts the motor off when the set depth is attained. The depth of the annular hole produced can be varied from 0.5 to 30 mm but for most materials is kept at 3 to 6 mm. The drilling time

is measured by a stopwatch.

In order to increase bit life, a coolant is sprayed into the drill hole for about 1 second at regular intervals of about 1 second during drilling. The coolant is water under normal conditions and water plus ethanol under low temperature conditions. No effects were observed in drilling time as the spraying interval was varied from continuous spray to no spray, and it was concluded that, at the low drill speeds and normal forces used with ARHT, the cooling fluid did not interfere with abrasion in the drilling process within the accuracy of the measurements, i.e., ±5%. However, the spraying interval is kept constant at about 1 second.

The effect of dulling of the drill bits with wear was evaluated by drilling standard materials at a variety of loads until the drilling rate began to be affected by dulling of the bits. Errors of greater than 5% were not observed when using a bit until about 50 measurements were taken. After about 70 measurements, dulling and plucking of diamonds caused the results to be non-repeatable. In the practice of taking measurements, therefore, bits were discarded after 30 measurements. Each bit was calibrated by drilling to a fixed depth and at a fixed load in a standard material (the Navajo sandstone). All measurments were related to that material.

Operation

In the field operation of ARHT, the instrument is most conveniently used in the vertical or near vertical positions, but can be used at all angles. However, at angles much over 90^{o} to the verticle, the weight of the instrument becomes uncomfortable and errors due to operator fatigue

become important. The field operation requires two people: one to hold the instrument securely against the rock surface to be tested, and the other to manipulate the depth gauge, stage controls, stopwatch and coolant. Prior to each measurement, a small preparatory hole (up to 0.5 mm deep) is drilled to insure total bit contact with the surface. Depth and load are chosen so that drilling to the set depth will take between 30 and 300 seconds. For much shorter times, errors of several seconds will constitute too large a percentage of the measurement, while for much longer times operator fatigue interferes with the measurement. Under these circumstances of orientation and drilling time, reproducibility of the measurements is about ±5%. Larger scatter indicates heterogeneity in the physical properties of the material. These heterogeneities can be especially dramatic in weathered materials, where spatial variations in hardness can span two or three orders of magnitude over distances of several centimeters.

Standard Test Materials

Three rock types of different properties were chosen to test the instrument's operation and to establish the behavior of the general classes of geologic materials: clastic, chemical precipitate and igneous crystalline. The samples were selected for their relative homogeneity. Large pieces of each material were cut flat to eliminate surface effects.

The first rock type is represented by a homogeneous, fine to medium-grained portion of the Navajo sandstone. The sandstone is well-sorted, has an average grain size of 0.2 mm, and contains 97% quartz as detrital grains and authigenic overgrowths, with 2% calcite and 1%

hematite. For the purpose of this study, the sandstone can be characterized as composed of hard (H = 7 on Mohs scale) grains of quartz weakly bonded by cements of quartz, hematite and calcite. The second type is represented by a dense, medium-grained, equigranular, crystalline limestone consisting entirely of calcite with no trace minerals observed. The limestone can be characterized for this study as soft (H = 3) grains of calcite strongly bonded by calcite cement. For the third class of materials, a coarse-grained gabbro was chosen. The rock is made up of a variety of hard (H = 5 to 7) mineral grains strongly bonded in an igneous texture. The gabbro is a dark grey to black, holocrystalline, hypidiomorphic rock with interlocking laths of plagioclase up to 6 mm in length. Mineralogically, the gabbro is composed of 67% plagioclase (An_{80}), 10% biotite, 8% enstatite, 4% augite, 7% opaques, 2% apatite and about 1% quartz in graphic intergrowth with the plagioclase.

A large single crystal of gypsum was also tested to observe the behavior of a material having well-defined Mohs and indentation hardness values. In addition to these natural materials, tests were carried out on an earthenware ceramic (60% talc, 40% Ball clay, fired to 1000° C), which fits into the third category, having grains of a variety of hardnesses (metamorphosed and unmetamorphosed clay minerals, H = 2 to 9) strongly bonded in a crystalline texture.

Results

Each of the test materials was drilled to a fixed depth under a variety of loads (normal forces). The wear rate (W), defined as the volume of material abraded per unit sliding distance of the abrading

Figure 2 (A) Wear rate, W, plotted against load, L, for the standard materials described in the text. (B) Penetration depth, D, plotted as a function of the drilling time, t, for the sandstone standard.

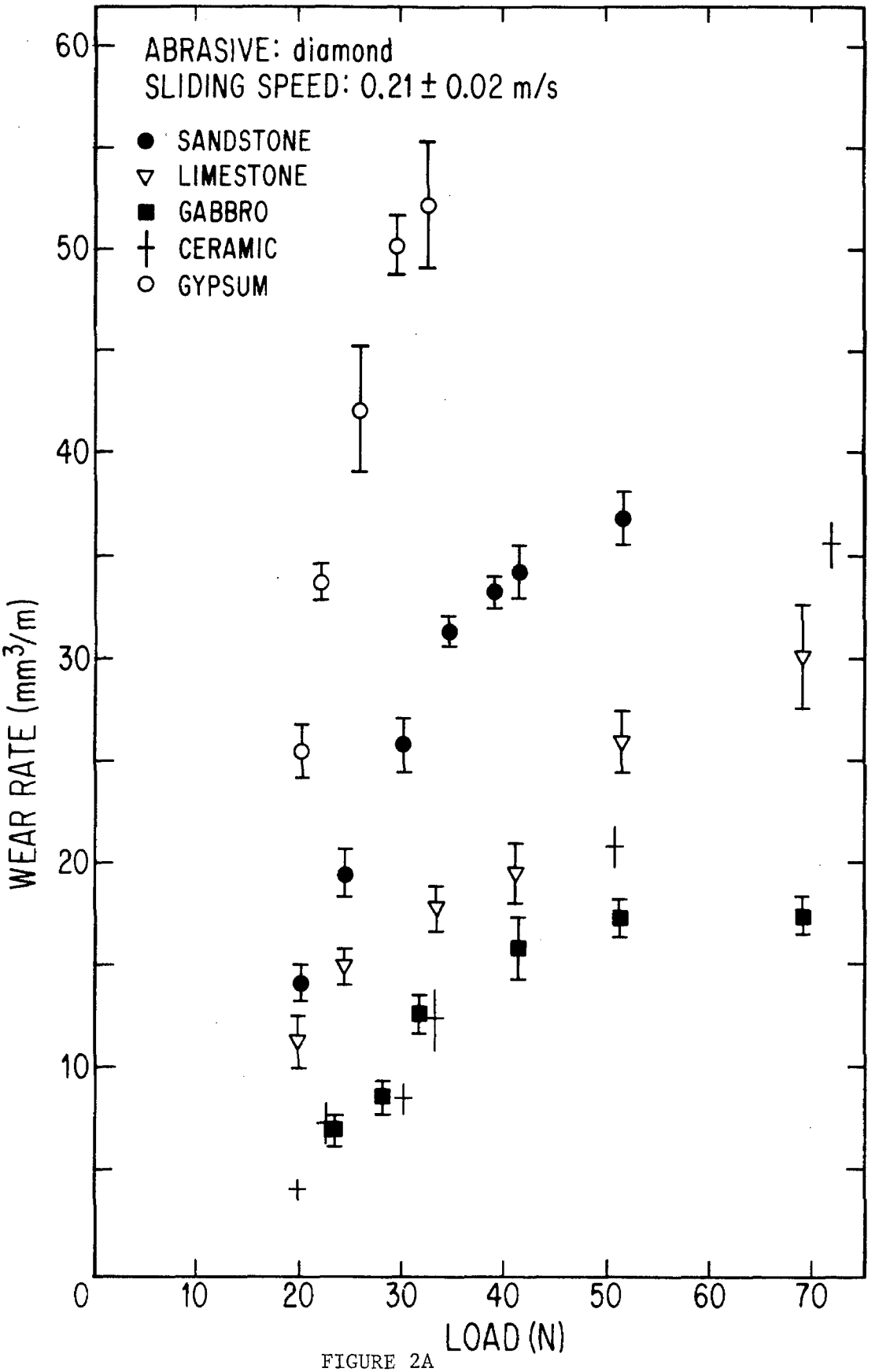
ABRASIVE: diamond
SLIDING SPEED: 0.21 ± 0.02 m/s
SANDSTONE
LIMESTONE
GABBRO
CERAMIC
GYPSUM
WEAR RATE (mm³/m)
LOAD (N)
0
10
20
30
40
50
60
70

FIGURE 2A

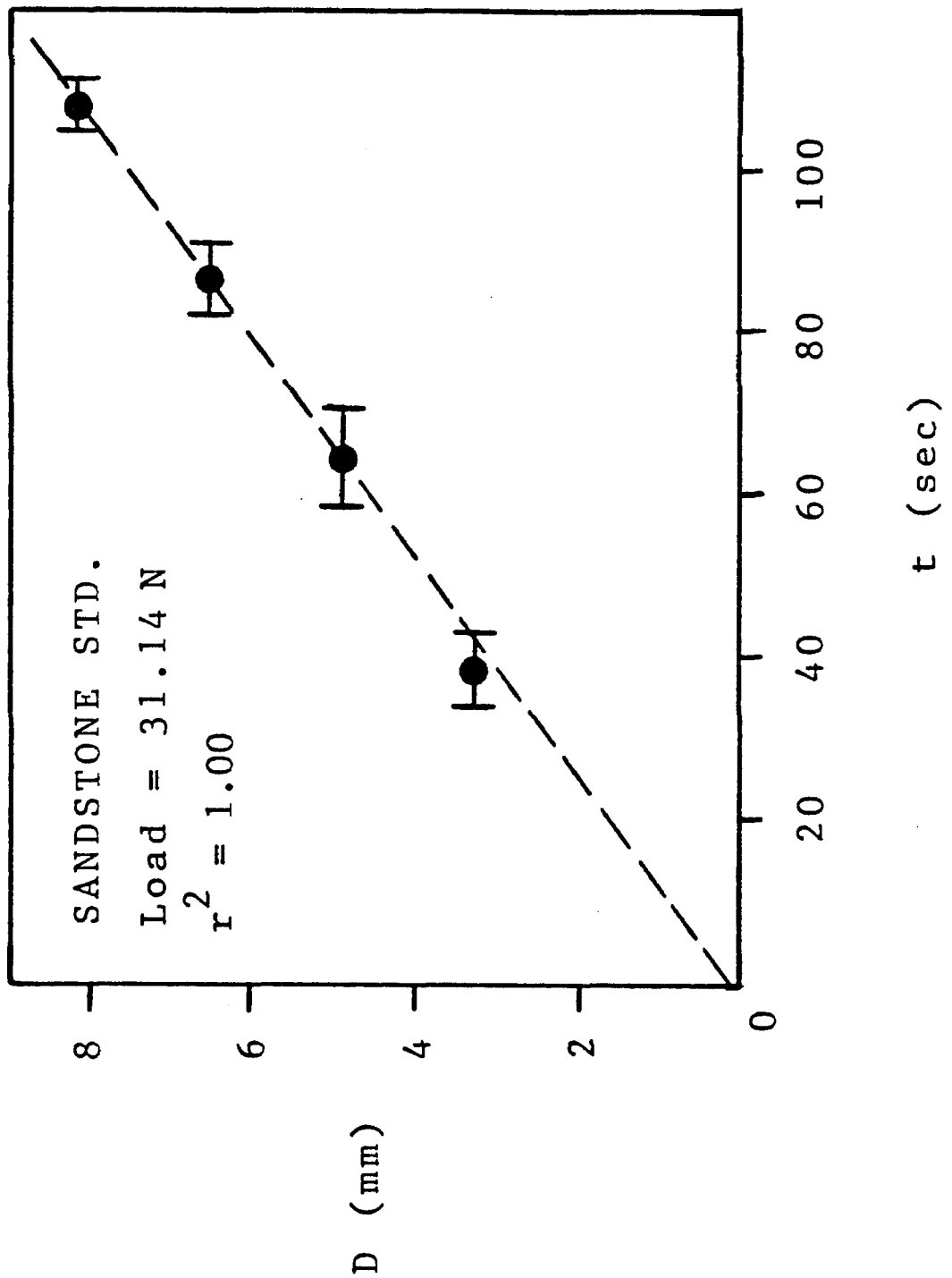

FIGURE 2B

agent over the abraded surface, can be calculated from the time, the total volume of material removed and the average sliding speed of the bit. The wear rate is, therefore, proportional to the reciprocal of the drilling time, and will be used in the following discussion. Figure 2B shows the penetration depth as a function of the drilling time for the sandstone standard. The drilling time is directly proportional to the penetration depth bearing out the relationship of t/D given in equation (1).

Figure 2A shows the wear rate plotted as a function of load. The relationship of wear to load is approximately linear for loads less than about 35 N, as would expected from the relationship of $L \cdot t$ in equation (1). However, for some of the materials this relationship does not hold at higher loads.

The relationship of wear to load is different for each of the geologic materials. For the loads normally employed by ARHT, the sandstone and gypsum are the most easily abraded. For the sandstone there is a marked change in slope at about 35 N, the wear rate approaching a constant value at higher loads. The gypsum may exhibit similar behavior at higher loads, but the softness of the material precludes drilling at higher loads because of binding of the bit. The limestone is next in ease of abrasion and does not have a marked slope change within the range of loads used by ARHT. The ceramic and the gabbro are the hardest materials and behave similarly at small loads. At loads above 45 N the gabbro approaches a constant wear rate whereas the ceramic shows no such effect.

For the sandstone and the gabbro, and probably for the gypsum, increasing the load above 35 to 45 N results in less increase in the

wear rate than a similar increase in load below 35 N. This represents a "saturation" effect in the drilling-rate response to increasing load. For the limestone and ceramic, the "saturation" load must be above the normal working loads of the machine. The saturation effect may be related to the grain size of the wear particles. The coring bit can become clogged by adherent wear debris, hindering increased penetration of the material by the diamonds as the load increases (Rabinowicz, 1965). Table 1 gives the grain-size distribution for the wear particles at a load of 30 N for each test material, and indicates definite differences in the wear-particle sizes. The ceramic wear particles are greatly skewed towards the small size fractions, with only a few particles above 5 μm and none above 50 μm. Since the grain size of the diamonds in the bit is 500 μm, these small wear particles should not interfere with abrasion in the load range used. However, going from the ceramic to the gabbro there is a continuous increase in the average wear particle size. Those materials that have larger wear particles exhibit a greater saturation effect in their corresponding curves in Figure 2, i.e., the effect is more complete and occurs at lower loads. Table 1 also gives values for the largest particle size observed for each material. Wear of the sandstone and gabbro is producing particles that are on the order of the grain size of the diamonds and interfere with the wear process at high loads. Therefore, when using ARHT in the field, loads should be chosen below the saturation load to insure the linear relationship between wear and load.

According to equation (1), the origin in Figure 2 should be a point common to all curves. Yet, some of the curves seem to intersect the abscissa at a load of about 7 N, indicating a threshold load below which

TABLE 1

GRAIN-SIZE DISTRIBUTION FOR WEAR PARTICLES AT L = 30 N

Wear Particle Size Range (μm)	Distribution (% Volume) Ceramic	Limestone	Gypsum	Sandstone	Gabbro
< 0.5	30	10	10	5	5
0.5 - 5.0	60	40	20	10	15
5.0 - 50.0	10	40	50	55	45
50.0 - 500.0	0	10	20	30	35
largest particle observed	15 μm	100 μm	150 μm	250 μm	400 μm

no wear takes place, or below which the relationship of wear rate to load changes dramatically. To a first approximation W seems to vary linearly with load at loads between about 20 and 40 N, and field operation of the instrument should be restricted to within this range to allow comparisons between values of H_a for different materials. A load of 38 N has been found to be appropriate for most rock types and most situations. The use of a standard load removes the problem of deviation in H_a with L, which arises when the W vs L curve of a material (Figure 2A) does not go through the origin.

Scanning electron microscopy of the abraded surface after the operation of ARHT illustrates the wear mechanisms involved. Figures 3a and 3b are micrographs of the abraded surface of the sandstone showing that brittle fracture is the only wear mechanism operating. On the other hand, the ceramic, gabbro, limestone and gypsum, shown in Figures 3c and 3d, all exhibit textures that have been interpreted as due to brittle fracture and plastic deformation (Mehrotra, 1983)

Mehrotra (1983) found that, in ceramic material subject to abrasion, the wear mechanisms were plastic deformation during mild wear and brittle fracture during severe wear, and both mechanisms could operate simultaneously over any given surface. The two different surface textures in Fig. 3c probably result from differences in the geometry of the abrasive grains in the coring bit. Each diamond grain supports varying amounts of the load during abrasion, and may be producing a different severity of wear. The presence of only brittle fracture in the sandstone reflects the weak bonding of the material.

Figure 3 Scanning electron micrographs of worn surfaces produced during the operation of ARHT. (a) Sandstone showing fractured quartz grains and quartz overgrowths with little evidence of plastic deformation. (b) Higher magnification view of (a). (c) Ceramic showing both plastic deformation (dark areas) and brittle fracture (light areas). The gabbro and limestone show similar features. (d) Higher magnification view of (c) showing boundary between areas of plastic deformation (left) and brittle fracture (right).

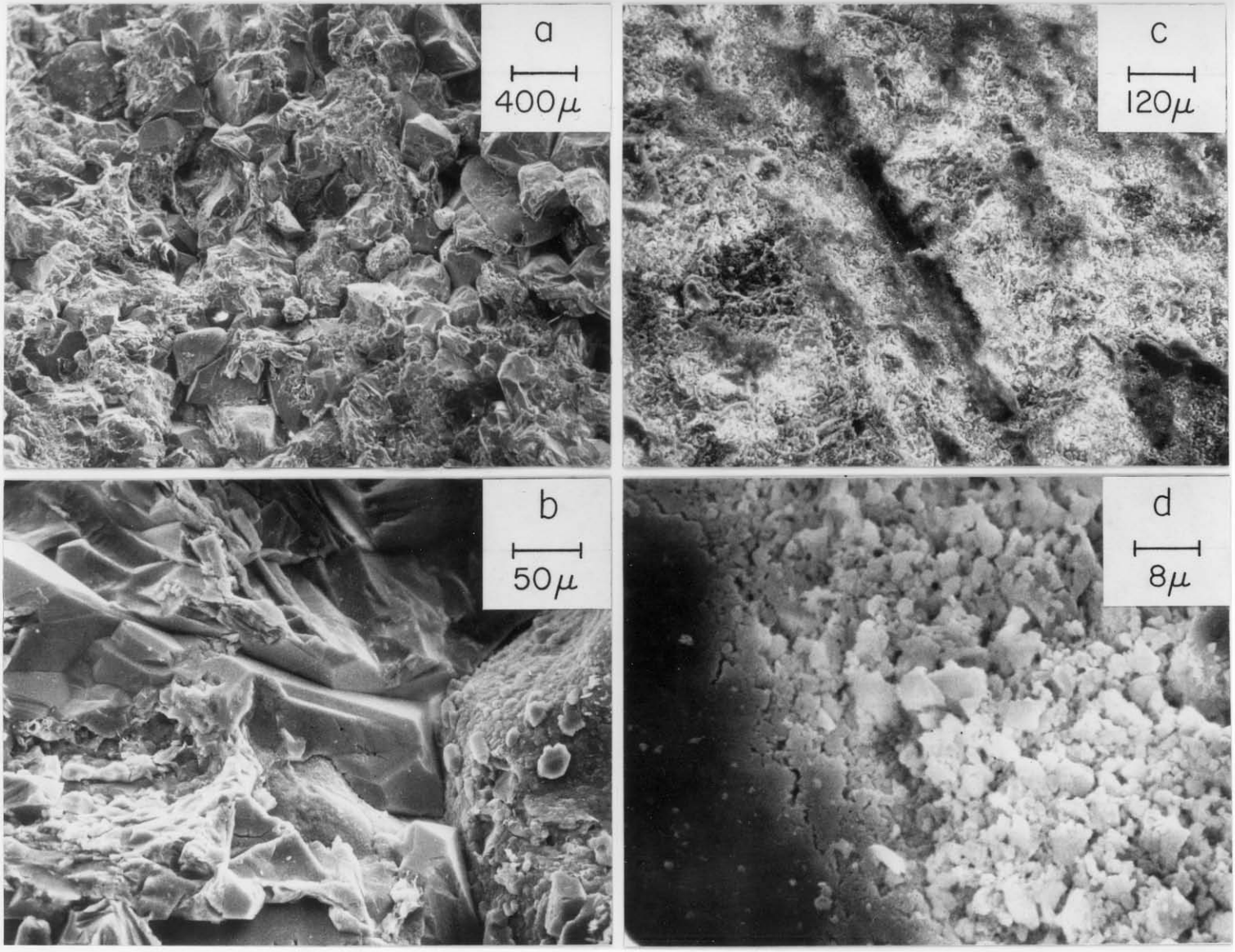
a
400μ
c
120μ
b
50μ
d
8μ

Mechanism of abrasive wear

Abrasive wear describes the process of material removal during the operation of ARHT. Abrasive wear arises when a hard, rough surface (diamond-studded bit) slides against a softer material, digs into it, and removes material as loose fragments.

For the abrading diamonds of the coring bit, a simplified model of the abrasive wear can be developed using the geometric assumptions of Figure 4. The diamonds are assumed to have a conical shape and, under a load, to penetrate the surface to a depth, x. Rabinowicz (1965) shows that, in the penetration by an individual diamond, the cross-sectional area of the diamond at the grain surface, a, is determined by the load on the diamond, ΔL, and the indentation hardness, p, of the indented material as follows:

$$\Delta L = p \cdot a = p \pi r^2 \qquad (3)$$

where r is the radius of the cone at the grain surface. The projected area of the penetrating cone in the vertical direction is rx, which is equal to $r^2 \tan \theta$ where θ is the angle between the diamond surface and the horizontal. When the cone moves through a distance, dl, the volume removed, dV, is given by:

$$dV = r \times dl = r^2 \tan\theta \, dl = \frac{\Delta L \tan\theta \, dl}{p \pi}$$

The resulting wear rate, W, summed over the whole system, in total volume of material removed per total sliding distance, is:

Figure 4 Geometric assumptions used in the development of abrasive wear theory.

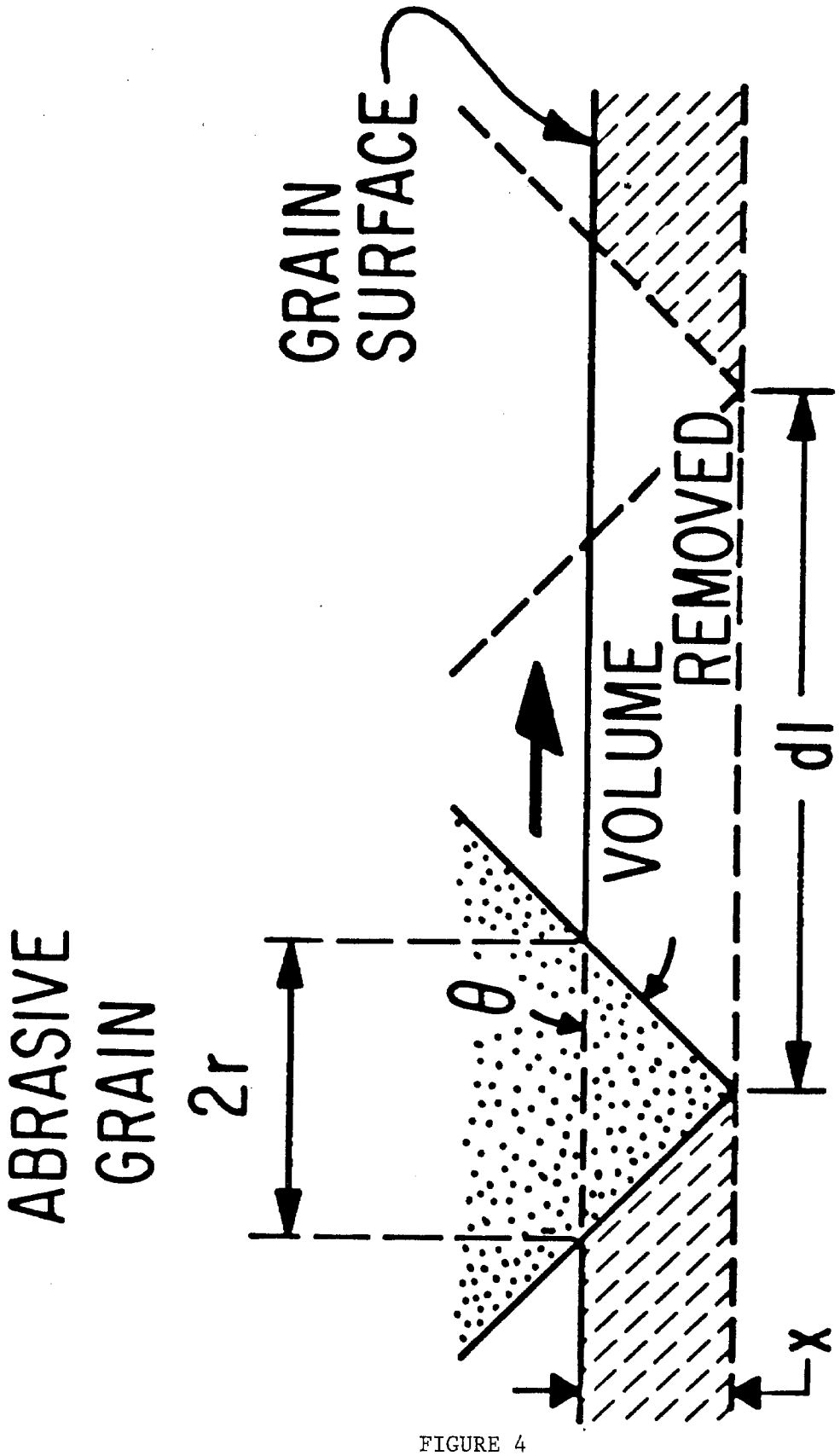

FIGURE 4

$$W = \frac{L \tan\theta}{p\pi} \qquad (4)$$

From equation (4) it can be seen that, if abrasive wear is the dominant mechanism acting in the removal of material, then the relationship of W to L should be linear. The slope of the line will be determined by θ and by the indentation hardness, p. For a fixed type of bit, θ is a constant, so that according to this model, the slope W/L should depend only on the hardness, p.

Evans and Marshall (1980) have modeled the abrasive mechanism of brittle fracture and derived a relationship of wear rate to load, analogous to equation (4), in which W varies as $L^{9/8}\ p^{-3/2}$ instead of $L^{1}\ p^{-1}$. A different functional relationship of W to L may explain why some of the curves in Figure 2 do not go through the origin.

Equation (4) together with the slope W/L, obtained from the data in Figure 2A, provides a determination of the hardness, p, of each material. As defined in the derivation of equation (4), p is the effective indentation hardness of the material as a whole and may bear little relationship to the hardness of the individual mineral grains, except in the case of gypsum since it is a single crystal.

Solving for p in equation (4), using the slopes from Figure 2A and a value for $\tan\theta/\pi$ of 0.1 (Archard, 1980), gives an effective indentation hardness for each material, given in Table 2. These values are extremely low compared to those of most minerals obtained from standard (DPN) indentation hardness tests, gypsum being about 30 kg/mm^2, calcite about 100 kg/mm^2 and quartz about 1000 kg/mm^2 (Rabinowicz, 1965). Choosing a value for $\tan\theta/\pi$ of 0.67 such that the calculated effective hardness for gypsum in Table 2 equals the experimental value

TABLE 2

INDENTATION HARDNESS, p (kg/mm^2), FROM EQUATION (4)

Materials \ $\tan\theta/\pi$	0.1	0.67
Gypsum	4.5	30
Sandstone	8.2	54
Limestone	10.9	72
Ceramic	20.0	133
Gabbro	20.4	136

of 30 kg/mm^2, leads to the adjusted values of p in column 3. For the the gabbro, this adjusted value is still a factor of 5 below the indentation hardness of most of the individual grains. Also, for such different types of rock materials, the values in Table 2 are very close to one another, suggesting that the mechanism of wear operating during the use of ARHT is much less sensitive to the hardness of the constituent minerals than to the intergranular cohesion. It remains to be seen if the p values in Table 2 can be related to other measures of intergranular cohesion in the individual rocks.

H_a vs p

H_a can be related to the hardness, p, through equations (1) and (4). If R is the mean radius of the bit, ω is the drill rotation rate, and A is the cross-sectional area of the annular hole produced during drilling then the effective hardness, p, is:

$$p = f H_a \qquad \text{where} \qquad f = \frac{10^5 R \omega \tan\theta}{\pi A}$$

f is a constant which is determined by the characteristics of the drill bit and the motor. p has a more fundamental meaning than H_a, and could be used as the experimental measure of abrasion hardness in place of H_a.

FIELD RESULTS

Although it would be valuable to obtain relationships of the wear rate to load for every material investigated using ARHT and to use them to determine the effective hardness, p, of each material, the number of measurements required to obtain each curve in Figure 2A is impractical

for field work and is unnecessary for answering initial questions, such as "Which rock is harder?"

For comparing the hardness of different rock masses or of different portions of the same rock it is convenient to use the same load (L) for each sample and determine the abrasion resistance hardness value for each measurement from equation (1).

ARHT was used to investigate the major field areas of this study. Abrasion resistance hardness values were determined for interior and exterior rock, and, when possible, for relatively unweathered rock. Table 3 gives measured values of H_a and C. C is greater than 1 for all of the rock types studied, indicating that indeed the rocks are either case-hardened or core-softened. As discussed earlier, the difference between case hardening and core softening concerns the evolution of the rock hardness during weathering. With case hardening, the hardness of the exterior zone of rock increases with time, while the hardness of the rock interior usually either remains the same or decreases. However, during core softening, the hardness of the exterior decreases with time, but to a lesser degree than the rock interior, resulting in a differential hardness similar to that developed during case hardening. The data from Table 3 demonstrate the differences between case hardening and core softening in terms of changes in the hardness with weathering. For the Catavina tonalite and the Ferrar dolerite, even though the hardness of the exterior zone has remained greater than that of the rock interior, the hardness of both has decreased with respect to the initial value, to an extreme degree in the tonalite and only moderately in the dolerite, indicating that both areas are core-softened. Most of the differential weathering occurring in crystalline

TABLE 3

ARHT Field Results

Locality	Rock Zone	Abrasion Resistance Hardness Values (10^5 N sec/m)	Coefficient of Relative Hardening
Tonalite	exterior	1.7 ± 0.6	
Catavina	interior	0.7 ± 0.4	2.3
Baja California	fresh tonalite	41.4 ± 2.5	
Ferrar dolerite	exterior	43.8 ± 8.3	
Labyrinth	interior	11.9 ± 2.1	3.7
Antarctica	fresh dolerite	64.5 ± 9.7	
Beacon sandstone	exterior	7.3 ± 0.5	
Farnell Valley	interior	2.9 ± 0.8	2.5
Antarctica	fresh sandstone	6.0 ± 0.3	
Bishop tuff	exterior	28.3 ± 2.8	
Butte Stream Cut	interior	1.6 ± 0.2	18.3
California	fresh tuff	17.0 ± 3.0	
Towel Creek tuff	exterior	0.11 ± .03	
Cottonwood Basin	interior	0.04 ± .03	2.8
Arizona			
Aztec sandstone	exterior	0.20 ± .02	
Valley of Fire	interior	0.16 ± .03	1.3
Nevada			

Figure 5 A core-softened boulder of the Vida granite exhibiting extensive cavernous weathering. The boulder is 3 meters wide.

rocks is core softening (Figure 5).

On the other hand, the Beacon sandstone exhibits case hardening in the classical sense. The crystallization of a secondary cement (silica) in the near-surface rock during weathering has increased the absolute hardness of the exterior zone of rock above the initial value, while the hardness of the rock interior has decreased. The Aztec sandstone and the Towel Creek Tuff have calcite as the major case-hardening agent. The interior rock itself is the unweathered material.

The Bishop Tuff is a rather unusual manifestation of case hardening. The exterior has become harder than the interior as a result of devitrification of the glassy matrix along joint planes. The effect on the hardness is dramatic, producing the highest value of C observed in any rock to date. Most values of C fall between 0 and 5.

The above results indicate that the effect that weathering will have on the abrasion hardness of a rock is complicated and depends on the type of rock as well as on which processes are involved in the weathering. For a sandstone, the redistribution of cement will greatly change the abrasion resistance of different portions of the rock. But for crystalline rocks, the effects of weathering are less obvious. The cohesion which holds a crystalline rock together can be disrupted in many ways. Disruption begins as soon as the rock moves from the P-T conditions of its origin. The initial disruption is microfracturing that results from the heterogeneous response of the different minerals to changes in temperature, pressure and stress. Subsequently, removal of material in solution, hydration or other alteration of primary phases and intergranular surface bonds, and crystallization of secondary minerals will further disrupt the internal cohesion of the rock. These

effects will produce a change in H_a with time, usually a decrease.

For fresh rock in which the intergranular cohesive strengths are comparable to the yield stresses of the constituent minerals, the abrasion of the rock should be controlled by the properties of the individual grains. But as weathering proceeds, these intergranular strengths will be reduced to below the yield stresses of the minerals, and the behavior of the rock in the face of abrasion will change. In studies of the weathering of the tonalite at Catavina (Chapter 4) the major effect of weathering is found to be the disruption of intergranular bonds by dissolution of feldspar and the formation of minor amounts of secondary kaolinite and quartz. The abrasion resistance of the rock decreases with increasing kaolinite content formed during weathering (Figure 6). Small differences in kaolinite content produce large variations in the hardness of the rock.

It is possible, therefore, to correlate changes in rock hardness with other parameters, such as changes in composition or exposure age, to obtain useful information on differential weathering mechanisms. The following chapters will expand upon this approach.

Figure 6 Hardness as a function of kaolinite content for different areas in a weathering tonalite boulder. The highly weathered interior has the highest kaolinite content, and the fresh rock has the least kaolinite (Chapter 4). The load, L, is given as the normal force, F_n

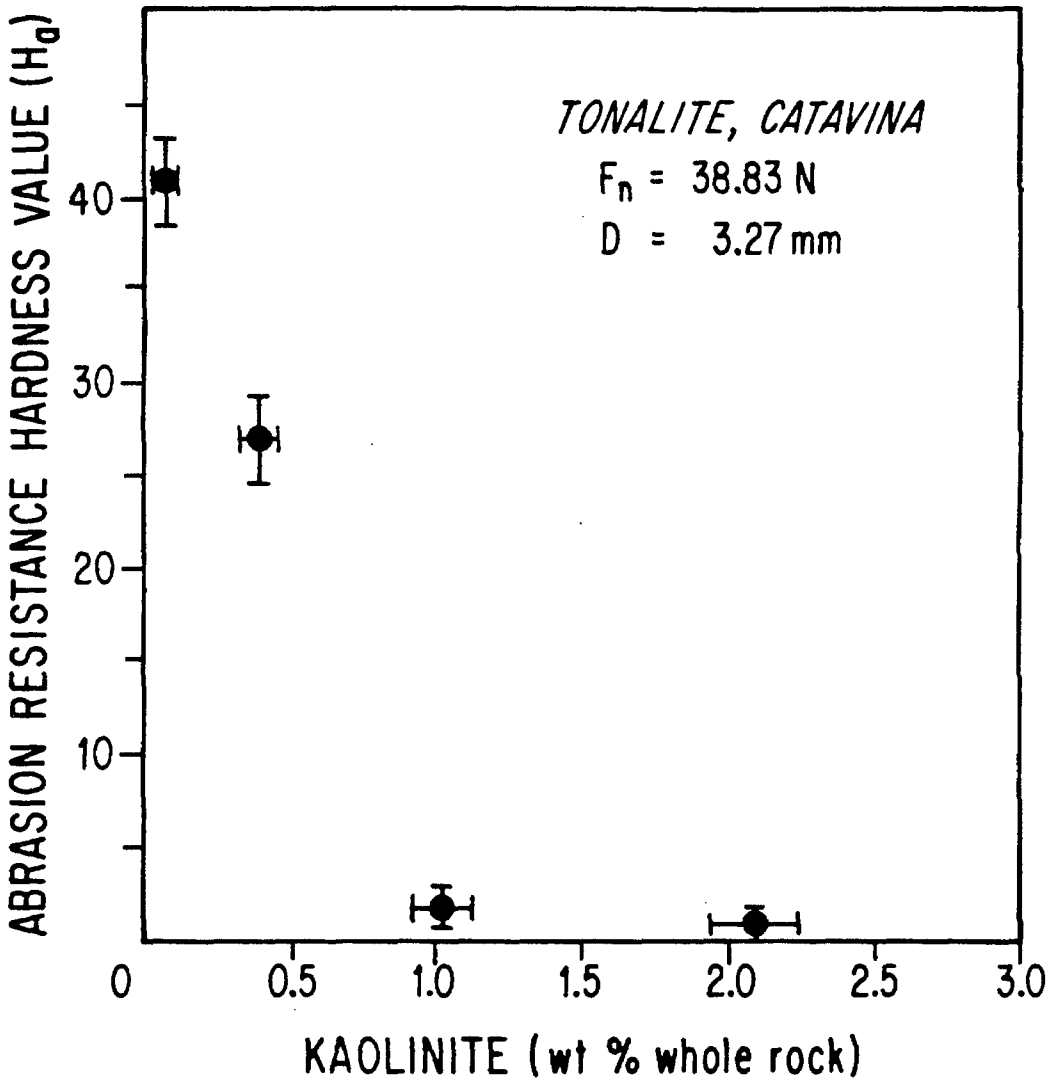
TONALITE, CATAVINA
F_n = 38.83 N
D = 3.27 mm
ABRASION RESISTANCE HARDNESS VALUE (H_a)
40
30
20
10
0
0.5
1.0
1.5
2.0
2.5
3.0
KAOLINITE (wt % whole rock)

FIGURE 6

CHAPTER 3

CASE-HARDENED AZTEC SANDSTONE

Cavernous weathering is particularly well developed in the Aztec Sandstone within the Valley of Fire, Nevada (Figure 7), where the differential effect is case hardening. The study area is located in the Valley of Fire, 60 km northeast of Las Vegas, Nevada. The dominant rock type in the area is the Jurassic Aztec Sandstone, a friable, fine-grained quartz sandstone, which is weakly cemented by hematite and minor amounts of calcium carbonate (for a detailed stragriphic discussion, see Longwell, et al., 1965).

CASE-HARDENED CRUST

Samples were obtained from a total of thirteen outcrops in the study area. The case-hardened crust within the Valley of Fire is usually between 0.5 and 5.0 mm thick, averaging approximately 1.5 mm. The crust is colored a lighter orange than the interior rock, and the boundary between crust and interior is abrupt.

The crust is not restricted to the unbroken surface of the outcrops but can be developed on surfaces inside cavernous depressions. Occasionally, the interior wall of a large cavernous depression is itself case-hardened and cavernous weathering can be developed in this interior wall.

The cavernous depressions are usually smooth-floored and spherical except where bedding has influenced erosion. Within the depressions active erosion is expressed as spallation and disintegration from the cavern walls. However, the floors usually have little eroded material

Figure 7 Representative outcrop of the Aztec Sandstone in the Valley of Fire, Nevada, showing well-developed cavernous weathering. The surface opening of the largest cavernous depression in center of image is 0.8 meters at its longest dimension. Also present in the upper left is a remnant of a once-extensive coating of desert varnish.

on them indicating rapid removal.

On parts of two outcrops a light yellow crust less than 0.5 mm thick is developed over the ubiquitous orange crust discussed above. The yellow crust is significantly harder and more resistant to abrasion than the orange crust and has a different chemistry.

SCANNING ELECTRON MICROSCOPY

Crust and interior rock samples were investigated using a scanning electron microscope equipped for energy dispersive X-ray analysis. The surface views shown in Figure 8 are representative of the study area. Figure 8a and 8b show micrographs of a section of the rock below the crust. The sandstone is very porous and there is a noticeable absence of intergranular fines. Submicron-sized hematite platelets cover all quartz-grain surfaces. The dominant clay mineral in both the case-hardened surface crust and the underlying rock is kaolinite, identified by X-ray diffraction and infrared spectroscopy.

Figures 8c and 8d show micrographs of the surface of the case-hardened crust (orange crust). X-ray analyses indicate that there is a coating, less than several microns thick, of fine-grained, Ca-bearing material on the quartz grains. Intergranular spaces are filled with fines which are mostly kaolinite. Hematite on grain surfaces is covered by the Ca-bearing coating and the fines.

INFRARED SPECTROSCOPY

X-ray powder diffraction reveals only quartz, kaolinite and hematite in both the case-hardened crust and the interior rock, although in different proportions: the crust has more kaolinite than the interior

Figure 8 Electronmicrograph of the interior and surface of the case-hardened Aztec Sandstone. (a) Micrograph of the rock below the crust, showing the abundant pore space between sand grains. (b) Higher magnification view of central portion of (a). (c) Micrograph of surface of case-hardened crust showing coating and the decreased porosity resulting from filling by kaolinite and calcite. (d) Higher magnification view of (c).

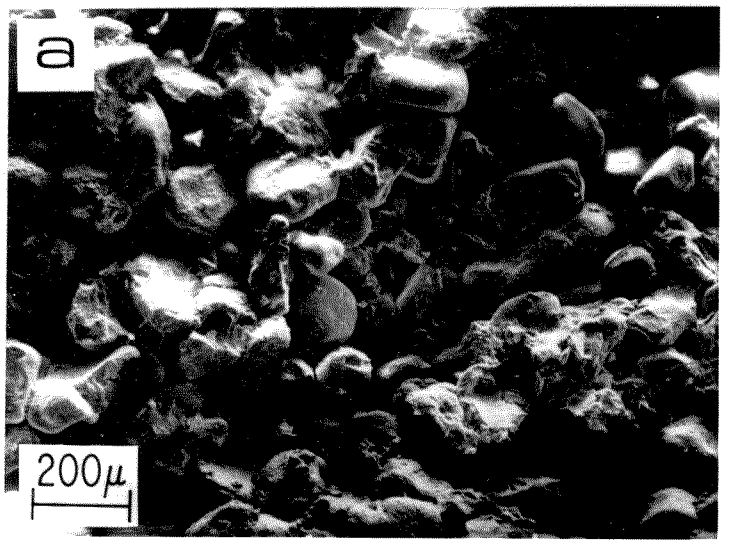
a
200μ

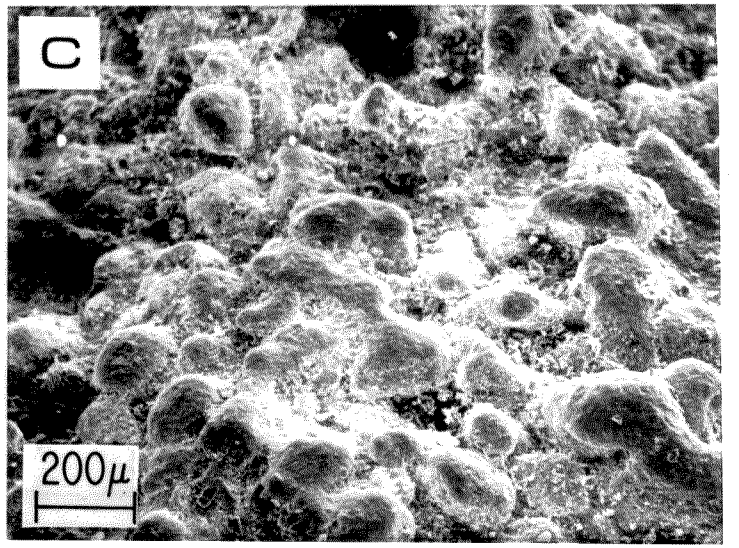
c
200μ

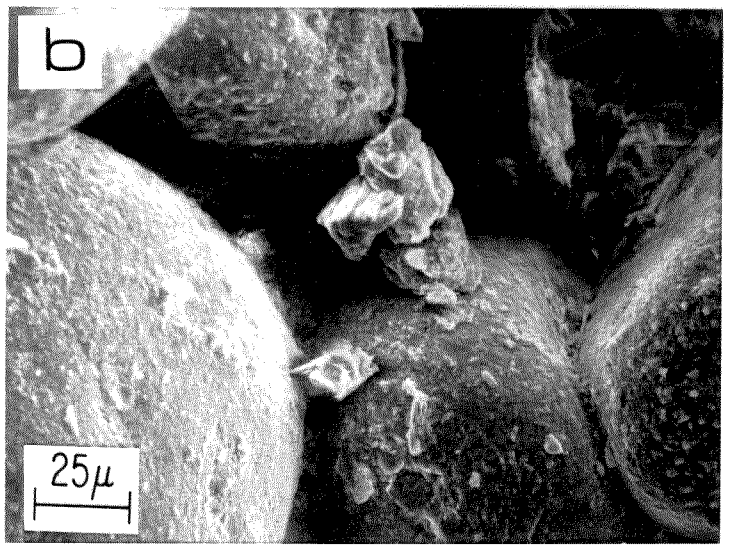
b
25μ

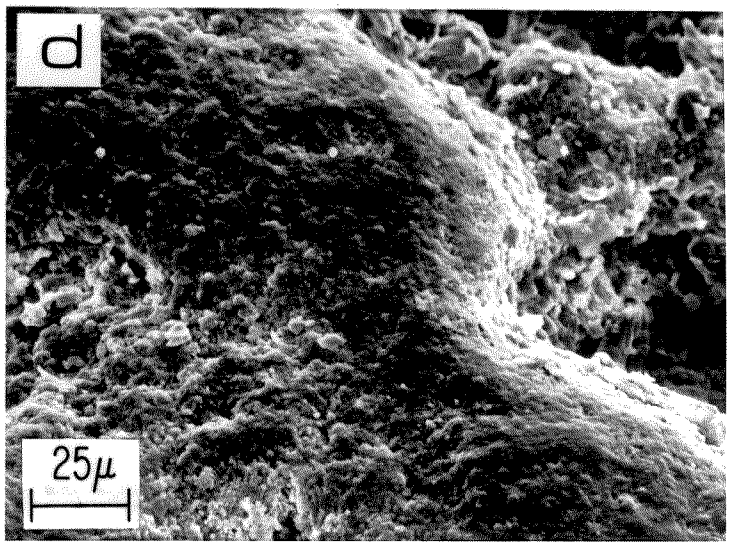
d
25μ

rock. Differences in the X-ray diffraction data between crust and interior rock occur only in the relative amount of kaolinite and quartz, the crust having much more kaolinite and slightly less quartz than the interior rock. Thus the cementing agent is either present in too low a concentration or is so fine-grained as to be X-ray amorphous. Removal of quartz grains above 40 μ results only in the relative increase of kaolinite and no appearence of the cementing agent in the diffraction data.

Infrared spectroscopy was employed because it is capable of identifying phases in small concentrations as well as X-ray amorphous material, and is also sensitive to the structural environment of hydrous components. Figures 9a and 9b show the infrared (IR) spectra for the interior rock and the case-hardened crust. In the spectrum of the interior rock, all absorption bands can be attributed to kaolinite and quartz with the exception of some adsorbed water features centered around 3450 cm^{-1} and 1625 cm^{-1}. Especially diagnostic are the absorptions between 3700 cm^{-1} and 3600 cm^{-1} corresponding to the hydrous groups of kaolinite. Kaolinite is the most abundant clay found in the Aztec Sandstone within the Valley of Fire, and is present in all samples studied. Kaolinite is always more abundant in the crust than in the interior rock, typically by a factor of 5.

In addition to absorptions related to quartz and kaolinite the spectrum of the case-hardened crust contains a broad absorption band centered at 1435 cm^{-1} and a sharper band at 873 cm^{-1}, both of which are absent in the interior rock. These two bands are the characteristic IR absorption features of calcite.

The IR spectra of the yellow crusts are different from those of the

Figure 9 Infrared spectra with major absorption bands labelled according to mineral species: quartz (Q), kaolinite (K), calcite (C), colemanite (B) and adsorbed water (W). (a) Infrared (IR) spectrum of case-hardened orange crust showing absorptions by calcite at 1435 cm^{-1} and 873 cm^{-1}. (b) IR spectrum of the interior of the case-hardened rock of (a). (c) IR spectrum of yellow crust showing absorptions due to colemanite. (d) IR spectrum of colemanite standard from Thompson Mine, Death Valley. (e) IR spectrum of kaolinite, orange crust and interior in the region of hydroxyl stretching showing the increase in kaolinite in the crust. (f) IR spectrum of standards and yellow crust showing presence of colemanite and kaolinite in yellow crust. Absorption by adsorbed water in the yellow crust has altered its broad water band relative to the colemanite standard.

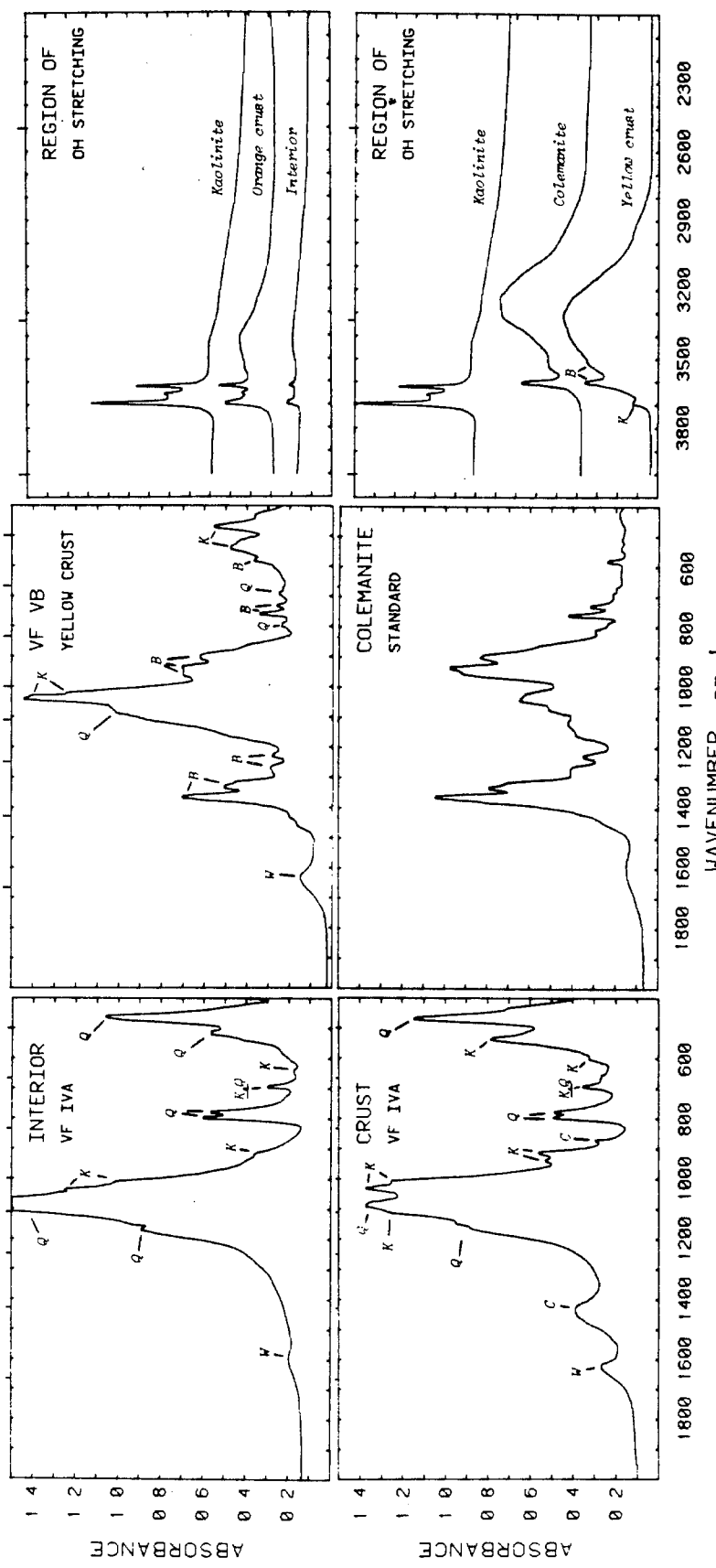
REGION OF
OH STRETCHING
Kaolinite
Orange crust
Interior
REGION OF
OH STRETCHING
Kaolinite
Colemanite
Yellow crust
VF VB
YELLOW CRUST
COLEMANITE
STANDARD
INTERIOR
VF IVA
CRUST
VF IVA
ABSORBANCE
ABSORBANCE
1800 1600 1400 1200 1000 800 600
3800 3500 3200 2900 2600 2300
WAVENUMBER, cm-1

FIGURE 9

orange crust. As with the orange crust, many absorption features are due to quartz and kaolinite. However, bands at 3600 cm^{-1}, 1367 cm^{-1}, 1334 cm^{-1}, 1318 cm^{-1}, 1270 cm^{-1} and 1227 cm^{-1} are the characteristic absorption features of the hydrated calcium borate, colemanite, $CaB_3O_4(OH)_3 \cdot H_2O$ (Figures 9d and 9f). No sulfates were found in the study area or in any sample analyses.

By comparison of the peak heights in sample spectra with those of the colemanite standard, the estimated amount of colemanite in the yellow crust is approximately 0.40 wt%. That colemanite appears as a hardening agent is surprising, but evaporite deposits of colemanite crop out and are mined at several locations within 20 km of the Valley of Fire, so that the supply of calcium borate in the form of eolian transported material is readily available.

CO_2 EXTRACTION

Because of the finely-particulate and interspersed nature of the carbonate in the crust, another method for determining the concentration of $CaCO_3$, as well as an independent verification of its presence, is dissolution of the crust in phosphoric acid, separation of the CO_2 evolved and determination of the amount of CO_2 by means of a manometer.

Table 4 shows the results for six case-hardened samples. The amount of $CaCO_3$ varies significantly between outcrops. As in all properties of the case-hardened crust within the study area, great local variations occur in hardness (friability), composition and thickness. Crust friability shows no systematic variation with $CaCO_3$ content as might be expected if $CaCO_3$ were solely responsible for the decrease in friability of the exterior.

TABLE 4 CO_2 EXTRACTION

Type of crust	sample	sample weight(g)	micromoles of CO_2	wt% $CaCO_3$
orange	VF VIII	2.706	8.76	0.033
interior	VF VIII	2.701	0.00	< 0.001
orange (pillar)	VF IVa	3.512	373.20	1.063
interior (pillar)	VF IVa	2.034	117.88	0.580
orange	VF XIII	5.192	2164.72	4.170
interior	VF XIII	3.573	0.00	< 0.001
orange	VF VIIa	0.311	0.67	0.004
orange	VF VIIb	0.313	0.95	0.005
orange	VF VIIc	0.311	1.10	0.006

There are two categories for interior samples: first, the samples obtained from inside the main part of the outcrop which is directly adjacent to deeper parts of the formation, and second, the samples collected from the interiors of structures surrounded by case-hardened crust, i.e., from the inside of pillars and knobs. When referring to interior samples, the samples are from the first category unless otherwise specified.

All interior samples studied from the first category did not produce any CO_2 above detection limits indicating that the amount of $CaCO_3$ in the interior of the rock is less than 0.001 wt%. Samples VF VII, VF VIII and VF XIII in Table 4 have interior samples from the first category. However, the interior sample taken from VF IVa in Table 4 was obtained from the interior of a pillar 4 cm in diameter and 27 cm long and contains significant amounts of $CaCO_3$. The pillar is case-hardened all the way around its exterior, but the interior of the pillar is as friable as the interior rock of the main body of the outcrop itself. However, even though the $CaCO_3$ content of the interior of the pillar is higher than that of most case-hardened crusts developed on the exterior of the main body of outcrops in the Valley of Fire, the interior is not hardened. This indicates that $CaCO_3$ alone is not sufficient to cause case-hardening at these concentrations in the study area. Other factors such as the presence of kaolinite or the mechanical distribution of the calcite must play a role.

FLUORESCENCE SPECTROSCOPY

Since both colemanite and calcite (due to impurities) are fluorescent minerals, their emission spectra may provide a clue to the

distribution of these minerals with depth in the case-hardened samples. Emission spectra for the surface of the orange crust and rock interior are shown in Figure 10a. The interior spectrum was taken from only 1.5 mm below the surface of the rock, immediately below the crust. The crust itself exhibits a broad band emission centered about 2682 cm^{-1}. The interior, however, is completely non-fluorescing. Because the crust contains 0.002 wt% MnO and ample Mn exists in the immediate environment as desert varnish, the calcite in the crust is probably fluorescing as a result of Mn^{2+} impurity. This type of emission and the relationship between crust and interior rock holds for all case-hardened samples studied. Immediately below the crust there is no emission. However, the spectra for different crusts differ significantly. Figure 10b shows the emission spectra for the surface of the yellow crust and the interior immediately below it. The spectrum for the surface of the yellow crust shows the overlap of two broad-band emissions; one centered about 1500 cm^{-1} and the other about 2409 cm^{-1}. Figure 10c shows the same spectrum along with that of the colemanite standard. The standard shows a broad band centered about 1455 cm^{-1} (along with several Raman lines). Since infrared spectroscopy of the yellow crust indicates the presence of colemanite, the emission about 1500 cm^{-1} for the crust is probably due to the colemanite. The band about 2409 cm^{-1} suggests that calcite coexists with the colemanite in the yellow crust (the thickness of which exceeds the penetration depth of the laser light). Figure 10d shows the emission spectrum for the orange crust immediately below the yellow crust. This spectrum is again dominated by calcite, although a slight shoulder suggests some colemanite is still present.

Figure 10 (A) Fluorescence spectra of the interior and of the surface of the case-hardened crust of sample VF IX. The spectra of the interior were taken immediately below the crust (1.5 mm beneath the exterior surface of the crust). (B) Fluorescence spectra of the surface of the yellow crust and the interior of sample VF Vb. (C) Fluorescence spectra of the yellow crust and the colemanite standard. (D) Fluorescence spectra of the orange crust immediately below the yellow crust of (B).

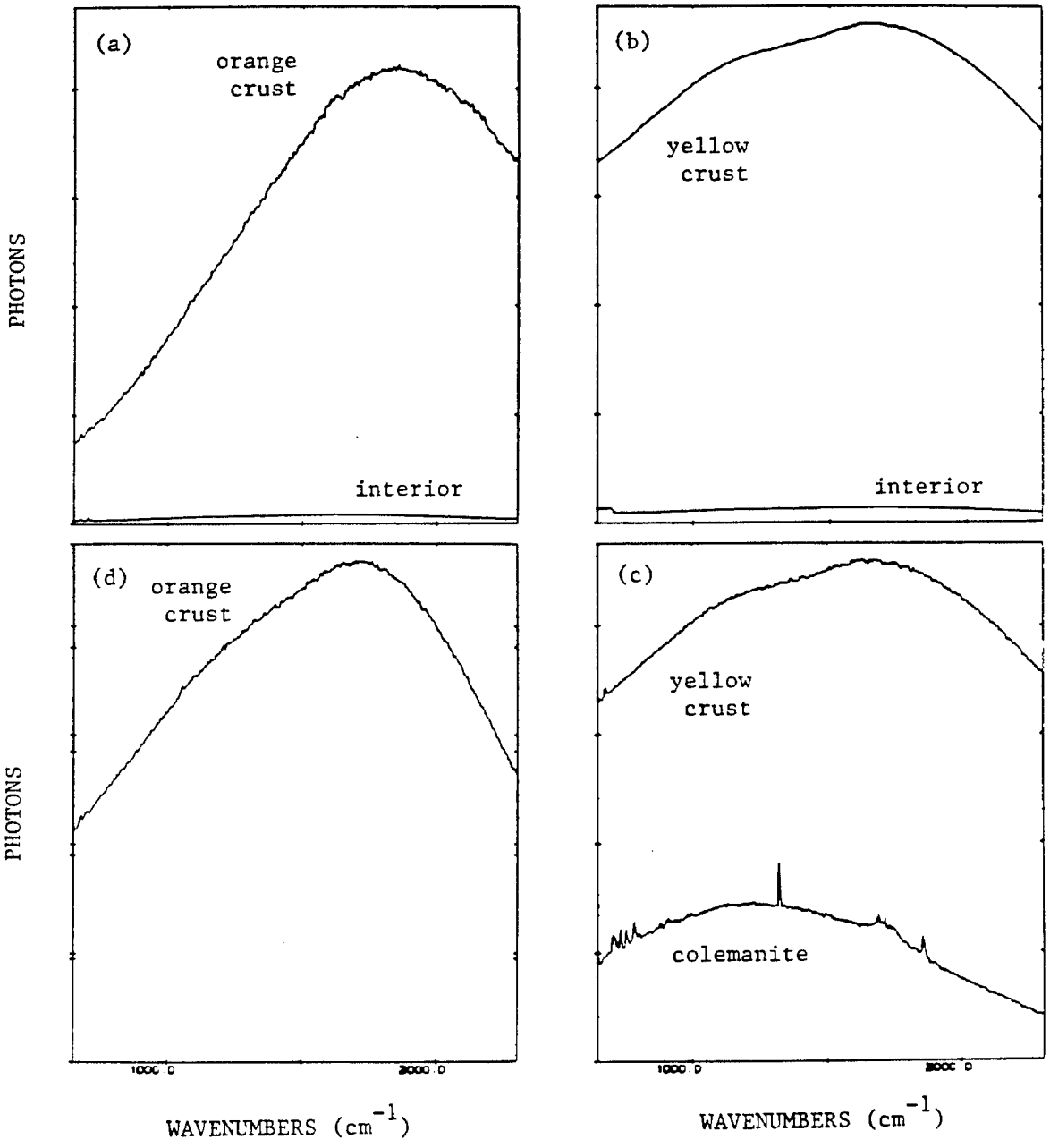
(a)
orange
crust
interior
(b)
yellow
crust
interior
PHOTONS
(d)
orange
crust
(c)
yellow
crust
colemanite
PHOTONS
WAVENUMBERS (cm-1)
WAVENUMBERS (cm-1)

FIGURE 10

RADIOGRAPHY

As a result of the identification of colemanite in the yellow crust by infrared spectroscopy, an alternative test for boron was attempted and proved successful. Although colemanite is volumetrically insignificant as a hardening agent relative to calcite, it is important as a tracer for how the other constituents may have been emplaced, and should help in deciding which differential weathering mechanisms are involved.

It is possible to identify and obtain an in situ distribution of boron with depth in case-hardened samples using a radiographic technique employed by Furst, et al. (1976). The $^{10}B(n,\alpha)^{7}Li$ nuclear reaction is used in conjunction with alpha-sensitive plastic track detectors to determine boron concentration and spatial position within polished, doubly-impregnated thin sections of case-hardened samples cut perpendicular to the crust.

This radiographic technique takes advantage of the large cross section for the (n,α) reaction of ^{10}B (3840 barns). Lithium is the only element which interferes with this technique via the $^{6}Li(n,\alpha)^{3}H$ reaction which has a cross section of only 950 barns. Coupled with the isotopic abundances of the two elements, Furst (1979) determined that for equal concentrations of Li and B, the efficiency for detecting Li relative to B is only 0.12. Considering the estimated amount of Li in the samples, interference should be negligible.

The amount of boron can be calculated from the tracks produced using the following relationship:

$$\text{Track density} = n\ f\ \sigma\ \tau\ \frac{R}{4}$$

where $n \equiv$ number of boron atoms/gram

$f \equiv$ neutron flux (nucleons/$cm^2 \cdot sec$)

$\sigma \equiv$ cross-sectional area (n,α) (cm^2/nucleon)

$\tau \equiv$ time of irradiation (seconds)

$R \equiv$ range of α particles in sample (grams/cm^2).

For this experiment, assuming all boron is in colemanite:

$R = 1.12 \times 10^{-3}$ g/cm^2

$f = 5.00 \times 10^8$ neutrons/$cm^2 \cdot sec$ (in thermal column)

$\alpha = 3840$ barns $= 3.84 \times 10^{-21}$ cm^2/nucleon

$\tau = 900$ sec.

Irradiation of case-hardened sample VF VIb (yellow crust) under such conditions produced a varying alpha track density with depth or distance from the rock exterior. Figure 11 shows the average of five track-counting traverses through the sample (Table 5). It is evident that almost all of the boron is contained within the case-hardened crust which is 1.5 mm thick on this sample.

Figure 11 indicates that the concentraion of colemanite in the yellow crust is about 0.10 wt%. This is a bit low compared to the values estimated from infrared spectroscopy (0.40 wt%). Yet, as in all case-hardened samples local variations are great and to be expected. Also, the extreme friability of the sample, even when impregnated, causes the polished surface to be very irregular. Void spaces caused by plucking of quartz grains are abundant and filled with epoxy. This greatly reduces the ability of the track detector to measure alpha production. Therefore, the values for the amount of colemanite in the

Figure 11 In situ distribution of colemanite with depth in case-hardened sample VF VI, as determined from the alpha track density after irradiation with thermal neutrons.

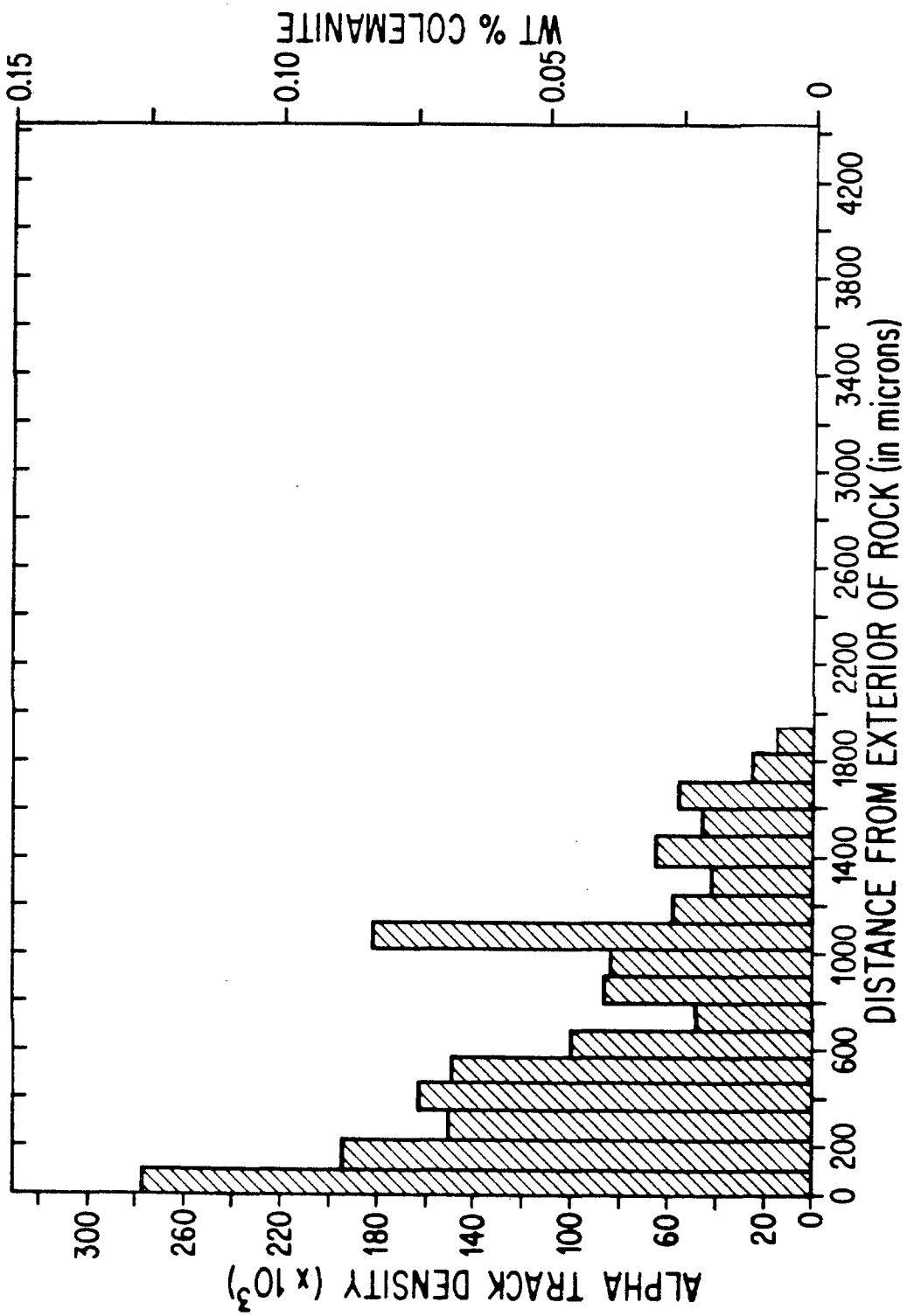
WT % COLEMANITE
0.15
0.10
0.05
0
ALPHA TRACK DENSITY (x 10³)
300
260
220
180
140
100
60
20
0
0 200 600 1000 1400 1800 2200 2600 3000 3400 3800 4200
DISTANCE FROM EXTERIOR OF ROCK (in microns)

FIGURE 11

TABLE 5

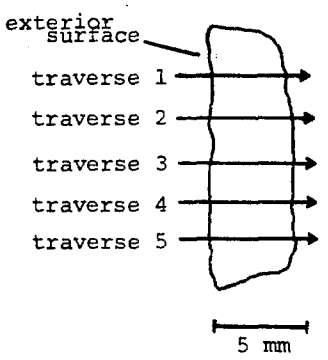

Neutron irradiation

flux = 5×10^8 neutrons cm^{-2} sec^{-1}

τ = 900 sec

Track density for Colemanite standard is 2.19×10^8 tracks/cm^2

TRACK DENSITY (track/cm^2 x 10^3)					distance from exterior (in microns)	average track density
traverse 1	traverse 2	traverse 3	traverse 4	traverse 5		
234	258	318	300	275	0 - 113	277
313	78	300	165	117	113 - 226	194
234	39	150	235	94	226 - 339	150
172	204	164	220	55	339 - 452	163
117	196	78	150	204	452 - 565	149
63	39	110	47	243	565 - 678	100
16	23	62	39	101	678 - 791	48
157	78	23	86	86	791 - 904	86
78	70	0	150	117	904 - 1017	83
198	258	55	274	125	1017 - 1130	182
47	125	0	94	23	1130 - 1243	58
0	86	0	39	86	1243 - 1356	42
0	62	86	155	16	1356 - 1469	63
39	39	23	125	8	1469 - 1582	46
62	94	47	62	8	1582 - 1695	55
0	31	0	70	0	1695 - 1808	25
23	16	0	23	0	1808 - 1921	15
0	0	0	0	0	1921 - 2034	0
0	0	0	0	0	2034 - 2147	0

crust determined by this radiographic technique should be regarded as lower limits for the actual values. By the same token, the friability of the sample also increases the possibility of contamination of the interior during polishing and probably smooths out any abrupt boundary in boron distribution with depth that may exist in the pristine sample.

DISCUSSION

Field observations and the experimental results can be summarized as follows: (1) rocks of the Aztec Sandstone within the Valley of Fire, Nevada, are extensively case-hardened; (2) case-hardening in the study area involves the presence of an induration crust (called the orange crust), usually between 0.5 and 5.0 mm thick, which has increased hardness and reduced friability over the interior rock, and differs from the interior in the amount of kaolinite (about a factor of five greater in the crust) and the presence of calcite (in concentrations between ≈0.001 and ≈5.0 wt%); (3) two out of thirteen outcrops sampled possessed a yellow crust overlying the orange crust and which, even though much thinner (less than 0.5 mm), was significantly harder. Like the orange crust, the yellow crust contained more kaolinite than the interior but also contained colemanite, $CaB_3O_4(OH)_3 \cdot H_2O$; (4) the interior boundary of the crusts are abrupt and the interior rock within the study area contains no calcite or colemanite above detection limits (≈0.001 wt%), and (5) thickness, physical properties, and calcite content of the case-hardened crusts within the study area show great local variations.

It is possible to speculate on the formation mechanism of the case-hardened crust in the Valley of Fire from these results. First, the crust is a non-pedogenic deposit of calcium carbonate cement. Quartz, hematite and some of the kaolinite are the host materials, existing

prior to induration, and constitute the interior of the rock.

Possible transport mechanisms for the carbonate, colemanite and kaolinite are wind and water. Groundwater containing dissolved carbonate could deposit the case-hardening agents at the surface as evaporite deposits cementing the surface materials. Although it is conceivable that enough calcite-poor Aztec Sandstone could be leached of carbonate to produce the crust on rock surfaces, this mechanism may not account for the case-hardened crusts that develop around small pillars, knobs and other protrusions which do not have access to leaching of the large volumes of rock required to supply the carbonate. These protusions often exhibit better developed crusts than surfaces on larger outcrops. Leaching of the Aztec Sandstone by groundwater also cannot account for the borate-containing crust. Leaching and redeposition of calcite has occurred in the study area as evidenced by botryoidal and vein-filling calcite deposits, but these occurrences do not relate to case-hardening in any observable way.

By far the more efficient and prevalent agent for transporting the necessary materials to the outer surface of the rock is the wind. Eolian transportation of fines composed of kaolinite, calcite and colemanite particles, as well as quartz and minor constituents, is common in the desert environment. Eolian transported material was regarded by Lattman (1973) to be the major source of $CaCO_3$ for cemented non-carbonate-bearing alluvial fan deposits. Of importance is the fact that windblown fines are able to reach all exposed rock surfaces and be deposited on them. Subsequent interaction with dew, groundwater or meteoric water, and recrystallization of the calcite throughout the surface rind is a probable formation mechanism for the crust within the study area.

Support for the eolian emplacement of the crust constituents as the differential mechanism in the Valley of Fire comes from observations of another kind of crust which forms on the stems of plants and from analyses of trapped fines from eolian particulate collectors. After a rain storm, transient crusts of wind transported fines coat the stems of small desert bushes (the Calovini effect). These crusts are several millimeters thick and crumble when removed. They are usually eroded quickly under the action of windblasting after they dry out. These crusts are of the same composition as the case-hardened crusts on the rock surfaces after the host grains have been removed; i.e., they are composed mostly of fine-grained kaolinite, quartz and calcite. Likewise, eolian transported particulates collected in an airborne-particulate collector over a period of two years from a height of one meter above the ground were also of this bulk mineralogy.

But the strongest indication of an eolian influence is the presence of colemanite. It can only be transported to the rock surface by the wind because, at the ambient temperatures and pressures of the rock surface, colemanite is not stable in aqueous solution and will recrystallize to the mineral meyerhofferite, $CaB_3O_3(OH)_5 \cdot H_2O$, whose IR spectrum is easily distinguished from that of colemanite (Appendix 1). This means that the colemanite in the yellow crust has not undergone significant recrystallization in the the yellow crust (less than several wt%) or else meyerhofferite would appear in the spectra of the yellow crust (Figure 9c). However, since the yellow crust is harder than the orange crust, colemanite is contributing to the differential weathering effect of case hardening if only by way of its inherent hardness (H = 4 to 4 $\frac{1}{2}$ compared to calcite's H = 3 and kaolinite's H = 2), further illustrating the effects that passive agents

such as colemanite and kaolinite can have on the physical properties of crusts. But calcite is still the important cementing agent even in the yellow crust, as indicated in Figure 10b.

Unlike $CaCO_3$, kaolinite is unable to penetrate very far into the rock. The thickness of the crust probably reflects this limit of penetration. It is difficult to distinguish the added kaolinite from the host kaolinite, but SEM studies show much of the kaolinite in the crust to be more rounded and finer-grained than in the interior which probably reflects an eolian origin. More studies must be done to determine the existence, nature and distribution of the two different kaolinite populations.

Dating the crust using ^{14}C in the calcite is a possibility, but the same problems arise as in dating K-horizons in soils by radiocarbon. It is difficult to determine the source of the carbonate and the amount of post-depositional recrystallization that could have introduced younger carbon. Since the coating is so fine-grained it might have been in complete equilibrium with atmospheric carbon when it crystallized. This may become apparent after some of the crusts have been dated. Also the crusts are probably the result of repeated episodes of recrystallization, and different areas on a microscopic scale may be of different ages. Still ^{14}C dating may be useful for relative age dating.

Kaolinite and fine-grained quartz are the major materials transported by the wind in the study area, and they also make up most of the case-hardened crust second to the primary quartz grains. All case-hardened crusts studied display an enrichment of kaolinite over the interior rock. It is at present impossible to determine whether the clays are a passive constituent in case hardening, present only because they are deposited along with the case-hardening agent, or whether the

clays are a critical component of the crust. It appears reasonable that the kaolinite acts as a space filler, reducing the amount of required cement to form a crust. The amount of calcite in most of the crusts is low (less than 0.01 wt%). Potter and Rossman (1977) discussed the role of clays in the formation of desert varnish and concluded that it was a necessary component of the varnish, although for different reasons.

DESERT VARNISH AND CRUST

Unlike desert varnish, the case-hardened crust is composed mostly of host rock (over 90 wt%) and is an induration phenomenon. Like varnish, however, the boundary between crust and interior is abrupt, and the origin of the case-hardening material (cement and deposited kaolinite) is external to the rock. Also like varnish, the major part of the deposited material is clay: ≈ 70% for varnish (Potter, 1979) and anywhere from 50% to 90% for case-hardened crusts. In fact, desert varnish contributes to case hardening in the study area by decreasing the friability of the exterior surface. However, desert varnish is itself coated with the same calcite-cemented crust that covers the unvarnished case-hardened rocks. The amount of kaolinite on the surface of the varnish relative to the orange crust is less and this may reflect a difference in the ability of the two surfaces to retain eolian deposited clay. Certainly the fresh sandstone surface has a greater porosity and surface roughness than the varnished surface and may retain either the case-hardening constituents or moisture longer than the varnished surface.

To describe the varnish as being case-hardened by the calcite is incorrect since the calcite coating on the varnish probably has no effect on the relative weathering rates between exterior and interior

which would result in cavernous weathering, the varnish itself being harder than the calcite coating. However, it is an important relationship as far as the age of the surface is concerned. Petroglyphs which occur in abundance within the study area are also coated with the indurating material and may be termed case-hardened. Although the age of the petroglyphs themselves are in doubt, this does put an upper limit on the age of the crust (or the time required to form it) of about 10,000 years.

SUMMARY

Field observations and the experimental results from the Valley of Fire, Nevada, can be summarized as follows: (1) rocks of the Aztec formation within the Valley of Fire are extensively case-hardened, (2) case-hardening in the study area involves the presence of an induration crust (called the orange crust), usually between 0.5 and 5.0 mm thick, which has increased hardness and reduced friability over the interior of the rock, and differs from the interior in the amount of kaolinite (about a factor of five greater in the crust) and the presence of calcite (in concentrations between ≃ 0.001 and ≃ 5.0 wt%), (3) two out of thirteen outcrops sampled possesed a second yellow crust overlying the orange crust and which, even though much thinner than the orange crust (less than 0.5 mm), was significantly harder. Like the orange crust, the yellow crust contained more kaolinite than the interior but also contained colemanite, $CaB_3O_4(OH)_3 \cdot H_2O$, (4) the interior edge of the crusts are abrupt and the interior rock within the study area contains no calcite or colemanite above detection limits (≃ 0.001 wt%). and (5) thickness, physical properties, and calcite content of the case-hardened crusts within the study area show great local variations.

CHAPTER 4

CORE-SOFTENED TONALITE

The tonalite is part of a pluton in the Peninsular Ranges Batholith, located near Catavina, at the northern end of the Jaraguay Block in central Baja California (Figure 13). The climate is arid with less than 5 inches of rainfall annually. The Cretaceous pluton exhibits cavernous weathering in much of its exposure (Figure 12) and forms topographic lows, with surrounding mesas capped by Pliocene basalts. The present erosion surface of the pluton has formed below the level of the exhumed old erosion surface of the early Cenozoic mentioned in many geomorphic studies of Baja California (Gastil et al. 1975).

Within the study area the pluton is a medium-grained, light-colored tonalite. Thin section point counts yield an average modal mineralogy of 65% plagioclase (An_{28}), 11% quartz, 5% potassium feldspar, 16% biotite, 3% hornblende, and trace amounts of zircon, titanite and epidote. The quartz exhibits a small degree of myrmekitic texture with plagioclase. The plagioclase is microantiperthitic with areas as high as 70% K-spar. In general, all grains appear fresh and unaltered in the unweathered rocks, except that hornblende occasionally exhibits alteration to epidote. Variations in bulk composition and mineralogy within the pluton are significant within distances of hundreds of meters. Modal amounts of hornblende range from 5% to less than 1% by weight within the study area and plagioclase compositions vary between An_{25} and An_{29}. As will be discussed later, these intraplutonic variations are often greater than the chemical variations owing to weathering, necessitating the use of indicators other than changes in composition to trace the effects of weathering on these rocks.

Figure 12 A representative core-softened tonalite boulder at Catavina, exhibiting cavernous weathering. The overhanging shell is 8 cm thick and the longest dimension of the cavernous hollow is just over 1 m.

Figure 13 Index map of field area in Baja California (After Gastil et al. 1975).

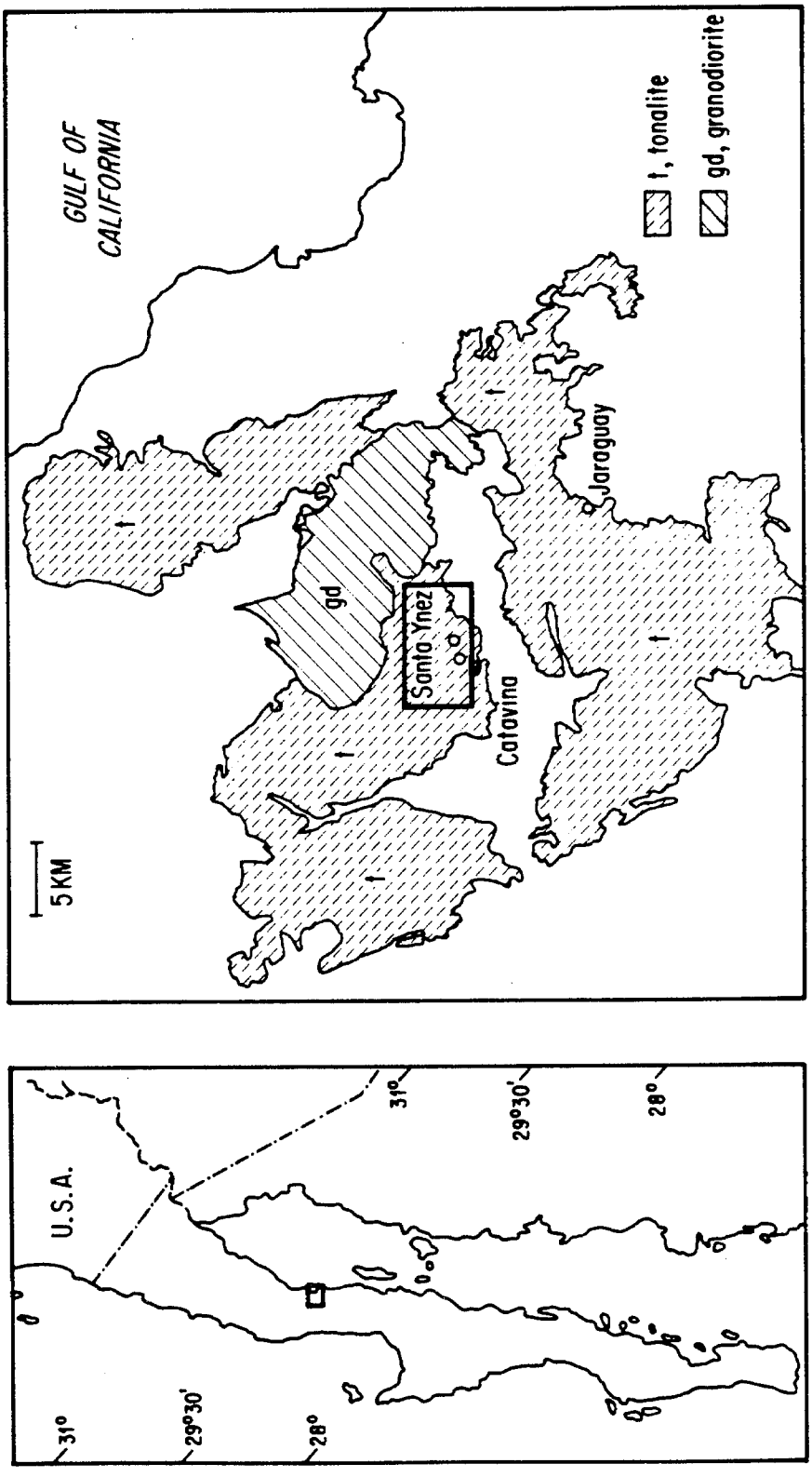
GULF OF CALIFORNIA
t, tonalite
gd, granodiorite
Jaraguay
Santa Ynez
Catavina
gd
t
5KM
U.S.A.
31°
29°30'
28°

FIGURE 13

The tonalite boulders sit in a soil of grus. Fresh outcrops are rare and restricted to areas recently exhumed by streams or road cuts. The surfaces of the weathered boulders are often coated with a weathering patina of various shades of brown. Individual cavernously weathered boulders are dominated by a single large cavern but may have several smaller holes in the overhanging shell or walls of the larger hollow. The interior walls of the cavernous hollow also have a weathering patina that may or may not be developed to the same extent as the respective exterior surface. Hard, thin (1-2 cm) exfoliation shells occur on some of the weathered boulders and are found on surfaces which do not exhibit cavernous weathering. The exfoliation shells have a weathering patina on both their outside and inside surfaces.

No soluble salts or salt weathering effects were seen in the tonalite in the study area. Eolian erosion effects are also absent although wind is an important agent for the removal of weathered debris. Insolation and frost action are expected to be insignificant in the study area and no evidence for their action was observed at Catavina. Although biological activity will, in general, increase the chemical reactivity of surface and interstitial solutions (Antweiler and Drever 1983), thus enhancing weathering, there is little such biological action at Catavina, and no observable relationship between biological activity and cavernous weathering.

Whole-rock chemical analyses of each rock zone of a representative, core-softened, cavernously weathered boulder (Figure 14) are shown in Table 6: (A) friable rock interior, (B) rock exterior and (C) exfoliation shells. The exfoliation shells are the least weathered material obtainable from the outcrop, as determined from petrographic examination, amount of clay minerals formed and the degree of hydration

Figure 14 Schematic cross-section through a core-softened tonalite boulder exhibiting cavernous weathering. Analyses are given in Table 6 for each weathering zone as well as for a sample from a nearby unweathered outcrop having slightly different mineralogy.

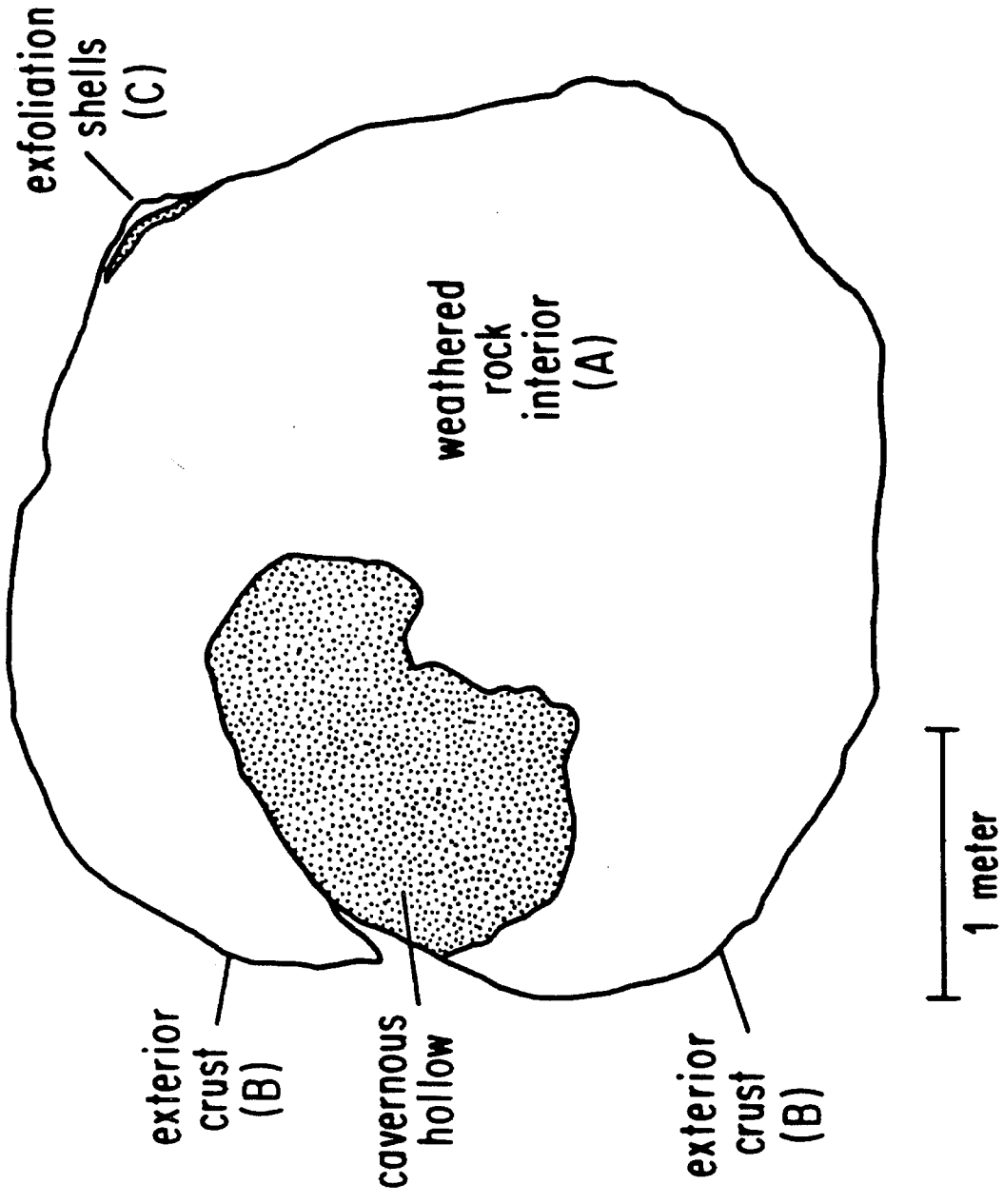
exfoliation shells (C)
weathered rock interior (A)
exterior crust (B)
cavernous hollow
exterior crust (B)
1 meter

FIGURE 14

TABLE 6

WHOLE ROCK CHEMISTRY

Oxide	Weathered Interior (A) (%)	Exterior Crust (B) (%)	Exfoliation Shells (C) (%)	Unweathered Boulder (D) (%)
Al_2O_3	15.5	15.2	15.4	15.6
SiO_2	66.9	69.8	70.1	66.2
Fe_2O_3	.98	1.48	1.00	1.13
FeO	1.15	.83	.85	2.48
MgO	.85	.91	.71	1.99
K_2O	1.57	1.53	3.37	2.15
Na_2O	4.80	4.98	4.13	4.44
CaO	2.76	2.92	2.47	4.04
TiO_2	.37	.39	.39	.57
MnO	< .1	< .1	< .1	< .1
H_2O	.53	.62	.40	.63
TOTAL	95.5 %[a]	98.8 %	99.0 %	99.6 %
Fe^{3+}/Fe^{2+}	.76	1.60	1.06	.41
Al_2O_3/SiO_2	.23	.22	.22	.24

[a]Weathered samples give low totals for whole rock powder and individual mineral chemical analyses due to matrix effects brought about by weathering, affecting SiO_2 and Al_2O_3 values while keeping Al_2O_3/SiO_2 ratios fairly constant.

of the biotites. The exfoliation shells are also the most coherent material in the outcrop. Assuming that throughout the boulder the initial chemical and mineralogical variations of the parent material were small, then we can view the present compositions of the three zones as being the result of three different weathering histories from a single parent material. Relatively fresh, unweathered rock (D) from a nearby outcrop recently exhumed by stream activity is included in Table 6 for comparison with the weathered material. This sample (D) differs from the weathered samples (A-C) mineralogically by initially having more hornblende (4% as opposed to 1%). For the three weathered zones of the boulder (A,B,C) TiO_2 has remained fairly constant with weathering. As would be expected with dissolution weathering, the ratio of Al_2O_3/SiO_2 has increased with weathering, although only slightly. Both the exterior crust and the exfoliation shells have Fe^{3+}/Fe^{2+} ratios greater than one, reflecting the precipitation of iron oxides near the rock surface, not greater oxidation of primary Fe^{2+} (see Table 9). The weathered zones A and B have lost a considerable amount of K_2O relative to the exfoliation shells and show a relative gain in Na_2O and CaO.

Comparing the results for this weathered boulder with the sample from the nearby unweathered outcrop (D) we see that the intraplutonic compositional variations are greater than those due to weathering with perhaps the exception of K_2O. Thin section analyses of nearby boulders also indicate variations of several weight percent in modal amounts of the major minerals. In light of such variation it may be erroneous to assume that the parent whole rock composition was really constant over the small volume of the boulder. Therefore, changes in bulk composition between different areas are not solely due to weathering and may not be a good parameter with which to characterize the weathering processes

that have given rise to the existing morphology. Indeed, the use of traditional ternary compositional diagrams such as kaolinization diagrams do not supply useful information in the present case, mainly because the bulk composition has undergone too little change as a result of weathering. It is necessary to look at changes in individual minerals and the growth of authigenic phases during weathering and how these affect the physical properties of the rock.

Differential weathering effects are extremely heterogeneous. Although the basic effects described above are seen in all core-softened boulders at Catavina, the details will differ from boulder to boulder. The scenario presented in this paper focuses on a single cavernously weathered boulder, with supporting data from several others, and from surrounding material.

FELDSPAR WEATHERING

In hand specimen the feldspar grains of the weathered rock have a powdery material on their surfaces. In thin section the feldspars in the weathered interior (A) are permeated with orthogonal sets of microfractures. Under the SEM the fine powdery material on grain surfaces can be seen as authigenic silica and alumino-silica bearing minerals on the basis of EDS analysis. Disaggregated samples were sonified and centrifuged to collect the <10 μm fraction. Infrared spectroscopy was used to identify the clay minerals. The spectra are dominated by kaolinite and quartz. IR spectra of whole rock powders were used to determine the wt% kaolinite in each of the rock zones of Figure 14. Table 7 gives the results. Comparing the kaolinite contents with the hardness data and general thin section and hand specimen observation, it is seen that the friability and weathered appearence of

TABLE 7

KAOLINITE CONTENTS

Sample areas (see fig. 3)	Kaolinite content (wt% whole rock) (%)
Weathered interior (A)	2.10 ± .2
Exterior crust (B)	1.05 ± .1
Exfoliation shells (C)	.40 ± .05
Unweathered boulder (D)	.10 ± .02

the rock zones are directly proportional to the kaolinite contents. Even the fresh rock (D) contains a small amount of kaolinite, indicating that some chemical weathering has occurred. The exfoliation shells have significantly lower kaolinite than the exterior surface which, in turn, has less than the friable interior. Thus kaolinite content can indicate the degree of chemical weathering that different areas of the rock have experienced.

Kaolinite and secondary quartz occur in mixed clusters on the surfaces of the primary mineral grains. This relationship is consistent with current hypotheses concerning the deposition of released alumina and silica as amorphous gels which subsequently crystallize to kaolinite and quartz (Yariv and Cross 1979; Loughnan 1969; Berner and Holdren 1979). Thin section analyses indicate that the interiors of the feldspar grains have been unaffected by kaolinization which has occurred along grain boundaries and fracture surfaces. Feldspar analyses (Table 8) show that little change in overall feldspar composition has occurred with weathering. There appears to be a small relative loss of Ca and Al with a complimentary gain in Na and Si. Since Al normally increases relative to Si during dissolution and weathering, these slight differences can best be explained as intraplutonic variations in the original composition.

Mixed layered illite/montmorillonite (80% illite) was found in the surrounding soils but not in the weathering rock material. Most desert soils retain the alkalies and alkaline earths owing to incomplete leaching. This favors the formation of mixed layered clay minerals (Devore 1958). However, incomplete leaching of the soil does not necessarily reflect the situation of the weathering boulder resting on top of the ground surface. At Catavina, the boulders are effectively

TABLE 8

PLAGIOCLASE CHEMISTRY

Oxide	Unweathered rock (%)	Weathered rock (%)
Al_2O_3	24.06	23.45
SiO_2	60.74	61.98
TiO_2	---[a]	.01
Na_2O	8.05	8.51
K_2O	.27	.31
CaO	5.97	5.28
FeO[b]	.08	.08
BaO	.04	.02
TOTALS	99.19 %	99.64 %
	$An_{28.6}$	$An_{25.1}$
Al_2O_3/SiO_2	.40	.38

[a] Below detection limits

[b] As total iron

leached while the soil is not. Thus kaolinite is the initial weathering clay product of the rock. Only after granular disintegration occurs and the material enters the soil profile does mixed layered illite/montmorillinite begin to form in the study area.

BIOTITE WEATHERING

In all samples of the weathered tonalite at Catavina, the biotites are only slightly altered chemically and retain much of their luster. X-ray diffraction patterns of the biotites from the rock zones of Figure 14 show no vermiculite or other intermediate weathering products forming from the biotites. Chemical analyses for biotites from each zone (Table 9) show that only minor changes in chemistry have occurred during weathering, such as an increase in the water content of the biotites. Although total iron has changed only slightly, the Fe^{3+}/Fe^{2+} ratio has increased substantially in the weathered samples, to almost double the unweathered value in the weathered interior. Figures 15a and 15b show SEM micrographs of the (001) surface of an unweathered and a weathered biotite. The sheets of the weathered biotite are in the process of separation and breakup. The dissolution of the biotites is not homogeneous, as some layers weather differently and more rapidly than others. Figures 15c and 15d are micrographs of the (110) surface of a weathering biotite. There are two types of layers: more resistant, smooth layers alternating with less resistant, recessed layers. Energy dispersive X-ray analyses of these areas show that the recessed layers have higher Fe concentrations (up to about 40%) than the more resistant layers. The (110) surfaces of these high-Fe layers appear highly etched and indicate that they are dissolving at a much faster rate than the low-Fe layers. Dissolution appears to be the major process of removal

Figure 15 Electron micrographs of biotite surfaces. (A) The (001) surface of an unweathered biotite. (B) The (001) surface of a weathered biotite. (C) Oblique view of the (110) surface of a biotite from a weathered boulder interior showing the alternating low and high-Fe layers (resistant and recessed layers, respectively). (D) Higher magnification view of (C) showing the etched (110) surface of a high-Fe layer. Scale bar is 10 μm in (A), (B) and (C), and 1 μm in (D).

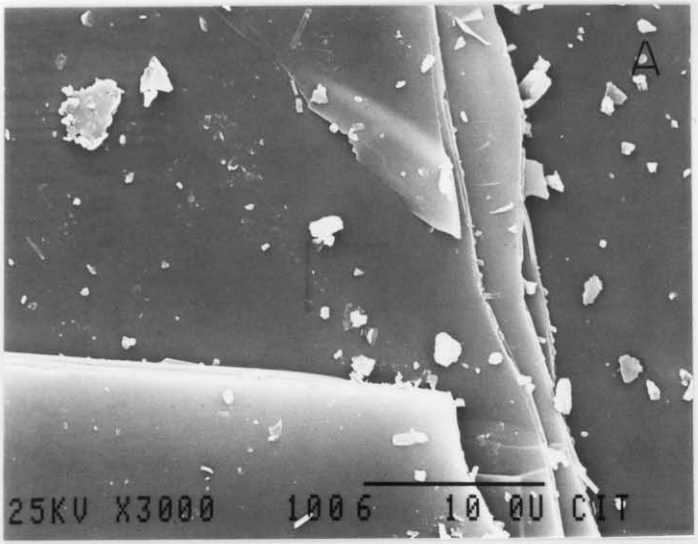
A
25KV X3000 1006 10.0U CIT

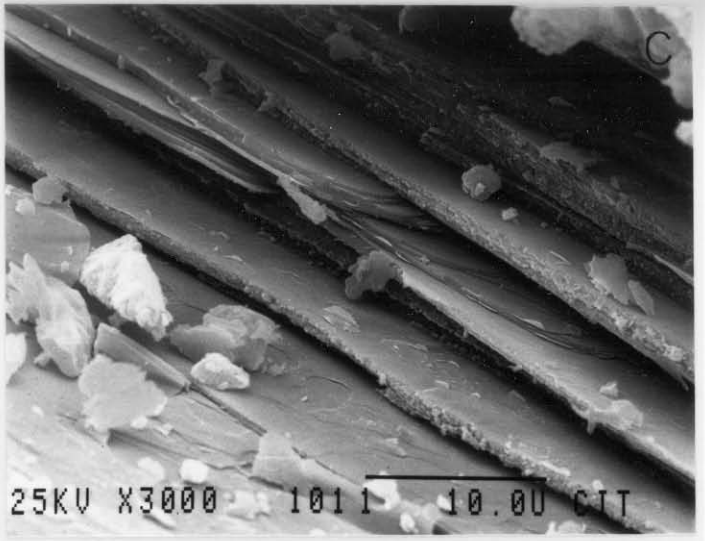
C
25KV X3000 1011 10.0U CIT

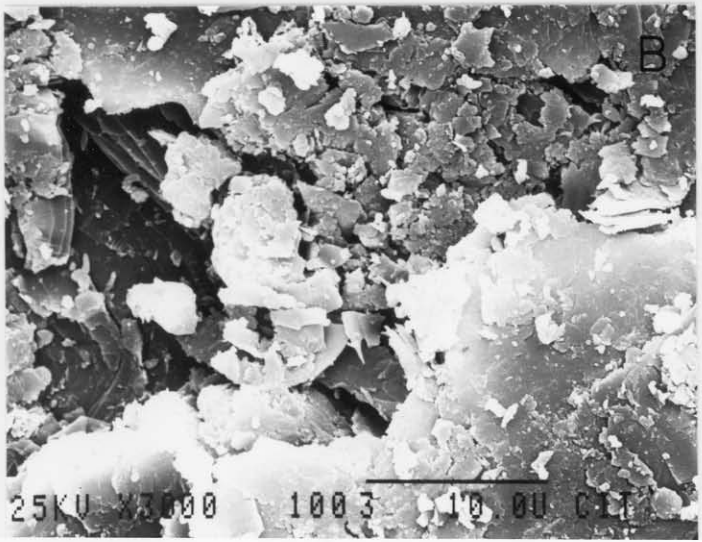
B
25KV X3000 1003 10.0U CIT

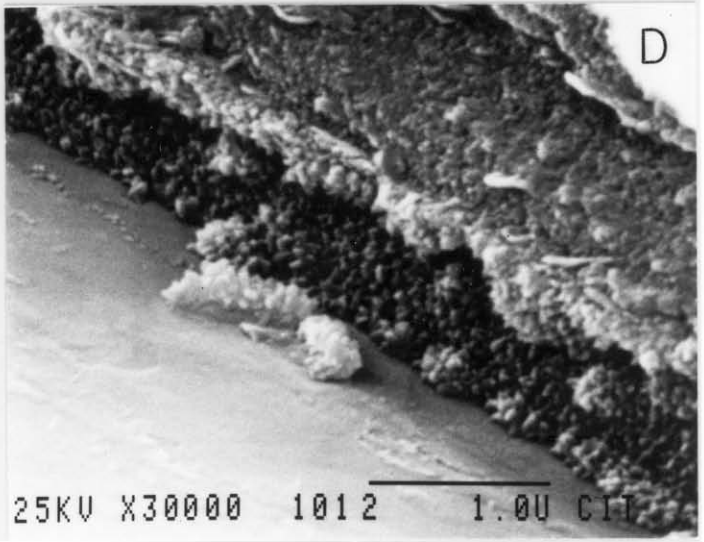
D
25KV X30000 1012 1.0U CIT

TABLE 9

BIOTITE CHEMISTRY

Oxide	Weathered Interior (A) (%)	Exterior Crust (B) (%)	Exfoliation Shells (C) (%)	Unweathered Boulder (D) (%)
Al_2O_3	14.57	15.45	14.00	14.58
SiO_2	36.29	35.82	35.30	37.13
TiO_2	3.66	3.84	3.48	2.97
Na_2O	.09	.58	.02	.06
K_2O	9.54	9.23	9.49	9.56
CaO[a]	---	---	---	---
MgO	9.55	9.46	9.08	11.10
FeO	12.20	11.64	14.57	14.58
Fe_2O_3	8.54	8.16	6.79	5.12
MnO	.41	.36	.44	.28
F	.17	.23	.07	.05
Cl	.03	.04	.02	.03
ZnO	.03	.20	.05	.10
H_2O	4.00	4.20	3.76	3.04
TOTALS	99.08 %	99.21 %	97.07 %	98.61 %
Fe^{3+}/Fe^{2+}	.63	.49	.42	.32

[a] Below detection limits

of the high-Fe material. The (110) surfaces of the low-Fe layers rarely have an etched appearance and more commonly show smooth fracture surfaces as though physical transport of fragments were most important in removing this material from its present position. Wilson and Farmer (1970) found that Fe-rich lamellae in hornblende were completely altered and removed during weathering while the rest of the hornblende remained essentially unweathered. The greater susceptibility to dissolution of Fe-rich silicates results from the ability of Fe to change in oxidation state during weathering, rendering the structure unstable.

Biotite loses Fe by the following reactions (Farmer et al. 1971):

1) loss of hydroxyl protons (reversible)

$$KFe_3^{2+}(Si_3ALO_{10})(OH)_2 + \frac{1}{2}\,O_2 \rightarrow KFe^{2+}Fe_2^{3+}O_2(Si_3AlO_{10}) + H_2O$$

2) loss of octahedral iron (irreversible)

$$KFe_3^{2+}\,(Si_3AlO_{10})(OH_2) + \frac{3}{4}\,O_2 + \frac{1}{2}\,H_2O \rightarrow KFe_2^{3+}(Si_3AlO_{10})(OH)_2 + FeOOH$$

with the precipitation of amorphous or crystalline Fe-hydroxides. According to Fischer and Schwertmann (1975) hematite forms from the aggregation of the hydroxides and subsequent dehydration. Under conditions present at the rock surface in Catavina, i.e., periodic dessication under strong sunlight, low organic contents, and high Eh, dehydration to hematite is favored over the formation of goethite. Using scanning electron microscopy on the Catavina samples these hematite aggregates are seen in association with the other secondary minerals in both the interior and exterior of the rock, but occur in

greater abundance towards the rock surface.

OTHER WEATHERING PRODUCTS

Trace amounts of authigenic calcite and gypsum have been found in weathered samples of the tonalite using scanning electron microscopy. The calcite occurs as irregular masses which have incorporated small grains of secondary kaolinite and quartz during growth. CO_2 monometry indicates that calcite totals less than 0.001 wt% in the weathered rocks. Gypsum is even less abundant than calcite.

Based upon thin-section study, X-ray diffraction and scanning electron microscopy, hornblende remains essentially unweathered in these rocks. What small amount of iron is supplied by hornblende breakdown is far outweighed by iron supplied from biotite weathering.

HARDNESS TESTING

The hardness, as manifested in the abrasion resistance, of the different rock zones in Figure 14 was measured using the abrasion resistance hardness tester (Chapter 2). At Catavina, C is 2.26 ± 0.3, indicating a moderate degree of relative hardening. The relationship between H_a and kaolinite content was shown in Figure 6. Abrasion resistance hardness values vary inversely with kaolinite contents, suggesting that kaolinite formation is related to changes in the rock's physical properties.

DISCUSSION

Although hematite occurs in exterior coatings at Catavina, its presence is not a contributor to the differential hardness between the exterior and the interior. Exteriors often have no coatings while the

friable interior walls of cavernous hollows sometimes have considerable accumulations of hematite. The presence of such accumulations on the friable interior walls has decreased their friability relative to similar interior walls not having such accumulations (i.e., they do have a minor local case-hardening effect). However, the presence of a case-hardening cement is of secondary importance compared to kaolinization and the degree of chemical weathering undergone by different areas. The friable rock interior has undergone considerably more chemical weathering and has had more kaolinite formed than the exterior. The hard exfoliation shells contain even less kaolinite. The dissolution of feldspar and quartz surfaces and the formation of kaolinite have had the most profound effects on the rock's physical properties.

Therefore, the tonalite at Catavina has actually become core-softened as a result of differential weathering rates between the rock interior and exterior. This is different from the classical examples of case hardening in which the exterior becomes harder and more resistant to weathering than the original rock prior to weathering, usually as the result of precipitation of a secondary phase at the rock surface (Anderson 1931; Conca and Rossman 1982).

WATER PERMEABILITY AND INFILTRATION INTO CORE-SOFTENED BOULDERS

Core softening depends upon the relative degree of chemical weathering between different areas of the rock which in turn depends upon the changes in moisture content of those areas. The effect that core softening has on the water content and flux within a boulder, and what this means for the continued development of the cavern, will be modelled under the simplest conditions of one-dimensional flow, where the gravitational head is much smaller than the matric suction (a

condition satisfied for infiltration over the small volume of an initially dry boulder).

Infiltration of water into a non-saturated boulder and its subsequent redistribution is described by unsaturated flow, in which Darcy's law takes the form;

$$q = - K(\psi)\ \nabla H \qquad (1)$$

where q is the flux density (i.e., the volume of water flowing through a unit cross-sectional area per unit time), ∇H is the hydraulic gradient (supplied by either a pressure head, gravitational head or matric suction head) and K is the hydraulic conductivity (or water permeability) which is a function of the matric suction, ψ. Matric suction is the negative pressure or suction generated by both capillary and water film effects (Swartzendruber 1969). The hydraulic conductivity, K, is a product of the intrinsic permeability of the material and the fluidity of the water.

The flow equation in one-dimension describing the change in volumetric water content, θ, with time, t, can be obtained by differentiating Darcy's law with respect to distance from the surface, x:

$$\frac{\partial \theta}{\partial t} = - \frac{\partial q}{\partial x}$$

For an unsaturated system where the hydraulic gradient is dominated by matric suction (as in the present case), the flow equation becomes:

$$\frac{\partial \theta}{\partial t} = \frac{\partial}{\partial x} \left[K(\psi) \frac{\partial \psi}{\partial x} \right] \qquad (2)$$

If K remains fairly constant, then equation (2) reduces to:

$$\frac{\partial \theta}{\partial t} = K \frac{\partial^2 \psi}{\partial x^2} \qquad (3)$$

Green and Ampt (1911) developed a simplified approach to the solution of equation (3). Their principal assumptions are that the wetting front is distinct and sharp, and that the matric suction at this wetting front is effectively constant. This approach gives the infiltration rate, i, and the maximum depth of infiltration, L_f, as (Hillel 1971):

$$i = \Delta\theta \left[\frac{K}{2t} \frac{\Delta H}{\Delta \theta} \right]^{1/2} \qquad (4)$$

$$L_f = \left[2tK \frac{\Delta H}{\Delta \theta} \right]^{1/2} \qquad (5)$$

where $\Delta\theta$ is the difference between the initial and final water contents of the rock ($\Delta\theta$ equals the porosity for an initially dry boulder that becomes saturated upon infiltration), and ΔH is the change in hydraulic pressure or matric suction from the point of infiltration to the wetting front.

Figure 16 is a cross section of an idealized core-softened boulder which will provide the parameters for the following model calculations, and is based upon observations from several field areas including Catavina. The boulder, 3 meters in diameter, has a single cavern 1 meter in diameter, and an exterior less-weathered zone 10 cm thick. The interior of the boulder is uniformly weathered. Material immediately behind the cavern interior wall to a depth of 1 cm is the most highly weathered material in the rock and constitutes a third zone. Included

Figure 16 Cross section through an idealized core-softened boulder undergoing infiltration by rainwater. Hydraulic conductivities, K, are shown for the different zones of the boulder, exterior (K_c), interior (K_u), cavern interior wall (K_w) and basal zone (K_b), and for the soil (K_s). Porosity values (f) are given for the same zones. Boundaries between different zones are indicated by dotted lines. Direction of water flow in the boulder is approximated by arrows.

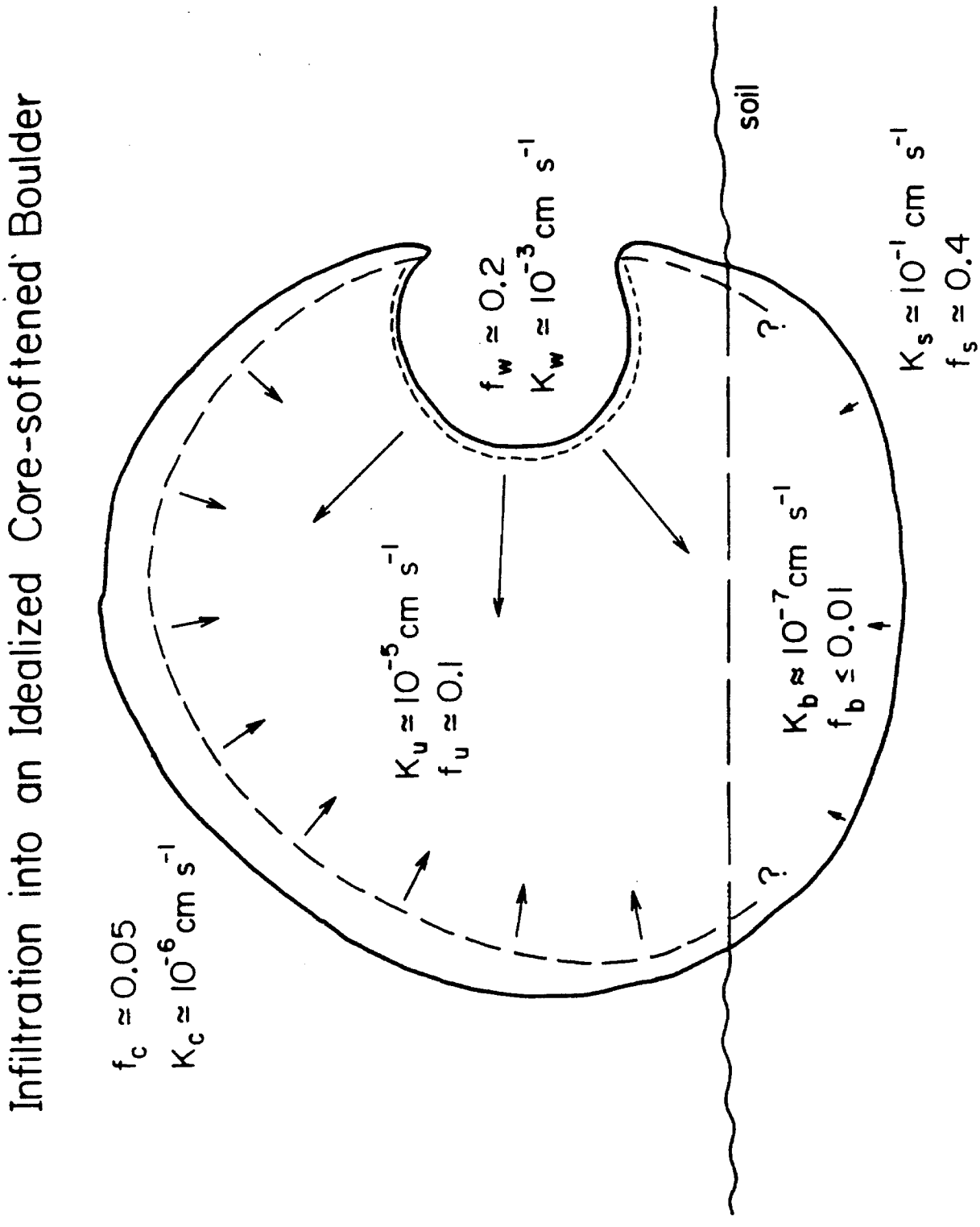
Infiltration into an Idealized Core-softened Boulder
soil
$f_c \approx 0.05$
$K_c \approx 10^{-6}$ cm s^{-1}
$K_u \approx 10^{-5}$ cm s^{-1}
$f_u \approx 0.1$
$f_w \approx 0.2$
$K_w \approx 10^{-3}$ cm s^{-1}
$K_b \approx 10^{-7}$ cm s^{-1}
$f_b \leq 0.01$
$K_s \approx 10^{-1}$ cm s^{-1}
$f_s \approx 0.4$
?
?

FIGURE 16

in this idealization is a basal zone near or at the soil horizon. Many boulders in the field exhibit a basal zone which is much less weathered than any of the above zones. The boulder is embedded in the surrounding soil to a depth of 1 meter. These conditions, while by no means universal, are approximated in many field areas.

Hydraulic conductivities of different zones for core-softened boulders were measured under saturated conditions using a permeameter designed for rock material (methods for permeameters are reviewed by Klute 1965). Hydraulic conductivities for differentially weathered rock varied considerably, from less than 10^{-9} cm/s to as high as 10^{-3} cm/s (approximately 10^{-6} darcy to over 1 darcy). In general, interior values were at least an order of magnitude above exterior values with highly weathered zones several orders of magnitude above the conductivities of the exterior. In Figure 16, the different zones of rock are assigned values of hydraulic conductivity, K, and porosity, f, based on relationships observed in the field.

In the present case of the weathering tonalite, differences in permeability between different zones of the boulder result more from changes in the number and extent of interconnecting passageways than from changes in their fundamental properties (Norton and Knapp 1977). Thus, the matric suction will remain fairly constant between different zones in the dry state, and will be assigned a value of 10^{3} cm, a reasonable estimate based on the fine nature of the pore structure (Lambe and Whitman 1969).

Infiltration of water into the boulder will be modelled for steady-state infiltration from all surfaces; i.e., water is supplied to the surface by rain at a rate greater than infiltration, as will happen for the duration of a major storm. Overall infiltration can be divided into

three parts: infiltration through the cavern interior wall, through the exterior zone and through the basal zone. Equation (5) can be used to determine the time required to saturate each zone after the onset of the storm. These saturation times are given in Table 10. It can be seen from Table 10 that infiltration from the cavern wall into the boulder interior begins almost immediately, and that the time required to saturate the entire boulder by infiltration through the cavern wall will be:

$$t = \frac{0.1\ (300\ \text{cm})^2}{2\ (10^{-5}\ \text{cm/sec})\ (10^3\ \text{cm})} = 4.5 \times 10^5\ \text{sec}$$

or just over 5 days. Compared to this, saturation of the boulder by infiltration through the exterior will take considerably longer, over 50 days.

After infiltration stops, either when the boulder is saturated or the storm ends, the rock will begin to dry out. The drying process occurs in two stages (Hillel 1971): (1) an early, constant-rate stage, during which the evaporation rate is determined by the external and surface conditions, and (2) a falling-rate stage, during which the evaporation rate from the rock is lower and is determined by the material's conductivity.

The flow equation for drying will be similar to equation (2) (Gardner and Hillel 1962). However, the solution can not be approximated by Green and Ampt's approach because the assumptions used for a discreet wetting front do not hold for this situation. Therefore, it is assumed that the evaporation rate is low enough so that all depths are losing water at the same rate per unit volume, making water loss independent of depth. For mathematical convenience, let x be the

TABLE 10

SATURATION TIMES

Time required to saturate particular zone

zone (see fig. 6)	time (sec)
cavern interior wall	.1
exterior	2.5×10^3
basal zone	5.0×10^5

Time required to saturate entire boulder by infiltration through particular zone

zone (see fig. 6)	time (sec)
cavern interior wall	4.5×10^5
exterior	4.5×10^6
basal zone	4.5×10^7

distance to the rock surface from the opposite end of the drying profile. If E is the rate of water loss per unit volume per unit time, then:

$$\frac{\partial \theta}{\partial t} = K \frac{\partial^2 \psi}{\partial x^2} = - E$$

for constant conductivity. Integrating gives:

$$- E x = K \frac{\partial \psi}{\partial x} + \text{constant}$$

the constant of integration being zero for no flow across the boundary x = 0, i.e., no water flow into the opposite side of the boulder. For a given suction gradient the total water loss will vary with the hydraulic conductivity, K. Therefore, even though no rate calculations can be made without information on the suction gradient during dessication for the boulder in Figure 16, there will be an order of magnitude more flow through the cavern interior wall than through the exterior regardless of the suction gradient.

During the initial stage, water moves outward in response to the evaporation-induced suction gradient at the surface. The rate can remain fairly constant as the increasing suction gradient due to decreased water content tends to compensate for the decreasing hydraulic conductivity (Hillel 1971). Eventually, the water content, θ, becomes so low that no more water is supplied to the surface, the suction gradient is at a maximum, and the surface becomes air-dry. The second stage begins, and is accompanied by an inward-moving drying front. Movement of water from this front to the surface occurs by vapor diffusion. After the surface is brought to dryness Gardner (1959)

determined that the evaporative flux, q_e, takes a similar form to equation (4):

$$q_e = \Delta\theta \left[\frac{D}{\pi t} \right]^{1/2}$$

where D is the diffusivity of the material. Normally D is related to the hydraulic conductivity, K, by the following (Hillel 1971):

$$D(\theta) = K(\theta) \frac{d\psi}{d\theta}$$

both being functions of the water content. For a given matric suction, ψ, and water content, θ, the evaporative flux will vary with $K^{1/2}$, indicating that during the second stage of drying the moisture flux through the cavern wall will again be greater than through the exterior.

Thus the main effect that core softening has on the moisture regime of the boulder is the change in the hydraulic conductivities of the different zones, and the resultant change in the water flux, q. The lower conductivity of the exterior will reduce the flow of the underlying material during both infiltration and dessication (the effect will be the same for a case-hardened material). Since the amount and chemical reactivity of the interstitial water will determine the amount of chemical weathering that occurs, then, for similarly reactive waters over the volume of the boulder, the material behind the cavern interior wall will show the greatest weathering effects due to the highest fluxes.

ORIGIN OF CORE SOFTENING

The above model calculations indicate that core softening is a

stable, self-reinforcing process that should continue to operate until either the boulder is totally hollow or the system is externally perturbed. Once the cavern is initiated, by whatever mechanism, it will begin to affect the flux of water, both during infiltration and dessication. During early stages of cavern development, these effects will be only local, but will increase with time as the cavern enlarges and more moisture is diverted through the cavern wall. As the cavern develops, a zone with the highest degree of weathering should precede it into the boulder.

The exact causes of core softening and cavern initiation remain problematical, but most likely result from the combined action of a variety of mechanisms, as discussed in Chapter 1. At Catavina, the development of core softening and cavernous weathering is probably a function of differences in the moisture flux and reactivity. It has been observed by the authors that the levels of the basal zones of differentially weathered rocks are related to the soil horizon (either present or past horizons) and basal zones often form the floors of the caverns. Many caverns appear to be initiated at the soil surface-rock interface. Dragovich (1969) discusses the importance of the soil surface-rock interface in terms of a more rapid weathering rate due to increased moisture content and thermal effects through temperature cycling. The water existing in the upper soil horizon will have higher chemical reactivities due to increased dissolved CO_2 and organic acids (Antweiler and Drever 1983; D. Melchior, personal communication). Also, the wetness gradient, $\partial\theta/\partial x$, across the rock-soil interface will be smaller than the gradient across the rock-atmosphere interface during drying because of the higher soil humidity relative to the atmosphere, thus lowering the water flux through the base during dessication, an

effect which will be important mainly in arid environments.

There is an important size-dependence of core softening implied by equation (5). The larger the boulder, the longer it will take for infiltration into the interior, such that a size range will be reached for a particular situation where the boulder cannot become core-softened as a whole, although locally differential effects will develop. Similarly, the smaller the boulder the less important will be differences in infiltration rates, and the rock will weather more evenly.

SUMMARY

The weathering effects on the tonalite at Catavina, Baja California can be summarized as follows: (1) kaolinite, quartz and hematite are the major weathering products formed, and calcite and gypsum have formed in trace amounts, (2) biotite has undergone loss of Fe^{2+} without major breakdown in structure and without the formation of a measureable amount of phases such as vermiculite or chlorite-saponite, but weathering has increased the water content of the biotite, (3) feldspar has weathered along cleavage surfaces and grain boundaries to supply Al and (along with minor dissolution of quartz) Si for the formation of kaolinite and secondary quartz (mixed layer illite/montmorillinite clays were not found in the weathered samples, but were found in the surrounding soils), (4) less kaolinite is present in the exterior than in the more friable interior, and the feldspars are not as highly fractured in the exterior as they are in the interior,(5) most of the hematite occurs towards the rock surfaces, and (6) the degree of relative hardening of the exterior (C) was equal to 2.26 ± 0.3, abrasion resistance hardness values (H_a) inversely correlate with kaolinite contents.

These observations indicate that tonalite boulders at Catavina are core-softened as a result of greater kaolinization of the interior.

Model calculations for one-dimensional flow within a tonalite boulder indicate that core-softening influences the flow of water by changing the hydraulic conductivities (water permeabilities) of different areas, thus increasing the flux of water through the cavern interior wall relative to the exterior.

CHAPTER 5

DIFFERENTIAL WEATHERING IN THE ANTARCTIC

The primary field areas are located in the Dry Valleys of Southern Victoria Land, especially the Labyrinth. The Labyrinth is an area of anastomosing troughs and ridges cut into the Ferrar dolerite b sill at the upper end of Wright Valley, Antarctica (Figure 17). Its origin has been vigorously debated and various hypotheses reported (Selby and Wilson, 1971). The dolerite exhibits cavernous weathering as a result of the differential weathering effect of core softening (Figure 18).

The study area includes the Labyrinth plus isolated examples from neighboring Dry Valleys for comparison. The Labyrinth is developed in the Ferrar dolerite b sill, a ~200 meter thick intrusion between the Beacon Sandstone and the Dais granite (McKelvey and Webb, 1962). Within the study area, the b sill is composed of zoned plagioclase ($An_{\sim 55}$) and three pyroxenes; augite, pigeonite and hypersthene. Accessory minerals include biotite, amphibole and opaques. Considerable amounts of quartz, amphibole and alkali feldspar occur in and near the granophyre at the top of the sill, which crops out at several localities in the Labyrinth.

The dolerite is exposed as brownish-red ridges and dull-grey troughs (Figure 17). The highly jointed dolerite is undergoing mass wasting within the Labyrinth, forming large talus piles of angular blocks (Figure 19). The brownish-red color of much of the dolerite is due to an iron-stained silica coating developed at the rock surface and to various depths (up to 2 cm). The effect of this coating on weathering is of prime importance and will be discussed below. Intermediate-sized blocks can have their exteriors broken into peculiar patterns of polyhedra (Figure 20). The dull-grey color of the

Figure 17 The Labyrinth in Upper Wright Valley. The foreground field of view is 30 km. Note the brownish-red color (dark) of the ridges in contrast to the dull-grey color (light) of the troughs. [Photograph by Ingrid Klich]

Figure 18 A boulder of the Ferrar dolerite exhibiting cavernous weathering as a result of core softening. Note the influence of joints on the morphology. Boulder is 1.5 meters across.

troughs is caused by the presence of a fine eolian polish on the rock surface developed primarily in the direction of the winter winds (Figure 21) which are several times stronger on average than the summer winds.

Salt accumulations are common in the arid, poorly drained Dry Valleys, and salt weathering effects are evident (Claridge, 1965; Johnston, 1972; Selby, 1977). Salt crystals were observed between flakes of rock inside cavernous hollows and at the soil-rock interface, and appeared effective in removing already weathered and porous materials. When possible, these salts were collected and identified. The results are given in Table 11 and will be discussed below.

It is important to realize that in the Dry Valleys liquid water can be locally abundant during the warmer parts of the austral summer (late December and January), derived from precipitated snow, which melts quickly during this period, and as meltwater from perennial ice and snow. Even though the water does not usually move any considerable distance from its source, its capacity to transport solutes can be large, and the precipitates from local water accumulations can have dramatic effects on rock weathering (Figure 22).

These features are developed to widely varying degrees at different locations in the Labyrinth (and elsewhere in the Dry Valleys) with weathering effects being more dramatic closer to Upper Wright Glacier.

Hardness data on rocks from the Labyrinth and other Dry Valleys are shown in Table 12. The one sigma errors given are due primarily to spatial variations in hardness between different sampling points on the surface, separated by only centimenters. These variations, attributed to weathering, can be large. Machine error accounts for only ±5%.

C is greater than 1 for all samples indicating case hardening or

Figure 19 A talus pile of angular dolerite blocks formed by mass wasting of the jointed ridge. The two people in bottom right-hand corner give scale.

Figure 20 A dolerite block in the Labyrinth exhibiting expansion polyhedra in its outer surface. Block is 1 meter across.

Figure 21 A dolerite block in a Labyrinth trough. (Top) The west face of the block has been severely eroded and fluted by the austral winter winds, and has developed the dull-grey color characteristic of the eolian polish. (Bottom) The east face, however, facing away from the winter winds, retains its brown-coated polyhedral surface. The surrounding rocks in the area mimic these effects.

TABLE 12 ABRASION RESISTANCE HARDNESS VALUES OF ANTARCTIC SAMPLES

Outcrop No.	Locality	Description		H_a (10^5 N sec/m)	
1	Labyrinth	unweathered dolerite from sill b		64.5 ± 9.7	
2	Labyrinth	extremely weathered dolerite from sill b		5.9 ± 0.3	
3	Labyrinth	core-softened dolerite boulder from sill b exhibiting cavernous weathering and having expansion polyhedra	exterior	43.8 ± 8.3	C = 3.7
			interior	11.9 ± 2.1	
4	Labyrinth	core-softened dolerite boulder from sill b exhibiting cavernous weathering and having expansion polyhedra	exterior	22.7 ± 2.1	C = 1.4
			interior	16.2 ± 4.3	
5	Labyrinth	core-softened dolerite outcrop from sill b having expansion polyhedra but little cavernous weathering	exterior	28.4 ± 4.9	C = 1.5
			interior	19.2 ± 3.1	
6	Victoria Valley	core-softened dolerite outcrop from sill a exhibiting cavernous weathering but no expansion polyhedra	exterior	28.0 ± 2.4	C = 3.5
			interior	7.9 ± 0.5	
7	Farnell Valley	case-hardened boulder of Beacon sandstone exhibiting slight cavernous weathering	exterior	7.3 ± 0.5	C = 2.5
			interior	2.9 ± 0.8	
8	Farnell Valley	unweathered boulder of Beacon sandstone		6.0 ± 0.3	
9	Taylor Valley	core-softened boulder of Vida granite exhibiting extensive cavernous weathering	exterior	45.6 ± 3.1	C = 2.0
			interior	23.0 ± 3.5	

core softening. Comparing the values of H_a for the exteriors and interiors to that of the relatively unweathered material indicates that core softening is the differential weathering effect developed in the crystalline rocks (dolerite and granite) whereas case hardening is the effect observed in the sandstones. This is consistent with the author's general observation, from field areas in the southwestern United States and Mexico, that crystalline materials core-soften while clastic materials (including tuff) case-harden.

With the existing data it is difficult to relate the values of H_a and C to the presence of cavernous weathering or expansion polyhedra. All differentially weathered dolerite samples exhibited the brown coating, but outcrop numbers 3 - 6 (Table 12) are examples where either cavernous weathering or polyhedra, or both, were not present, and numerous occurrences of each were observed in the field.

WEATHERING PRODUCTS

The dolerite in the Labyrinth undergoes a modest amount of chemical weathering, especially towards the Upper Wright Glacier. This can be seen in the form of the often-cited surface stain, the dissolution of feldspars and pyroxenes, the hydration of biotite, and the formation of the weathering products secondary quartz, kaolinite and vermiculite. The weathering products are poorly crystalline, giving weak, ill-defined X-ray patterns and broad infrared absorption bands. As would be expected, these products are similar to those found in Antarctic soils (Claridge, 1965) with the exception of kaolinite, which can form in the more completely leached environments characteristic of many rocks sitting above poorly leached soils.

The weathering is heterogeneous, and only occasionally are blocks

Figure 22 Precipitation of the iron-stained silica coating from local runoff on a dolerite cliff face undergoing mass wasting. The surface shown was dry at the time the photograph was taken. Field of view is 2 meters.

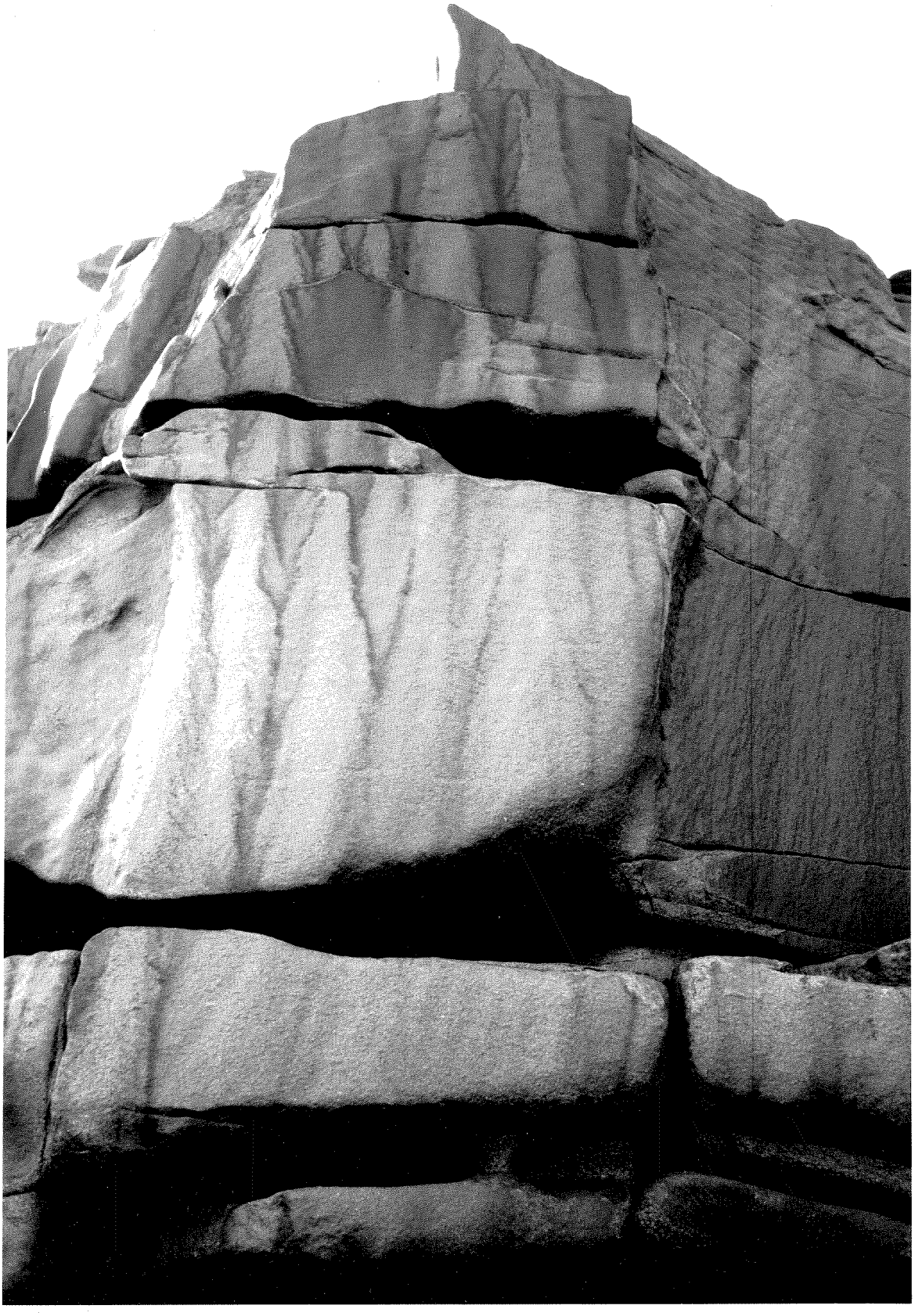

weathered enough to be disaggregated by hand. Weathering is greatest at the soil-rock interface and in the interior of the blocks. The polyhedra show, relatively, the least weathering effects even when the entire block is highly weathered and the polyhedra themselves contain the above-mentioned weathering products. Usually before this point is reached the polyhedra spall off and weather at a slower rate separately from the rest of the block.

The brown coating which covers so much of the exposed dolerite is an iron-stained, silica coating anywhere from several to hundreds of microns thick. This coating may also act as an induration agent to depths of a few centimeters. Field relations indicate that it is precipitated from solutions on exposed rock surfaces (Figure 22) and along internal joint planes. Viewed under the scanning electron microscope, the coating is very smooth (Figure 23), and it is difficult, given its thinness and the cryptocrystalline nature of the minerals, to determine the degree of crystallinity of the SiO_2 or the phase of the iron oxide/hydroxide. Much thicker coatings developed on the Beacon Sandstone are quartz in optical continuity with primary grains, suggesting that similar coatings also contain crystalline quartz. The presence of a silica coating reduces both the permeability of the rock and the chemical reactivity of the surface.

All coated and polished surfaces are quite smooth, as opposed to uncoated and unpolished surfaces (Figure 26), and appear similar under low magnification (Figures 23A, 24A and 25A). But at higher magnifications they are all distinct. The brown coating on the dolerite is thin and smooth on the scale of microns (Figure 23C), while the eolian polish is rough (Figure 25). The difference between the brown coating and the eolian polish is that the eolian polish is mechanical in

Figure 23 Electronmicrographs of the smooth surface of a brown-coated dolerite block. (Magnification increases from A to D as shown in the scale bars for Figures 23 - 26). Surface appears smooth through magnification range and EDS spectra indicate increased silicon at surface to several microns depth.

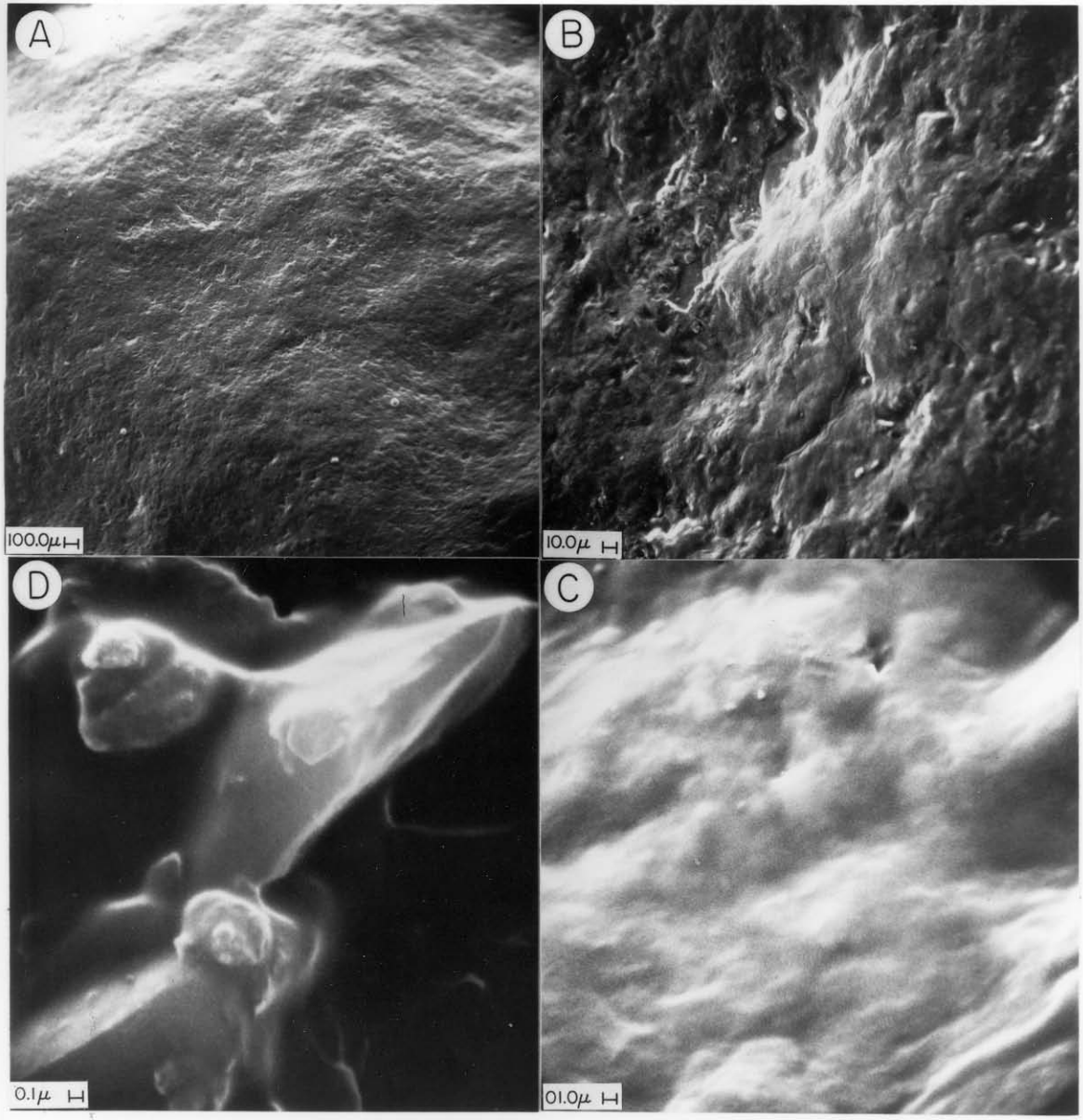
A
100.0μ H
B
10.0μ H
D
0.1μ H
C
01.0μ H

Figure 24 Electronmicrographs of the surface of case-hardened Beacon Sandstone. Surface is smooth at low magnifications but is rough on the scale of tens of microns (C and D) and is made of interlocking sheaves of quartz.

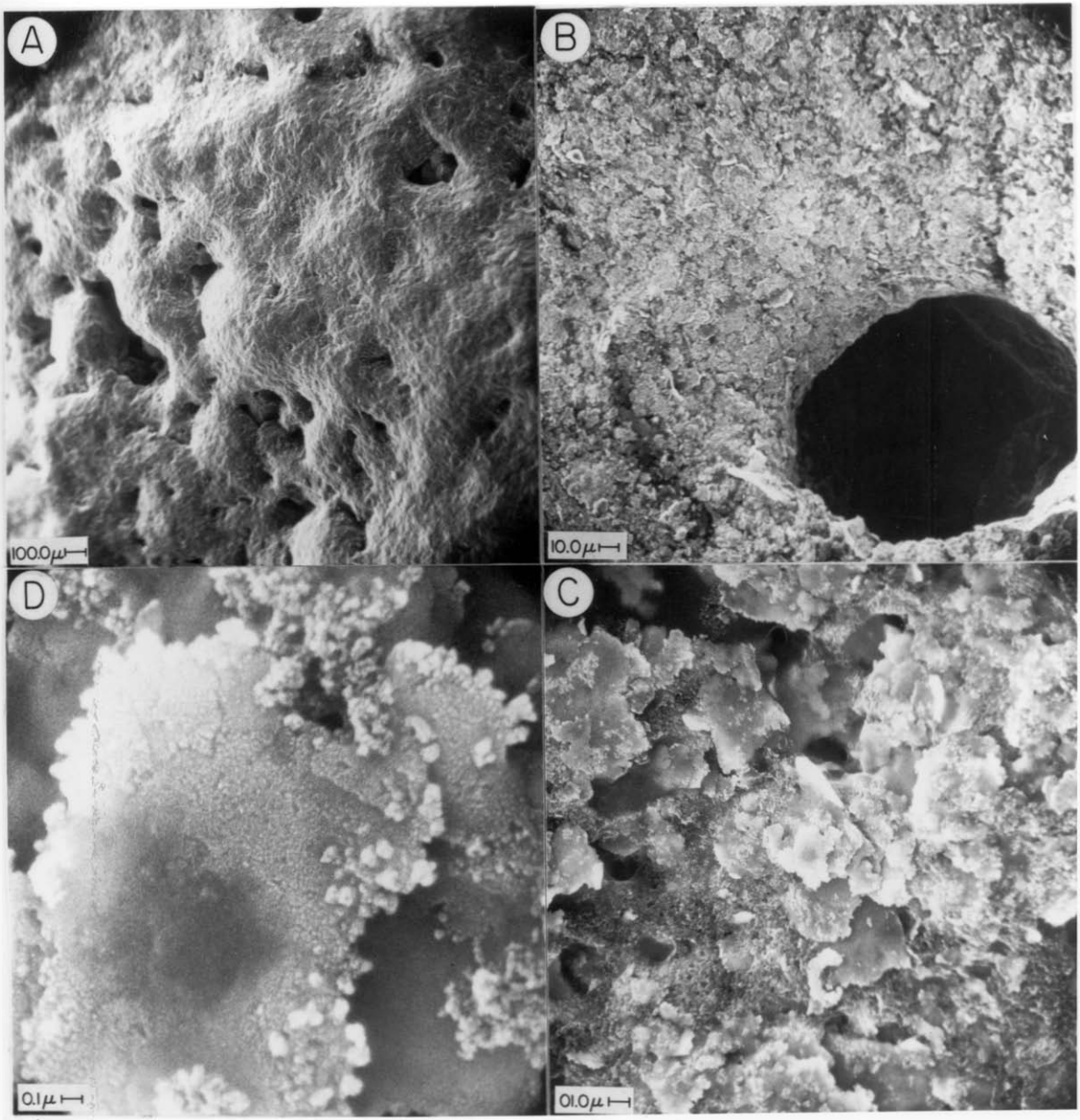
A
100.0μ
B
10.0μ
D
0.1μ
C
01.0μ

Figure 25 Electronmicrographs of a dolerite surface having the eolian polish. While appearing smooth at low magnification (A), at higher magnification the surface is seen to be a mosaic of broken primary grain surfaces and impacted fragments of plagioclase and pyroxene.

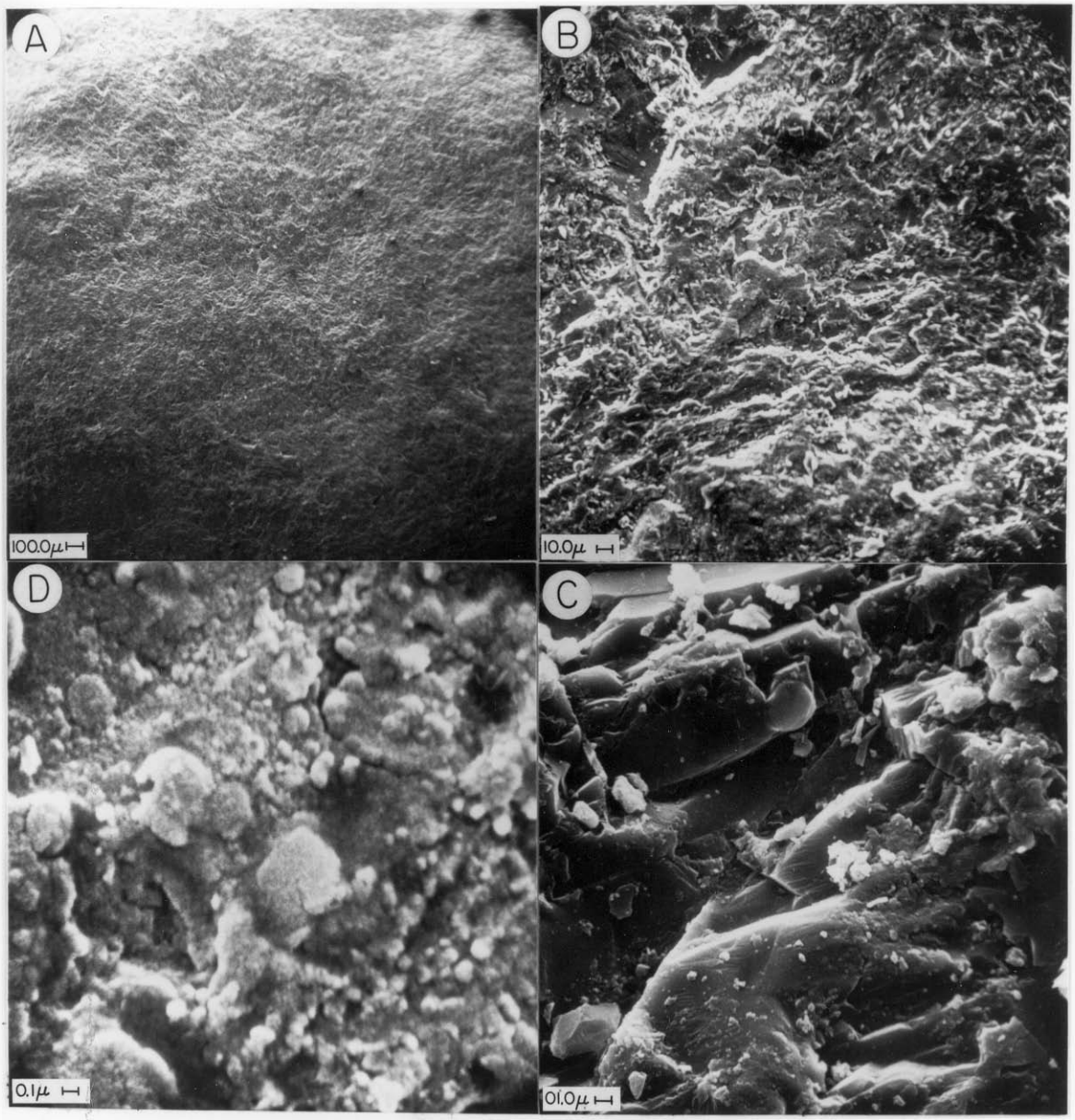
A
100.0μ
B
10.0μ
D
0.1μ
C
10.0μ

Figure 26 Electronmicrographs of an uncoated and unpolished dolerite surface, which is rough on all scales and shows fresh striations and cleavage surfaces on the primary mineral grains.

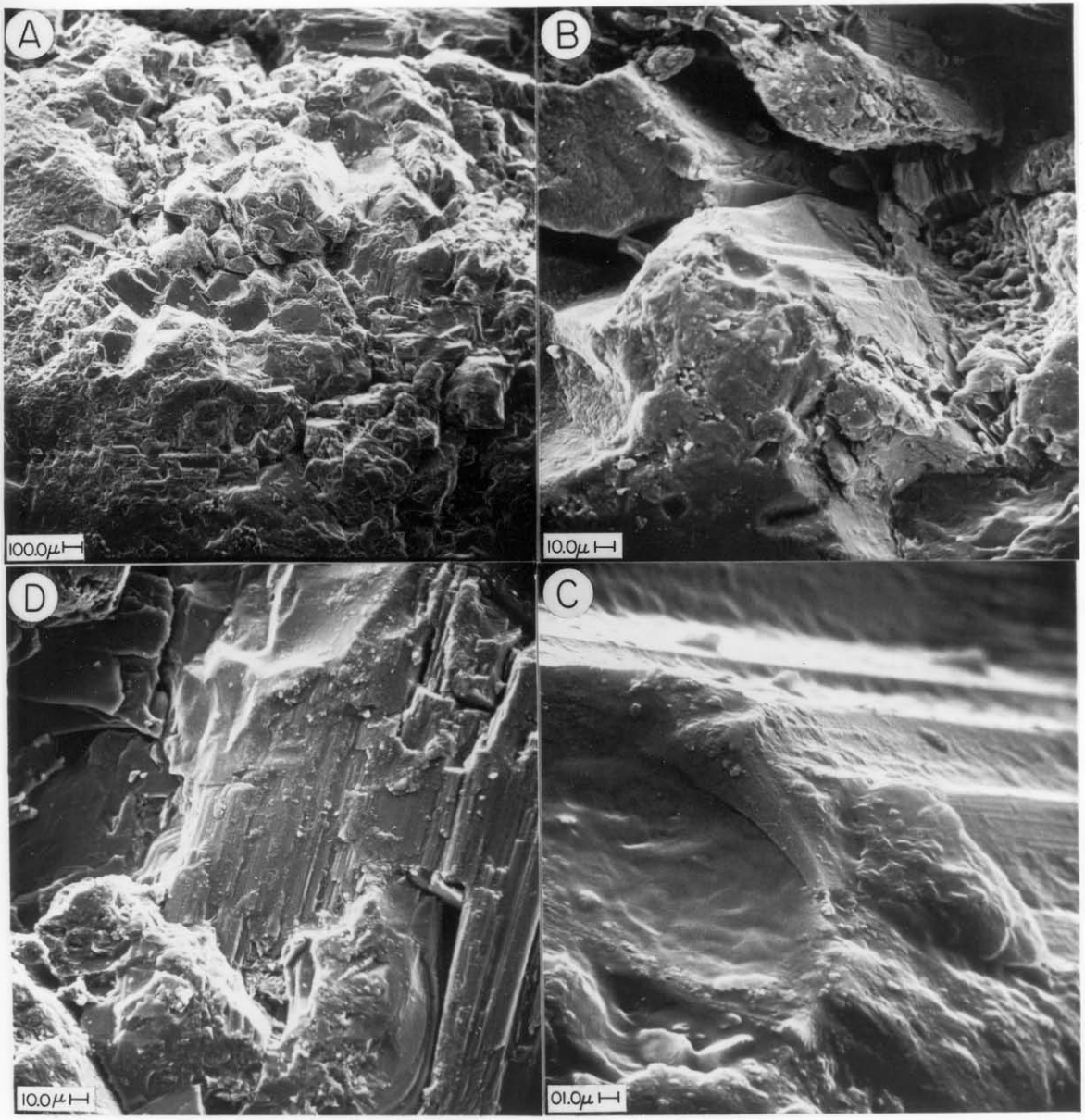
A
100.0μ
B
10.0μ
D
10.0μ
C
01.0μ

nature, formed by repeated impact of wind-driven particles and is simply a mosaic of fine-grained fragments of felspar and pyroxene which decreases the surface roughness as well as its porosity and permeability.

Surprisingly, the silica coating on the sandstone is also rough on the scale of microns, being made of interlocking sheaves of quartz which grow by precipitation and coalescence of fine-grained particles on their surfaces and along their edges (Figure 24D). This difference in morphology between the dolerite and sandstone coatings may reflect their different substrates; i.e., for the sandstone, quartz is precipitating on pre-existing quartz surfaces with high initial porosity, whereas for the dolerite, quartz is precipitating on surfaces of plagioclase and pyroxene with negligible porosity. Both the kinetic effect of nucleation and the longer moisture residence times for a porous material should favor precipitation of larger crystals of quartz on the sandstone while only cryptocrystalline quartz or amorphous silica on the dolerite.

BIOLOGICAL EFFECTS

Studies by Friedmann (1982) have shown the presence of endolithic micro-organisms living below rock surfaces in the Dry Valleys, and during the present study many such colonies were observed. According to Friedmann, a narrow subsurface zone in the rock has a favorable microclimate for a population dominated by cryptoendolithic lichens and cyanobacteria. Friedmann found that the lichens' biological activity results in local mobilization of iron compounds and causes rock weathering with a characteristic pattern of exfoliation. Friedmann's studies centered around the Beacon sandstone, but chasmoendolithic colonies were found inhabiting the cracks and fissures of granites,

granodiorites and dolerites. However, the igneous rocks do not show the exfoliation patterns owing to the endoliths that characterize the sandstones.

Since the cavernous weathering in the Dry Valleys is found more often on the igneous and metamorphic rocks, and since the morphology and distribution of the cavernous hollows in them differs considerably from those produced by the endolithic microorganisms of the type described by Friedmann, the role of such organisms in overall cavernous weathering is restricted to specific sites on the sandstones in the Dry Valleys and was not included in this study.

SALTS AND SALT WEATHERING

A large variety of soluble salts have been found in the Antarctic Dry Valleys in soils, on rock surfaces and in saline lakes and ponds. It is possible in some cases to correlate the salt composition with environmental and transport conditions, proximity to seawater, rock type, etc., but for salt accumulations occurring on rock surfaces uncertainties arise because of long exposure ages for outcrops and the non-uniform nature of the weathering and transport processes. Thus, Table 11 illustrates that the composition of these salts cannot be related to rock type, environment or proximity to seawater alone. The salts are determined by which ions dominate the saturated solution at the time of precipitation, the phase being determined by the ambient conditions of P, T and X_{H_2O}. In the Dry Valleys where complete leaching is rare, aqueous transport short-ranged, and residence times for soluble salts long, it is often impossible to define the source of the ions which make up the salts involved in differential weathering.

Explanations for the origin of the salts in the Dry Valleys center

TABLE 11 SALTS IN THE DRY VALLEYS

Locality	Rock Type and Morphology	Position of Salt on Rock	Salt	Elevation	Distance from Ocean
Labyrinth	dolerite sill b CW and CS cliff face	between actively spalling flakes on interior wall individual crystals	$NaNO_3$ (soda niter)	1100 m	70 km
Lower Wright Valley	dolerite sill a small cobble slight CW, no CS	underside of rock at soil-rock interface massive	$Ca(SO_4) \cdot {}^1/_2 H_2O$ (bassanite)	200 m	40 km
Victoria Valley	dolerite sill a large boulder CW and CS	between actively spalling flakes on interior wall individual crystals	NaCl (halite)	500 m	40 km
Granite Knolls	Irizar Granite large boulder CW and CS	on interior wall massive	$CaCO_3$ (calcite)	1000 m	25 km
Bull Pass	granophyre of dolerite sill a large boulder CW and CS	on interior wall massive	$Ca(SO_4) \cdot 2H_2O$ (gypsum)	800 m	45 km
Bull Pass	Vida Granite CW and CS large boulder	on interior wall individual crystals	NaCl (halite)	800 m	45 km
Bull Pass	rhyolite dike small cobble slight CW, no CS	underside of rock at soil-rock interface massive	NaCl (halite)	1000 m	45 km
Farnell Valley	Beacon Sandstone small boulder CH but little CW	crust on side of rock massive	$Ca(SO_4) \cdot 2H_2O$ (gypsum)	1800 m	90 km

CW ≡ rock is cavernously weathered CS ≡ rock is core-softened CH ≡ rock is case-hardened

on marine sources, chemical weathering, volcanic aerosols, leaching of sedimentary, metasedimentary and volcanic rocks, and atmospheric precipitation (Gibson, 1962; Claridge and Campbell, 1977, Linkletter, 1970). Many hypotheses are based on evidence from specific localities and can not be generalized to include the entire Dry Valley system. The great spatial heterogeneity of weathering and transport processes in this region suggests that all of the above origins are responsible to some degree for the salts present in any one situation, and that each case must be investigated separately. An example of this concerns the problem of the source of nitrates. Claridge and Campbell (1968) discuss the accumulation of nitrate deposits in Antarctica by precipitation from the atmosphere. However, their study environment is quite different from the interior cavern walls of the Labyrinth where $NaNO_3$ is found between actively spalling rock flakes. As mentioned above, throughout the Labyrinth endolithic microorganisms as well as surface lichens were found in local abundance. Unexposed joint surfaces in the dolerite are an especially favorable niche for chasmoendolithic colonies described by Friedmann (1982). Many colonies were found living near a cavern which yielded $NaNO_3$ as the dominant salt (Table 11). Such metabolic products are a likely source of nitrate. Aqueous transport through the joint system is the likely mechanism for transport to the immediate area of the cavern (see transport model below).

Salts will precipitate where there is a tendency for solutions to become oversaturated. In the Dry Valleys, this occurs most often at an interface, e.g., water-atmosphere, soil-atmosphere, rock atmosphere and rock-soil interfaces. The solution oversaturates mainly as a result of evaporation across the interface. The salt will accumulate where there is net deposition, i.e., little subsequent erosion or redissolution,

such as the interior walls of cavernous hollows, soil-rock interfaces, poorly leached soils and the bottoms of saline ponds.

In a differentially weathered rock exhibiting case hardening or core softening it has been shown (Chapter 4) that the differences in permeability between the rock interior and exterior result in the greatest water flux being through the cavern interior wall. If the solutions have significant dissolved salts then the interior walls will have the greatest salt accumu-lations on the rock, a situation which is observed in the field (Figure 27).

It is possible for these salts to be involved in salt weathering, but only if conditions are favorable. These conditions include sufficiently high porosities (Goudie, 1974; Evans, 1970), oversaturation of the solution and favorable surface tension associations; i.e., the phase boundary surface tension between the salt and the rock must be greater than the sum of the phase boundary surface tensions between the salt and solution and between the rock and solution (Evans, 1970). Weyl (1959) determined that if the solution is kept supersaturated with respect to the crystallizing salt, then precipitation in the area of contact will take place as long as the supersaturation divided by the stress coefficient of solubility is greater than the average effective normal stress between the grains. These conditions will vary with the properties of the rock, the salt, the solution and the environment.

In general, it has been found that if there exists sufficient porosity the effectiveness of the various salts in disaggregating solid material is ranked as follows (Goudie, 1974; Evans, 1970; Cooke, 1979):

sulfates > carbonates, nitrates > chlorides.

Figure 27 Calcite accumulations on the interior wall of a differentially weathered granite boulder from Granite Knolls. Boulder is 1.5 meters across.

Salts of all four anion groups occur on the interior walls of cavernous hollows in the Antarctic (Table 11) and are probably actively removing material by salt weathering. The solutions are kept oversaturated by rapid evaporation in the arid environment of the Dry Valleys, and the condition of sufficient porosity is achieved by chemical weathering of the crystalline rocks and by the initial porosity of the sandstone.

WEATHERING PROCESSES

It is possible to hypothesize which weathering processes dominate in the Dry Valleys by observing how the Beacon sandstone and the Ferrar dolerite are affected differently by different processes. The dolerite is extremely susceptible to dissolution, hydration and chemical alteration, processes which are effective for mineral phases far out of equilibrium with the weathering environment. But the dolerite's initially low porosity and permeability (<0.1% and $<10^{-5}$ darcy, respectively) make it resistant to salt weathering, at least until chemical weathering has increased these properties to high enough values for salt weathering to become effective. This can be seen in the field, where salt weathering is observed to act only on dolerite material that already has significant weathering products such as vermiculite and kaolinite, and with permeabilities on the order of 10^{-3} darcy.

On the other hand, the Beacon sandstone with its high initial porosity and permeability (as much as 10% and 10^{-2} darcy) is extremely susceptible to salt weathering as opposed to chemical weathering. These observations agree with Goudie's (1974) experimental results in which he found that rock disintegration by salt weathering was effective only on rocks with initial porosities above about 1% and was a direct function

of the porosity. The diorite, granite and dolerite in his study were basically unaffected while the sandstones were greatly affected. Goudie also found that freeze-thaw, insolation, thermal expansion of salts and wetting-drying caused no mechanical breakdown of the rocks regardless of initial porosity, although freeze-thaw of salt solutions was effective for rocks with high initial porosities.

It can also be seen in the Dry Valleys that salt weathering of the Beacon sandstone is much more rapid than the chemical weathering of the dolerite. In the Beacon and its neighboring valleys the rock types exposed are slightly dominated by the Beacon sandstone over the dolerite. However, the overwhelmingly dominant rock type in the talus, debris of the valley floors, active rock glaciers and solifluction lobes is the dolerite, in remarkably unweathered condition. Indeed, the sandstone disappears entirely beyond about 15 meters from its source (Figure 28). The sandstone is quickly disaggregated by salt weathering. Scattered case-hardened sandstone cobbles do occur farther from their source owing to the decreased permeability and porosity afforded by the silica induration, but even these disappear before long.

During the downslope movement of the debris the dolerite blocks and cobbles can remain oriented along joint planes such that one surface remains up for most of its exposure history. Etch pits form and become enlarged as they trap the small amount of precipitation (Figure 29). The interiors of these pits do not have the brown coating which covers the rest of the rock's surface, and they contain clay minerals.

The lack of extensive cavernous weathering in the Beacon sandstone which shows well-developed case hardening is probably a result of the effectiveness of the salt weathering in this rock type in the Dry Valleys. Cavernous weathering requires not only differential weathering

Figure 28 Source rock, talus and debris flows in Farnell Valley, illustrating the lack of Beacon sandstone float and debris moving away from the source, and the dominance of Ferrar dolerite in the valley floor debris.

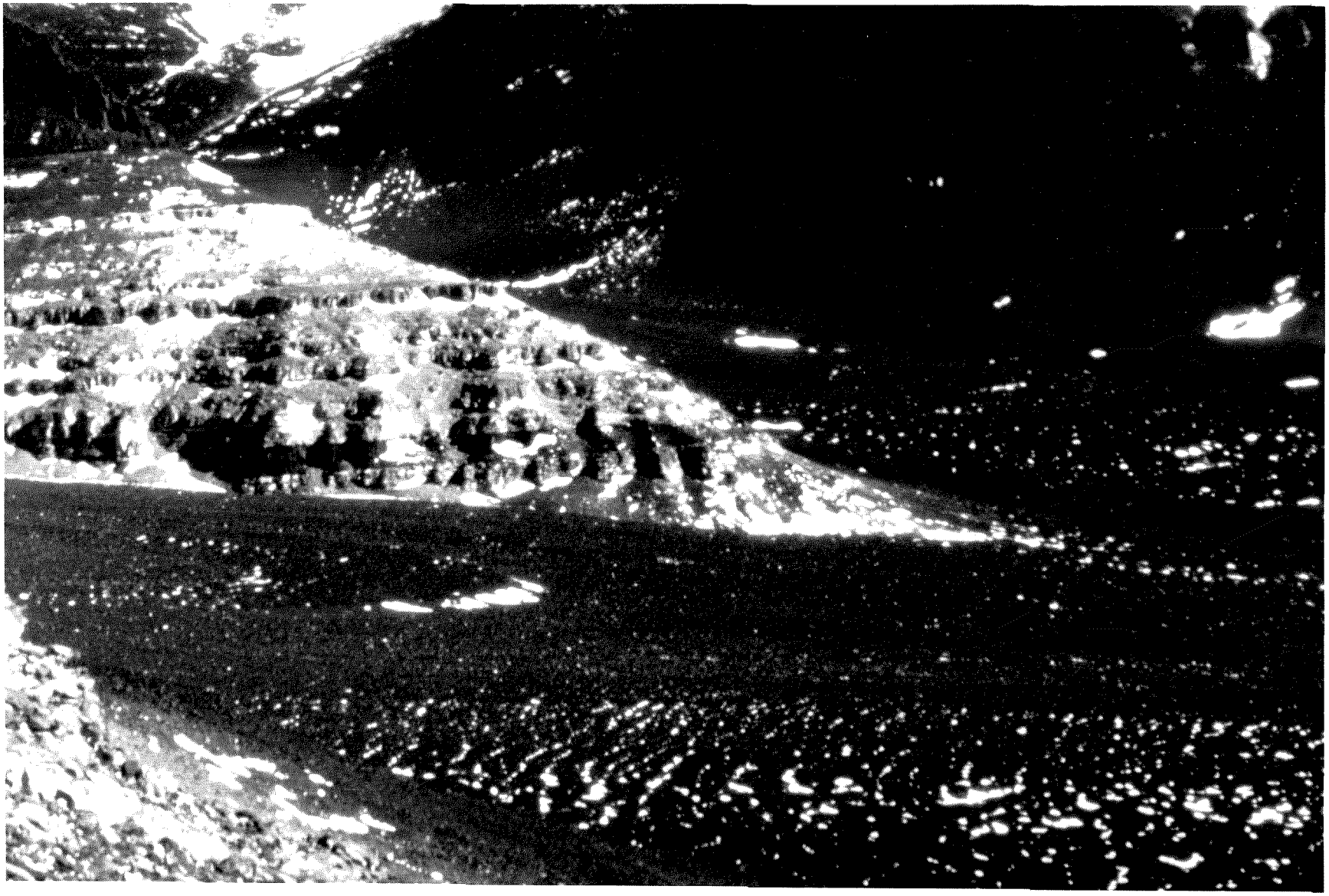

Figure 29 Etch pits commonly found in Ferrar dolerite float from a Beacon Valley talus slope.

effects but enough time to allow existing weathering processes to manifest that difference as a cavernous hollow. The Beacon sandstone is weathering too rapidly to allow cavernous hollows to develop to any appreciable degree. What weathering hollows do exist are usually small and irregular.

EFFECT OF MECHANISMS ON PORE WATER FLOW

The main reason that differential weathering mechanisms such as the precipitation of the brown coating result in core softening is that they change the moisture regime of the rock. Regimes of individual blocks will vary widely with physical properties and environment. Infiltration into a block can occur from melting of snow and ice, surface runoff or uptake of surrounding and underlying soil water. The spatial variations in permeability and porosity that accompany the presence of a differential weathering effect such as core softening in the dolerite will produce a heterogeneous uptake and flow pattern within the block. Because of its low permeability, flow through the brown coated exterior is usually negligible compared to flow through the underlying material and uncoated surfaces, reducing, for instance, infiltration of precipitation and runoff through that surface. At the same time flow paths of soil moisture infiltrating upwards by capillarity into a block will be deflected around areas underlying the coated surface (or any area of lesser permeability). Because of the complex nature of the moisture regime of most blocks in the field, we can choose situations observed in the field that are simple enough to model and which will illustrate principles applicable to the more complex systems.

Many such situations occur in the Labyrinth and surrounding valleys, involving core-softened dolerite that have their top surfaces

covered with the brown coating, and one block was chosen for the present model. The blocks are submerged in a coarse soil to below the annual melt zone (just above the top of frozen ground) where the soil is saturated with liquid water during much of the austral summer. During the period of the field study, there was constant flow from the water zone through the rock interior to the uncoated surfaces, the rock being saturated and the flow rate determined by the evaporative flux, E. This situation is more common in lower Wright and Victoria Valleys and in Bull Pass, but does occur in the surrounding Dry Valleys. This system was chosen because it can be described by saturated flow, in which Darcy's law takes the form:

$$q = - K \nabla H$$

where q is the flux density (i.e., the volume of water flowing through a unit cross-sectional area per unit time), ∇H is the hydraulic gradient (supplied by either a pressure head, gravitational head or matric suction head), and K is the hydraulic conductivity (or water permeability), which is constant in the present case. Matric suction, ψ, is the negative pressure or suction generated by both capillary and water film effects (Swartzendruber, 1969). The hydraulic conductivity, K, is a product of the intrinsic permeability of the material and the fluidity of the water.

The flow equation describing the change in volumetric water content, θ, with time, t, can be obtained by differentiating Darcy's law with respect to distance, z:

$$\frac{\partial \theta}{\partial t} = - \frac{\partial q}{\partial z} = \frac{\partial}{\partial z} \left[K \frac{\partial H}{\partial z} \right]$$

The hydraulic head is a combination of a gravitational head (an elevation above some reference datum, z) and a matric suction head, $\partial\psi/\partial z$, such that:

$$\frac{\partial\theta}{\partial t} = \frac{\partial}{\partial z}\left[K \left(\frac{\partial\psi}{\partial z} + \nabla z \right)\right] = 0$$

where $\partial\theta/\partial t = 0$ for saturated flow in an incompressible medium such as rock. Because $\nabla z = 1$ for verticle flow and 0 for horizontal flow, and K is constant for constant θ, the above equation reduces to the Laplace equation:

$$\nabla^2\psi = 0 \qquad (1)$$

and can be solved in two dimensions. The boundary conditions for the system are given in Figure 30. The distance to the saturated soil horizon is denoted by h, which is not necessarily the hieght of the block. Simplifying assumptions are that the block is initially rectangular and the interior is homogeneous and isotropic with a measured hydraulic conductivity of 10^{-5} cm/s. Flow through the top of the block is zero due to the brown coating, and there is comparatively little evaporative loss to the coarse dry soil because its humidity is so much higher than atmospheric. Moisture loss is primarily through the exposed, uncoated vertical sides and is determined by atmospheric conditions. Total flux into the block is distributed evenly over the bottom surface and will be equal to the total evaporative flux from the exposed sides. The flow will be diverted towards the exposed sides as a result of changes in the matric suction owing to the presence of the

Figure 30 The boundary conditions for the dolerite-block saturated flow model. Heavy, black line denotes silica-coated surface.

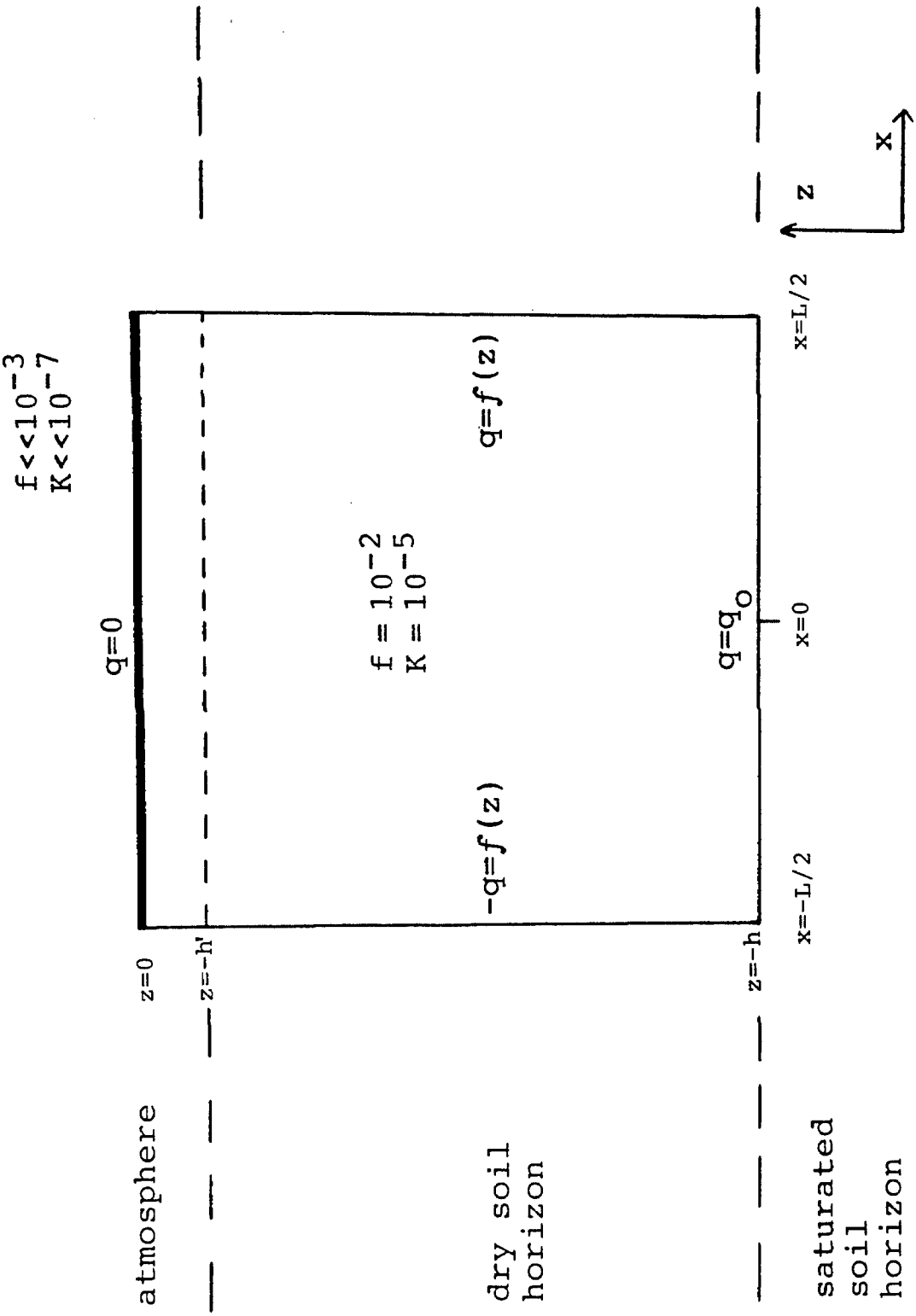
atmosphere
dry soil horizon
saturated soil horizon
z=0
z=-h'
z=-h
x=-L/2
x=0
x=L/2
q=0
q=f(z)
-q=f(z)
q=q_o
f = 10^-2
K = 10^-5
f<<10^-3
K<<10^-7
z
x
q=-Kvψ where ∇²ψ=0

FIGURE 30

coating. Solving equation (1) gives the matric suction and thus the flow rate as a function of position in the block (Figure 31 and Appendix 2).

The general form of the solution is:

$$\psi(x,z) = (z^2 - x^2)\frac{q_o}{2Kh} - \sum_{n=1}^{\infty} \frac{q_o hL \sin\left(\frac{n\pi h'}{h}\right)}{n^2\pi^2 h' K \sinh\left(\frac{n\pi L}{2h}\right)} \cosh\left(\frac{n\pi x}{h}\right) \cos\left(\frac{n\pi z}{h}\right)$$

where K is the hydraulic conductivity, E is the evaporative flux, q_o is the flux through the bottom, L is the length of the block, h is the height and h' is the height of the exposed rock (Figure 30). For the present case, L = 100 cm, h = 100 cm, h' = 10 cm, E = 5×10^{-4} g cm^{-2} sec^{-1}, $q_o = 10^{-4}$ g cm^{-2} sec^{-1} and K = 10^{-5} cm sec^{-1}. Figure 31A shows $\psi(x,z)$ as a function of position in the block. It can be seen that flow through the block is heterogeneous; i.e., some areas experience greater flow than others. The shape of the matric suction contours shown in Figure 31B is similar to the morphology developed in these rocks after long exposure to this situation, and occurs in granitic erratics as well as in the dolerite blocks. Overhanging roofs of cavernous hollows developed in these rocks are often straight as expected from the z=o surface of Figure 31B.

Most weathering situations will not be as amenable to solution as the one described above for a variety of reasons: 1) the hydraulic conductivity, K, may also be a function of x and z, 2) the system will usually be described by non-steady state, unsaturated flow, 3) the coating may have significant (but still low) permeability relative to the interior, and 4) there may be more than one moisture source. These

Figure 31 (A) The matric suction, ψ, subject to the boundary conditions of Figure 30, is plotted as a function of position within a dolerite block, and graphed as a surface in the Y-direction. (B) The contour lines for $\psi(x,z)$ projected onto the dolerite block. (C) View of $\psi(x,z)$ along the x-axis illustrating the change in flow, i.e., $\nabla\psi$, nearing the silica coated surface (z=o). Flow direction is perpendicular to the matric suction contours.

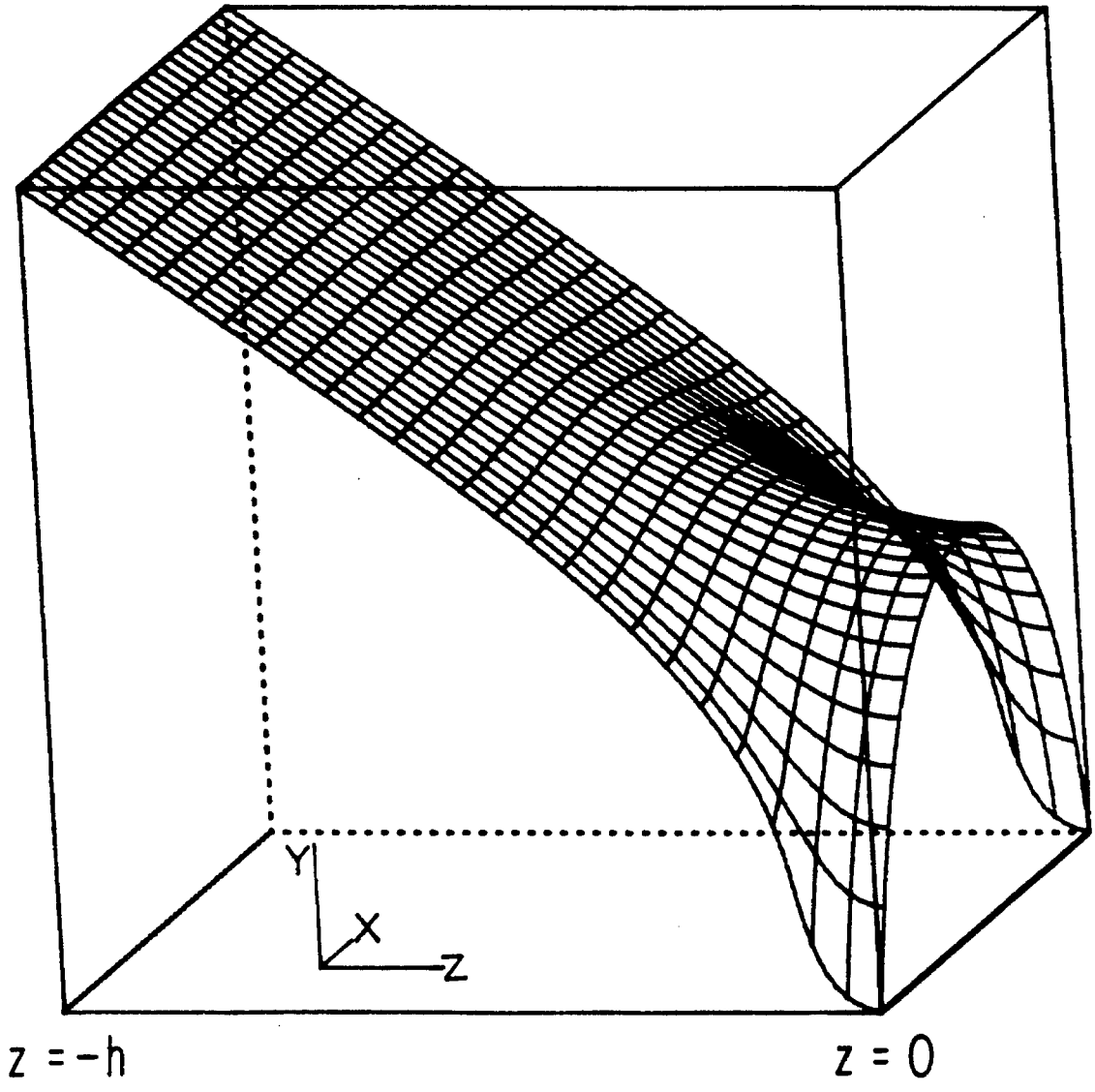

$\psi(x,z)$ for $q = -K\nabla\psi$ where $\nabla^2\psi = 0$

FIGURE 31A

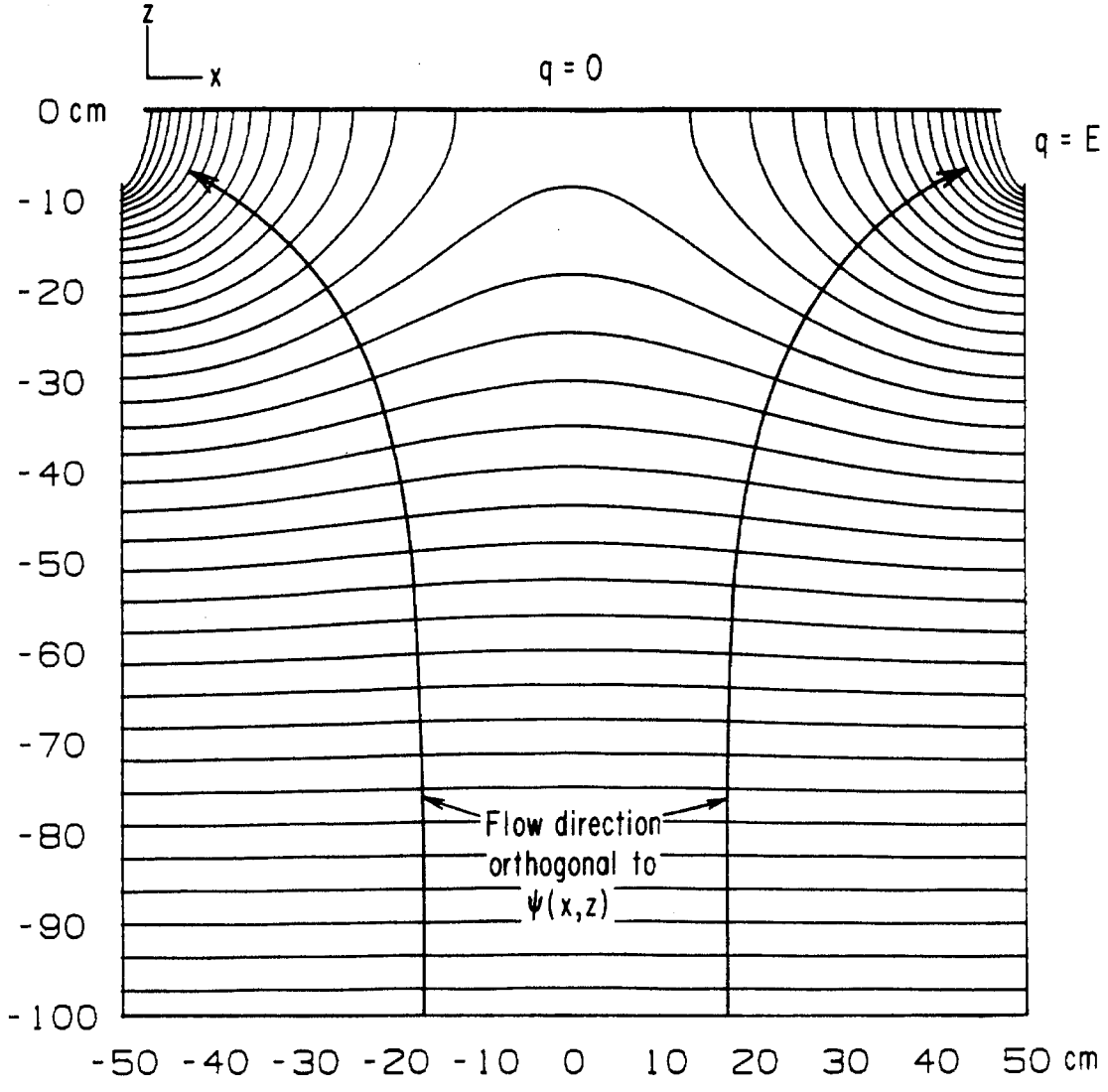
z
x
q = 0
q = E
0 cm
-10
-20
-30
-40
-50
-60
-70
-80
-90
-100
Flow direction
orthogonal to
ψ(x,z)
-50 -40 -30 -20 -10 0 10 20 30 40 50 cm

FIGURE 31B

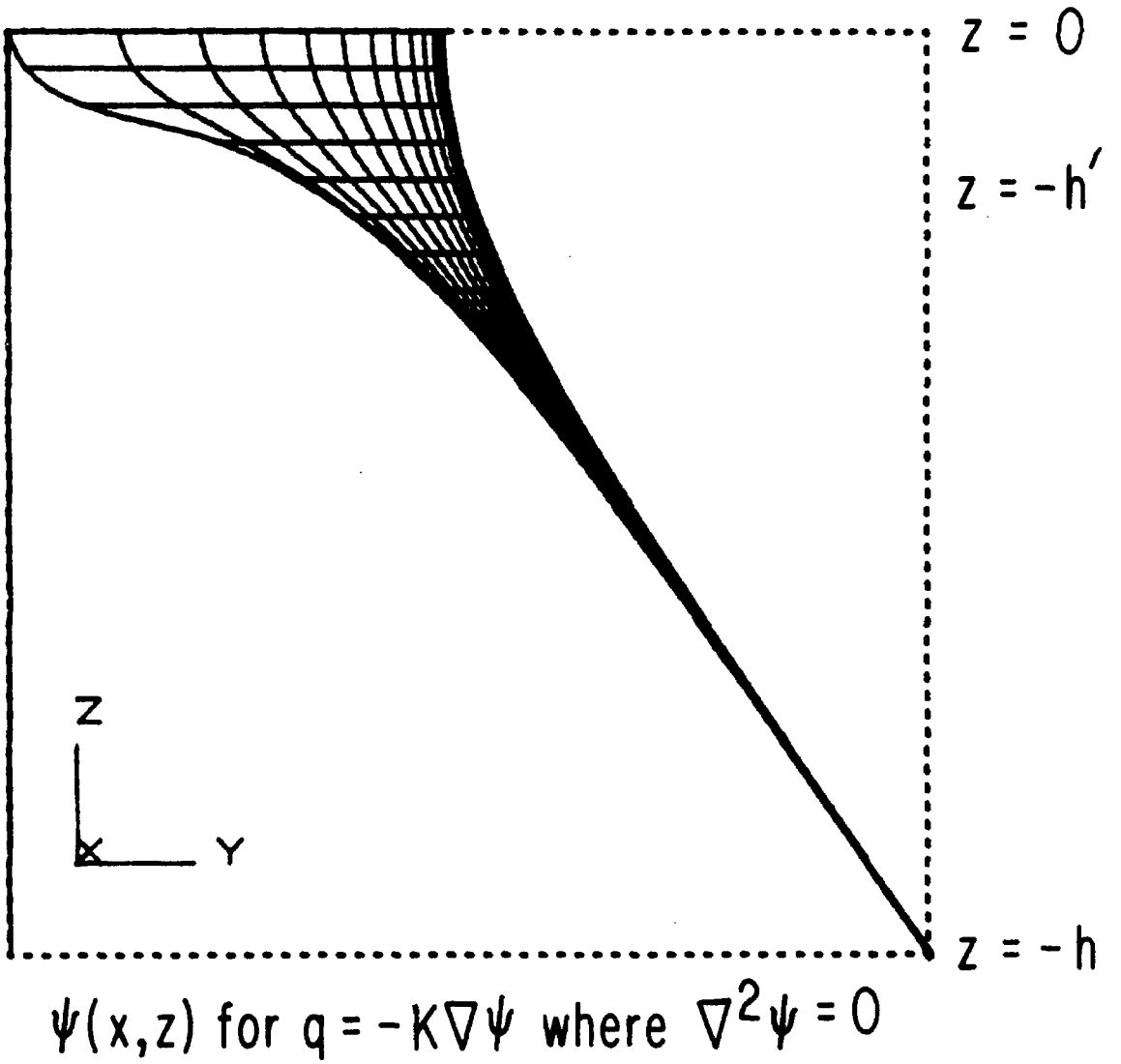

FIGURE 31C

variations will make the solutions more complex, but they will be qualitatively the same; i.e., spatial differences in the permeability resulting from differential weathering mechanisms will cause spatial differences in the moisture regime of the rock and may induce core softening.

To illustrate how these flow heterogeneities can be important in differential weathering, consider a parcel of water with a fixed composition in contact, but not equilibrium, with rock of fixed composition. Reactions will take place between the solution and the rock so as to bring about equilibrium. This equilibrium composition for the solution is the same whether the water is stationary or moving through the rock, as long as the material in contact with the solution is the same; i.e., the rock has an average composition with respect to the size of the parcel of water. The length of time required for the solution to attain this equilibrium composition, t_{eq}, depends most critically upon the surface reaction kinetics of the minerals (at least for silicate materials), such as the incongruent dissolution of the plagioclase in the dolerite. The residence time, t_{rs}, for the parcel of water is just the length of time it is in contact with the material. In the present case, t_{rs} is the flux, q, times the distance along the flow path through the block. The t_{eq} is fairly constant over the whole block (except at the rock-atmosphere interface) because of its relatively homogeneous composition. The greatest changes occur at the rock-atmosphere interface where large variations in temperature and solution chemistry occur.

If $t_{eq} \gg t_{rs}$, then variations in flux will not produce significant differences in the amount of chemical weathering experienced by different areas of the rock and the rock will weather homogeneously. If

$t_{eq} << t_{rs}$, then the solution will saturate quickly relative to the flux, and the water entry points will sustain the majority of the chemical weathering. However, if t_{eq} and t_{rs} are close to the same magnitude, then chemical weathering will be sensitive to variations in the flux and, all other parameters being equal, the morphology should depend upon the shape of the flux curves. The cavern retreats from the rock-soil interface because of its greater reactivity due to increased dissolved $CO_2(g)$ and $O_2(g)$ from the atmosphere, and its higher temperature from exposure to the atmosphere and sunlight.

It appears as though the condition $t_{eq} \approx t_{rs}$ is commonly satisfied in weathering environments, especially arid environments (Conca and Rossman, 1985) where the total amount of water is low while the fluxes are high. Together with differential effects, this contributes to the abundance of cavernous morphology and the variety of weathering forms found in arid regions.

SUMMARY

In the Labyrinth, the exteriors of dolerite joint blocks become indurated with an iron oxide-stained silica coating to depths up to several centimeters, mostly by precipitation from surface runoff over exposed surfaces and along joint planes. This usually occurs before blocks are mass-wasted into talus piles, but can occur on already-weathered blocks. Initial weathering is dominated by hydration and dissolution of primary minerals and the formation of poorly crystalline kaolinite, vermiculite and quartz.

Infiltration of moisture into the blocks is primarily through the soil-rock interface. Although the silica coating reduces the chemical reactivity of the exterior, its most important effect is reduction of

permeability, which diverts the flow of interstitial solutions away from this zone. The interior rock undergoes greater weathering than the exterior rock, and subsequent expansion can fragment the exterior zone into an array of polyhedral cracks, the boundaries of which weather more rapidly than the rest of the polyhedra, causing them to spall off of the block.

A fine eolian polish forms on rock surfaces in the Labyrinth troughs exposed to the austral winter winds. This polish also decreases the exterior permeability, and subsequent weathering, but is less dramatic in effect than the silica coating and results only rarely in cavernous hollows.

Outside the Labyrinth, the silica coating forms on the dolerite mostly on exposed surfaces which are at or near the soil level, from precipitation at the rock-atmosphere interface. Subsequent lowering of the soil level leaves these exteriors as higher-standing, resistant surfaces which can be undercut by weathering along their exposed vertical sides. The resulting morphology observed in the field mimics the contours of the matric suction produced by a two-dimensional model of saturated flow within a dolerite block.

CHAPTER 6

CASE HARDENING IN TWO VOLCANIC TUFFS

The Bishop Tuff in California and the Towel Creek Tuff in Arizona have developed the differential weathering effect of case hardening, but by completely different mechanisms. Each area will be discussed separately.

BISHOP TUFF

The Bishop Tuff is a widespread rhyolitic pyroclastic flow that was erupted about 725,000 years ago from the Long Valley caldera on the east flank of the Sierra Nevada (Bailey et.al., 1976; Dalrymple, 1967). Many exposures of the Bishop Tuff in the Mono Basin appear as joint blocks exhibiting differential weathering effects, which in the tuff west of Mono Craters has resulted in cavernous weathering (Figure 32), while east and south of Mono Craters the tuff shows little or no cavernous weathering (Figure 33).

The study area can be divided into three localities (Figure 34): 1) Aeolian Buttes, 2) Butte stream cut and 3) Mono Mills. The first two localities exhibit cavernous weathering, whereas the third does not. Where developed, the cavernous hollows are irregular in shape, up to meters in diameter, and were not observed to cross-cut joint boundaries. The interior walls of the hollows are in some cases a single smooth surface but in others consist of groups of coalescing shallow depressions separated by small ridges or septae. A cross section through a cavernously weathered block is shown in Figure 4.

All localities consist of joint-bounded blocks showing a high degree of pyroclastic welding. Exposed Bishop Tuff in the study area

Figure 32 Case-hardened joint blocks of the Bishop Tuff at Butte stream cut in Mono Basin exhibiting cavernous weathering.

Figure 33 Case-hardened joint blocks of Bishop Tuff at Mono Mills.

Figure 34 Study area showing extent of Bishop Tuff in Mono Basin.

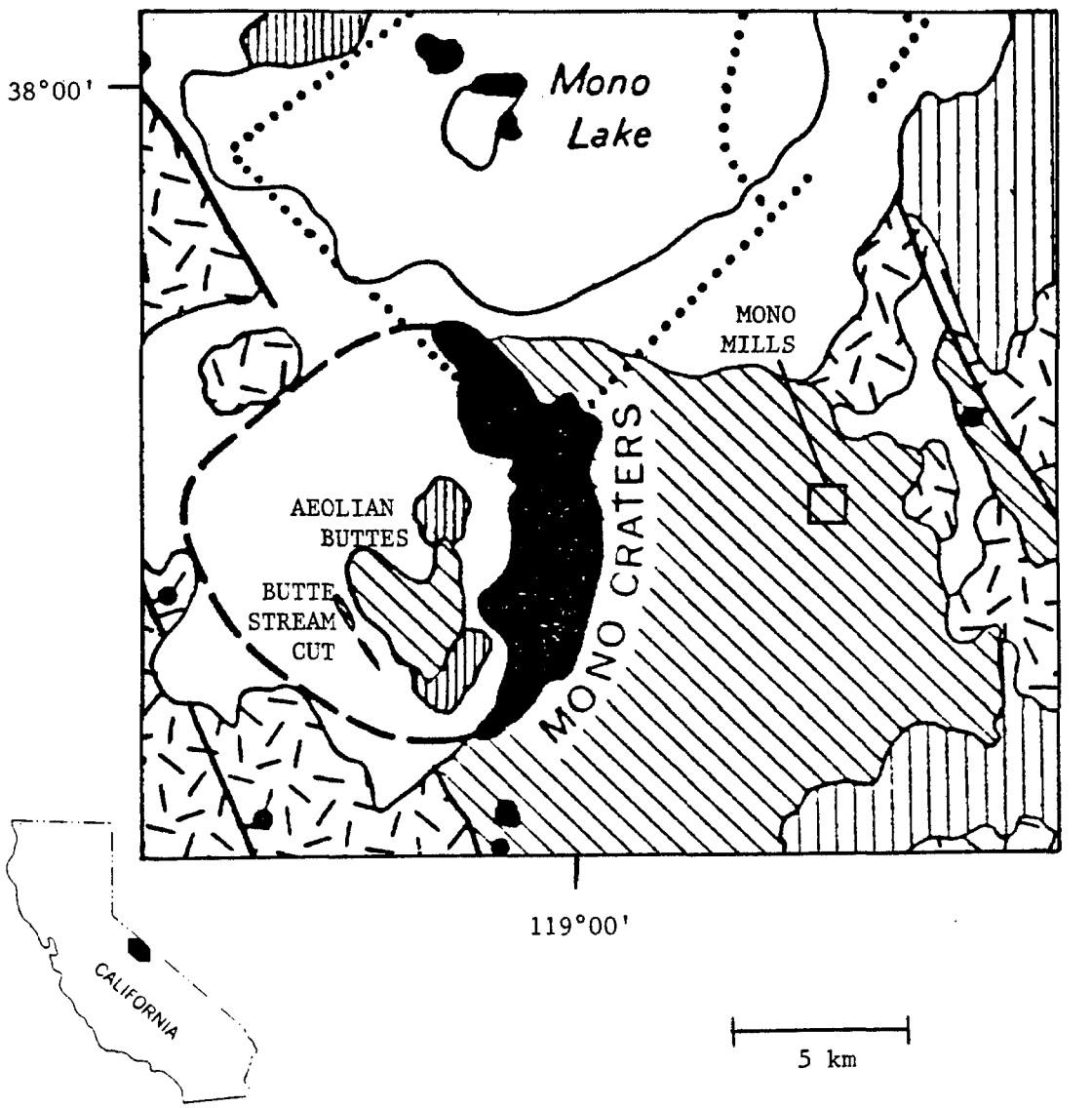
38°00'
Mono Lake
MONO MILLS
AEOLIAN BUTTES
BUTTE STREAM CUT
MONO CRATERS
119°00'
CALIFORNIA
5 km
EXPLANATION
Bishop Tuff
Rhyolite of Glass Mountain
Tertiary volcanic rocks
Geophysical boundary of Mono Basin
Mesozoic plutonic and metamorphic rocks
Alluvium and glacial deposits
Mono Craters ring fracture zone
Holocene rhyolite and rhyodacite
Postcaldera basaltic rocks
Postcaldera rhyolite and rhyodacite
Normal fault
Ball and bar on downthrown side

FIGURE 34

most resembles the welded vitric zone of Sheridan (1965) in petrologic character except that local devitrification of the matrix and glass fragments has occurred.

The non-uniform nature of the devitrification is the primary cause of the spatial variations in the rock hardness which has given rise to the case hardening. Joint block interiors have undergone little devitrification, generally restricted to glass fragments, whereas the exteriors have devitrified to an average depth of approximately a centimeter. These hardened exterior plates are planar zones which occur along relict joint surfaces. These zones are much harder than other parts of the tuff and have a groundmass which has devitrified to cryptocrystalline cristobalite and alkaline feldspar (Figure 37). In hand specimen, the plates appear as dark, almost translucent, zones of noticeably harder material that commonly overhang weathered hollows or stand out in relief (Figure 33). Phenocrysts have remained largely unweathered in both the devitrified and non-devitrified material.

The nature of the devitrification in the exterior plates differs from the hydration of obsidian described in many past studies (Friedman, et al., 1966). In the exterior plates, discrete microcrystals of cristobalite and alkaline feldspar have formed, not perlite as in hydration of obsidian, and these will be discussed below.

Hardness measurements were made on the Bishop Tuff in each of the localities (Table 13). The Bishop Tuff is case-hardened in the classical sense. However, the degree of relative hardening, as indicated by C, for the localities exhibiting cavernous weathering are the highest ever recorded, while for Mono Mills the value of C is in the normal range of 1 to 5 usually observed in case-hardened materials (Conca, 1985). In the presence of such extreme differential effects, it

Figure 35 Small cavernous hollow in the Bishop Tuff consisting of coalescing pits with septae.

Figure 36 Cross section through a cavernously weathered, case-hardened tuff block depicting the different rock zones.

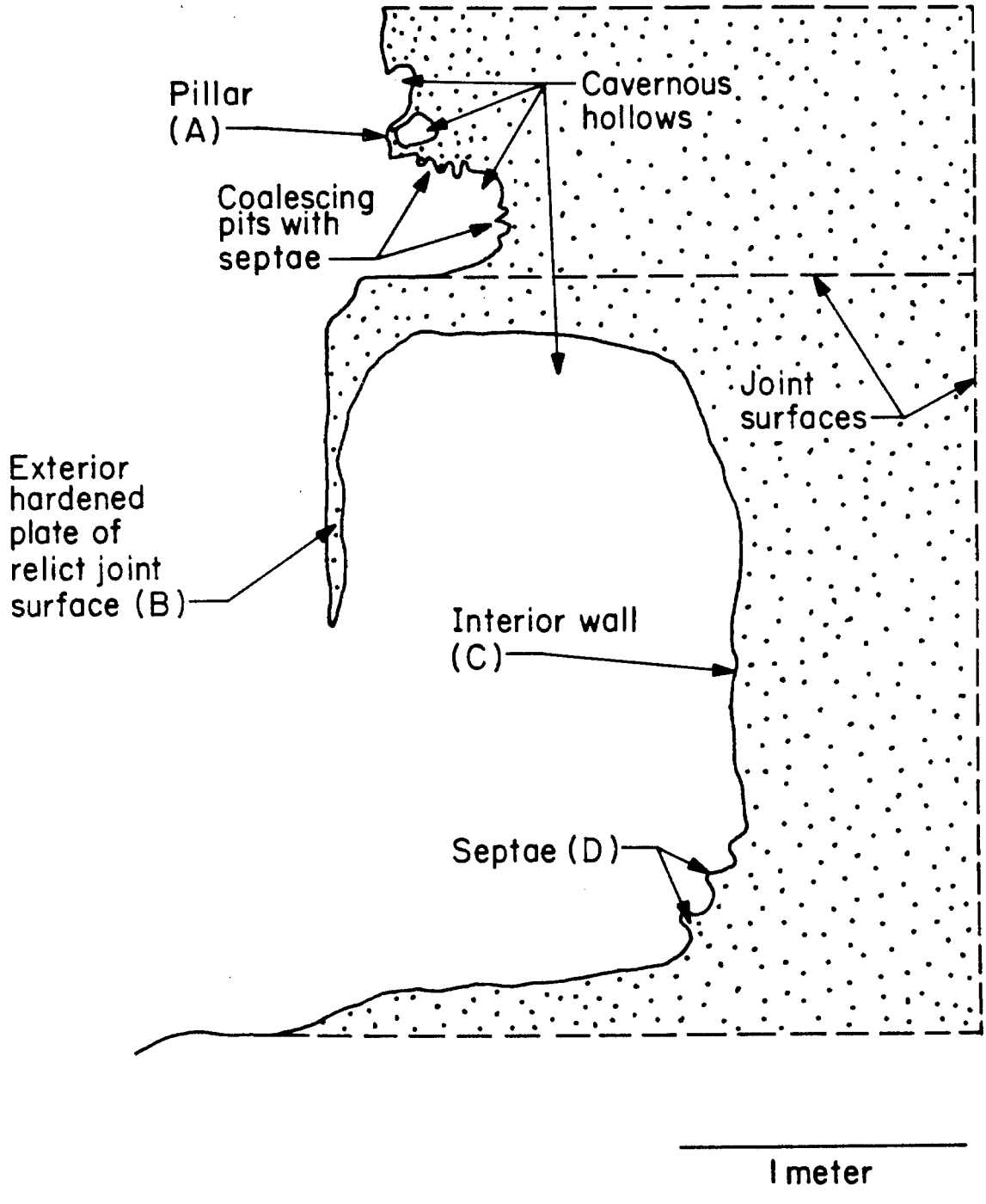
Pillar
(A)
Cavernous
hollows
Coalescing
pits with
septae
Joint
surfaces
Exterior
hardened
plate of
relict joint
surface (B)
Interior wall
(C)
Septae (D)
1 meter

FIGURE 36

Figure 37 Photomicrograph in plane polarized light (top) and crossed nicols (bottom) of the boundary between the devitrified exterior plates (right) and the interior (left).

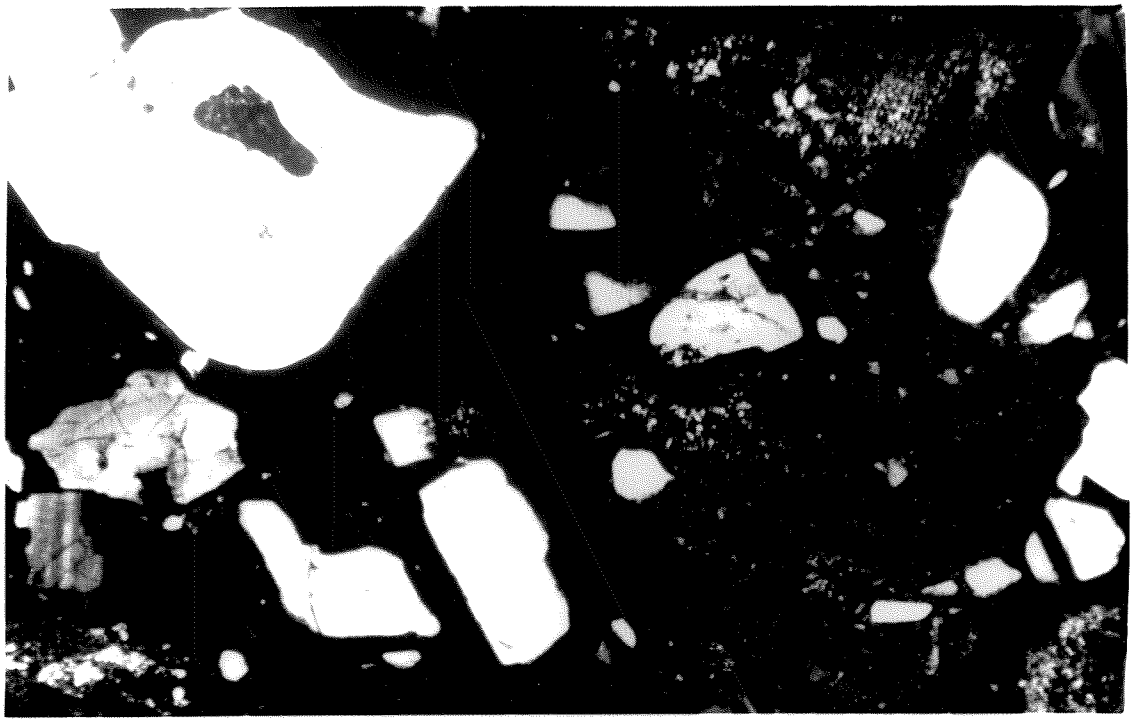

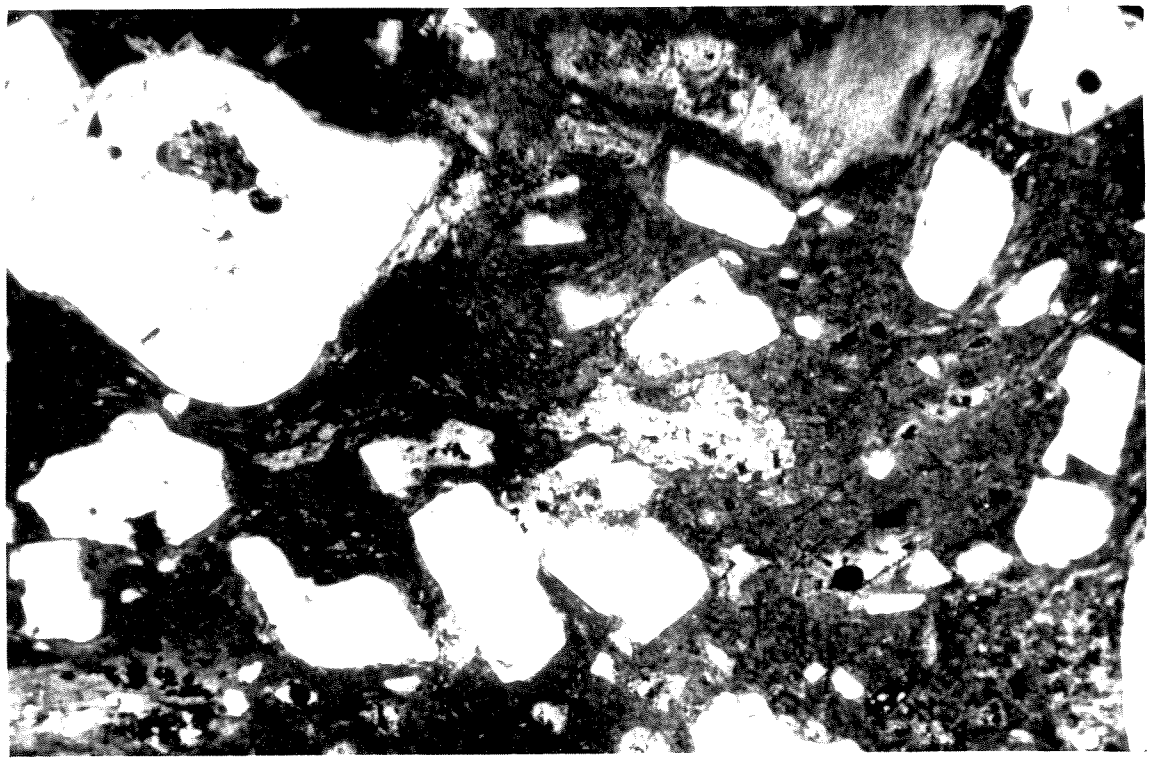

is little wonder that cavernous weathering has developed.

The relationship between the hardness values for the three localities is dependent upon the amount of time that the material has been exposed to weathering. The hardness data indicate that the development of cavernous weathering in the Bishop tuff depends upon enhancement of the initial differences in the physical properties between the interior and exterior of the tuff blocks by exposure to weathering over time.

Although it is difficult to determine exposure ages for each of the localities, it is possible to determine their relative exposure ages and to put some limits on the absolute ages (Sieh, personal communication). The tuff at Aeolian Buttes has been exposed the longest, having escaped burial under Quaternary glacial deposits, and is highly weathered. Aeolian Buttes existed as a hill during Tahoe time, and there is no reason to believe that the top of the butte has been covered by deposits in the last two hundred thousand years. There are no streams cutting the top of the butte and no evidence of other rapid removal of tuff. It is unlikely that tuff could survive exposure in this area for more than a couple of hundred thousand years, so a reasonable guess for the lifetime of Bishop Tuff on the top of Aeolian Buttes is about 200,000 years.

Although there is great uncertainty as to the absolute exposure age of the top of the butte, a reasonable limit for the exposure age is ~130,000 to ~200,000 years BP.

The material in Butte stream cut was exposed after deposition of Tahoe age till (Kistler, 1966). According to Gillespie (1982), the latest Tahoe is 65,000 years BP (Tahoe II). June Lake basalt (10,000 to 20,000 years BP) was deposited against the stream cut, indicating its

TABLE 13

ARHT FIELD RESULTS FOR THE BISHOP TUFF

Locality	Rock Zone	Abrasion Resistance Hardness Values (10^5 N sec/m)	Coefficient of Relative Hardening	Approximate Exposure Age (years BP)
Mono Mills not cavernously weathered	exterior	36.3 ± 2.3	2.5	3,000 $^{+2,000}_{-1,000}$
	interior	14.7 ± 2.7		
Butte stream cut exhibits cavernous weathering	exterior	28.3 ± 2.8	18.3	50,000 $^{+10,000}_{-10,000}$
	interior	1.6 ± 0.2		
Aeolian Buttes exhibits cavernous weathering	exterior	5.1 ± 0.4	39.2	150,000 $^{+50,000}_{-20,000}$
	interior	0.13 ± 0.04		

Figure 38 Variations of the coefficient of relative hardening with exposure age in the Bishop Tuff in Mono Basin.

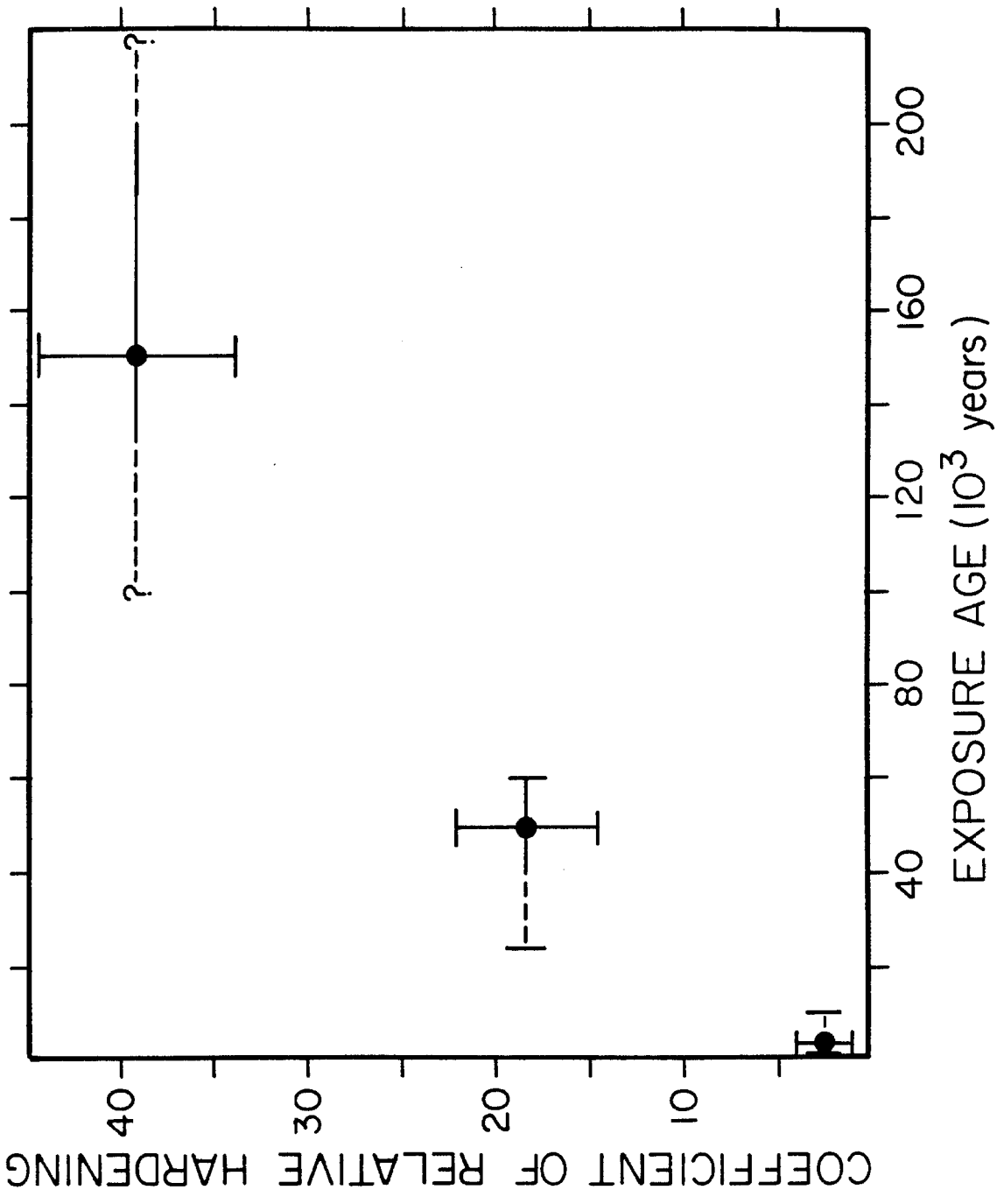
COEFFICIENT OF RELATIVE HARDENING
10
20
30
40
EXPOSURE AGE (10^3 years)
40
80
120
160
200
?
?

FIGURE 38

existence as an exposed cliff face by that time. The lower portion of the cliff, shown in Figure 32, is a less weathered bench which does not exhibit cavernous weathering. It was probably cut as an outwash channel during Tioga glaciation, and is much younger than the upper portion of the cliff face. Unfortunately, no hardness data has yet been obtained from this lower portion. It is likely that Butte stream cut began forming shortly after Tahoe glaciation, so that a reasonable exposure age is ~60,000 to ~40,000 years BP, but possibly including younger ages. From the very different degrees of weathering exhibited by the upper and lower portions of the cliff face, there is probably a significant time span between these exposure ages.

The tuff at Mono Mills is exposed in a young and small stream cut. The tuff appears fresh, although exposed material underlying the devitrified plates shows some weathering effects. The area is blanketed by Mono Craters tephra, extensive pyroclastic falls deposited sporadically from about 35,000 to 600 years BP. Since the total accumulation of tephra in the series of falls over the past several thousand years has been only about a meter, the tephra probably did not bury the wash to any appreciable depth. So a reasonable exposure age for the Mono Mills tuff is a few thousand years, possibly as much as 10,000 years.

Re-excavation of these stream cuts is a possibility that must be considered, and further field work needs to be done to better constrain these exposure ages. Yet, it is obvious that, for relative exposure ages, Aeolian Buttes is much older than Butte stream cut, which is much older than Mono Mills. Figure 38 shows the coefficient of relative hardness as a function of the estimated exposure ages (Table 13). The hardness values, H_a, of the exterior plates decrease with increasing age

at a slower rate than those of the interior, resulting in an increase in the coefficient of hardening with time. Better age dating and more hardness measurements from other areas will result in a more constrained relationship that may prove useful in dating geomorphic features in the Mono Basin area.

CHEMISTRY

A particular cavernously weathered, case-hardened block of tuff from Butte stream cut, exhibiting all of the properties described thus far, was investigated to observe chemical changes that may have occurred from weathering. Table 14 gives the whole rock chemistry for each of the rock zones depicted in Figure 36. Overall chemistry between zones is rather uniform, with Al and Si not having changed greatly. Most differences are probably due to variations in original composition and clast populations between different areas in the tuff. However, some changes have resulted from weathering, the most important being an increase in water content in the weathered interior materials. The increase in the amounts of Na, Ca, and K in the weathered materials results from their increased soluble salt contents (Table 15). IR spectroscopy identifies the principal salt of each cation as the nitrate: $NaNO_3$, KNO_3 and $Ca(NO_3)_2$.

Crystallization studies of vitreous silica (Wagstaff, et al., 1964) showed that several variables were important in devitrification of the vitreous silica. These were: 1) impurity content, 2) H_2O content of the glass and any ambient atmosphere, 3) reduction state of the glass, and 4) nucleation kinetics of the crystalline phases. H_2O increases the crystallization rate of a glass in two ways: by acting as an oxygen source and by weakening the glass structure through the formation of

TABLE 14

WHOLE ROCK CHEMISTRY

Oxide	Interior Septae (D) (%)	Interior Wall (C) (%)	Pillar (A) (%)	Exterior Plate (B) (%)
Al_2O_3	11.9	11.8	12.1	12.8
SiO_2	70.8	71.2	73.4	75.0
Fe_2O_3	1.19	1.09	1.20	1.08
MgO	0.35	0.22	0.12	0.27
K_2O	4.99	4.93	4.88	4.40
Na_2O	6.4	6.0	5.8	5.0
CaO	1.63	1.62	0.95	1.07
TiO_2	0.16	0.15	0.17	0.20
MnO	< 0.1	< 0.1	< 0.1	< 0.1
H_2O	2.8	2.8	1.1	1.6
TOTAL	100.3 %	99.9 %	99.8 %	101.5 %

TABLE 15

WHOLE ROCK SOLUBLE SALT CONTENTS

Rock Zone	Salt Content (%)
Pillar (A)	1.36 ± .01
Exterior Plate (B)	1.21 ± .01
Interior Septae (D)	2.30 ± .01
Interior Wall (C)	3.78 ± .01

hydroxyl groups (Mukherjee, et al., 1976).

The other important variable in devitrification is temperature, as can be seen in the large T-dependence of the growth rate of crystobalite from an Al_2O_3-SiO_2 glass at temperatures below the melting point (Brown and Kistler, 1959):

$$g = A\ T \exp(-B/T)$$

where g is the growth rate of a crystal face, T is temperature, A and B are compositionally dependent constants. A more valid expression for the crystal growth rate at very low temperatures is given by Kny and Nauer (1978):

$$g \approx \frac{f\ k\ T}{3\pi a_o^2 \eta}$$

where f is the fraction of crystal-surface area of interfacial adsorption sites, k is the Boltzmann constant, a_o is the molecular diameter and η is the viscosity of the glass. Kny and Nauer calculate crystallization times for alkali-silicate glasses at 300 K to be longer than 10^7 years for dry samples and longer than 10^4 years for wet samples. Therefore, the presence of H_2O seems necessary for devitrification to occur in the Bishop Tuff exterior plates over the time period of interest. However, the presence of H_2O is not enough because later interaction of the block interior with meteoric water at lower temperatures has not produced devitrification, even after intense weathering for up to 10^5 years. Elevated temperatures seem to have been necessary for the devitrification.

The water contents of the highly weathered materials (C and D in

Table 14) are twice that of the exterior plate as a result of weathering. The pillar (A) has less water than the exterior plate but is more weathered. There appear, then, to be two sources of H_2O in the tuff: one from hydrothermal fluids accessed through the joint system during the cooling of the tuff which resulted in the joint-aligned devitrification, and the other from later meteoric water involved in subsequent low-temperature weathering of the tuff.

Table 16 shows the kaolinite contents for each of the rock zones of Figure 36. The kaolinite is highest in zones A and B where the least chemical weathering has occurred. Zones C and D, the most highly weathered materials, have the least kaolinite. The kaolinite may be a hydrothermal alteration product formed at the same time as the devitrification (at high temperatures in the presence of water). The kaolinite content is highest in the two samples close to the joint surface (Figure 39), as would be expected in such a hypothesis.

TABLE 16

KAOLINITE CONTENTS

Rock Zone	Kaolinite Content (%)
Pillar (A)	2.37 ± .2
Exterior Plate (B)	2.05 ± .2
Interior Septae (D)	1.04 ± .1
Interior Wall (C)	0.94 ± .1

Figure 39 Plot of kaolinite vs distance from joint surface for materials of the tuff block shown in Figure 36.

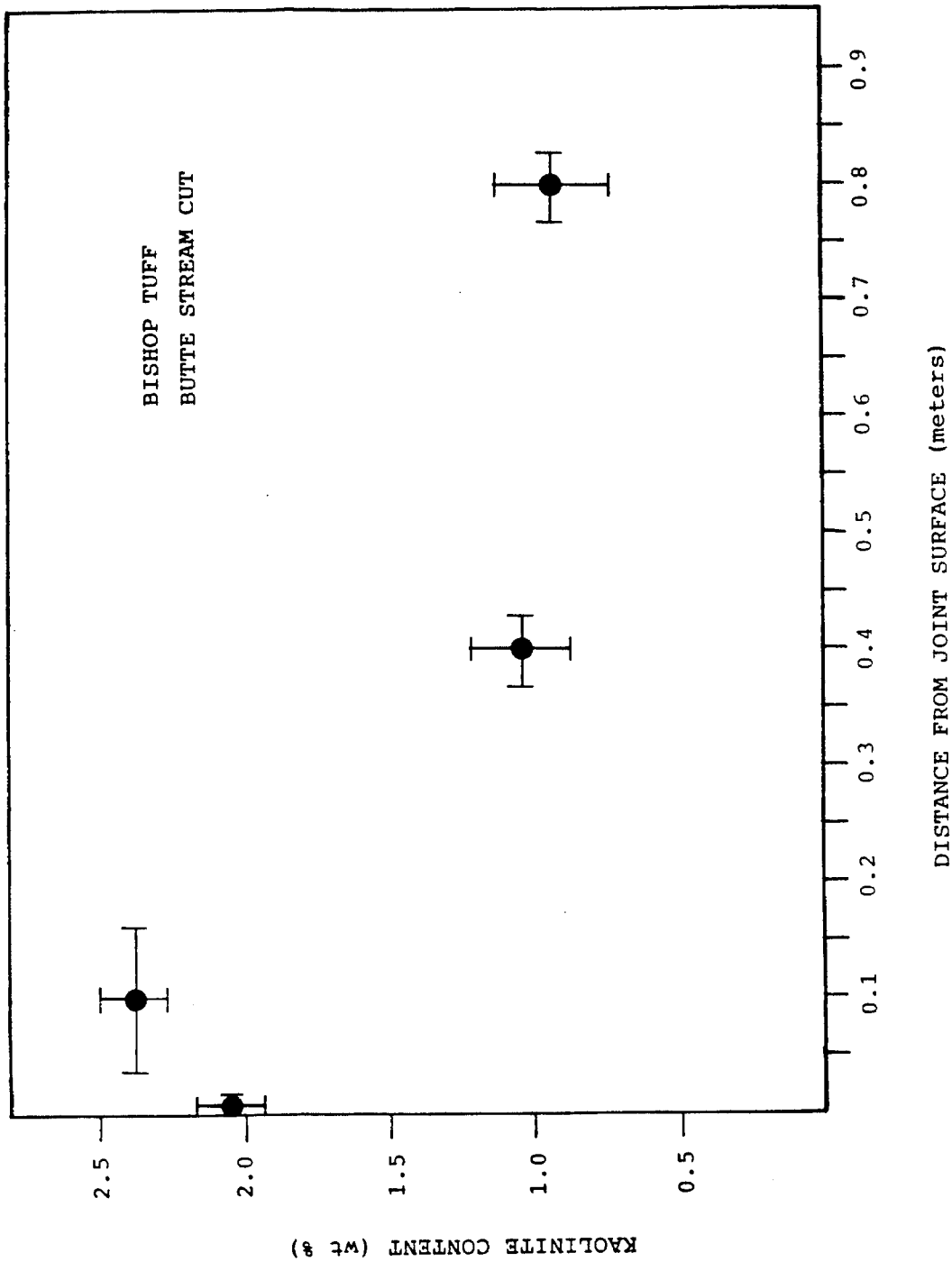
BISHOP TUFF
BUTTE STREAM CUT
KAOLINITE CONTENT (wt %)
2.5
2.0
1.5
1.0
0.5
0.1
0.2
0.3
0.4
0.5
0.6
0.7
0.8
0.9
DISTANCE FROM JOINT SURFACE (meters)

FIGURE 39

TOWEL CREEK TUFF

A portion of a dacitic ignimbrite of the Towel Creek Tuff in the arid environment of Cottonwood Basin, Arizona exhibits extensive cavernous weathering as a result of case hardening. Hollows of all sizes up to a meter occur with an abundance of the larger sizes (Figure 40). Within the study area the ignimbrite weathers into cylindrical cones or "tepees" that are spotted with cavernous hollows. The morphology of the hollows are spherical to elliptical with flat horizontal floors. Rock exteriors have a thin (< 1 mm) crust developed which is slightly more resistant to erosion than the interior as a result of the precipitation of minor amounts of calcite at the surface. The interior walls are sometimes coated with a brittle shell a few millimeters thick which armors the interior surface.

The ignimbrite is a whitish-pink, structureless, pyroclastic, non-welded deposit containing abundant pumiceous fragments of dacitic composition in a matrix primarily of glass (Lewis, 1983). Plagioclase is the most common crystal in the matrix (10% modal) and averages about 1 mm in length. Sanidine (and quartz), biotite and hornblende also occur in the matrix but are less abundant (< 5% modal). There is little layering in the tuff and the cavernous hollows do not seem stratigraphically controlled.

The ignimbrite within Cottonwood Basin shows some unusual structures (Figure 41). There is a shallow-dipping planar horizon of hard, calcite-cemented ignimbrite which forms cap rocks on many of the tepees. Scattered throughout the study area are vertical, U-shaped ovoids of the same calcite-cemented ignimbrite as the planar horizon and which intersect that horizon. The ovoids have friable cylindrical centers (vents) which penetrate downwards into the uncemented tuff.

Figure 40 View of Cottonwood Basin showing case-hardened, conical tepees of dacitic composition spotted with cavernous hollows.

These features were interpreted by Lewis (1983) as fossil fumeroles feeding a horizon of constant temperature and pressure with $CaCO_3$-saturated fluids. The ignimbrite is overlaid and underlaid by sandstone of the Verde formation which has an age of 7.8 to 6.0 m.y. in Cottonwood Basin (Lewis, 1983). After deposition of the ignimbrite, at >425°C (Lewis, 1983), water from the underlying Verde formation rich in $CaCO_3$ was driven by lithostatic pressure into the ignimbrite where it was heated. The water moved upwards through vents into the tuff until it became oversaturated with respect to $CaCO_3$ and deposited calcite in the surrounding material. Fossil fumeroles similar in form to those at Cottonwood Basin have been described in other areas (McDonald, 1972).

Another effect of the upward-migrating fluids was the oxidation of the matrix resulting in the formation of minor amounts of iron oxides which give the unit its uniform light pink color. Outside Cottonwood Basin the ignimbrite is white, shows no fumerolic structures and does not weather into Tepees or exhibit cavernous weathering.

Table 17 gives the calcite content of the matrix of the different rock zones (clast composition is similar for all materials) and the hardness values as determined by the abrasion resistance hardness tester (Chapter 2). The tuff hardened by fumerolic material has the highest calcite content and is the most resistant, ringing soundly when struck by a hammer. The fumerole vent material has less calcite and is more friable.

Although the exterior crust does not contain much calcite relative to the tuff inundated by fumerolic materials, it is measurable by CO_2 extraction methods, and imparts a measurable hardness to the exterior relative to the interior (coefficient of hardening is 2.8). Small amounts of calcite have been observed elsewhere to have large effects on

Figure 41 Cross section through a tepee exhibiting the features discussed in the text.

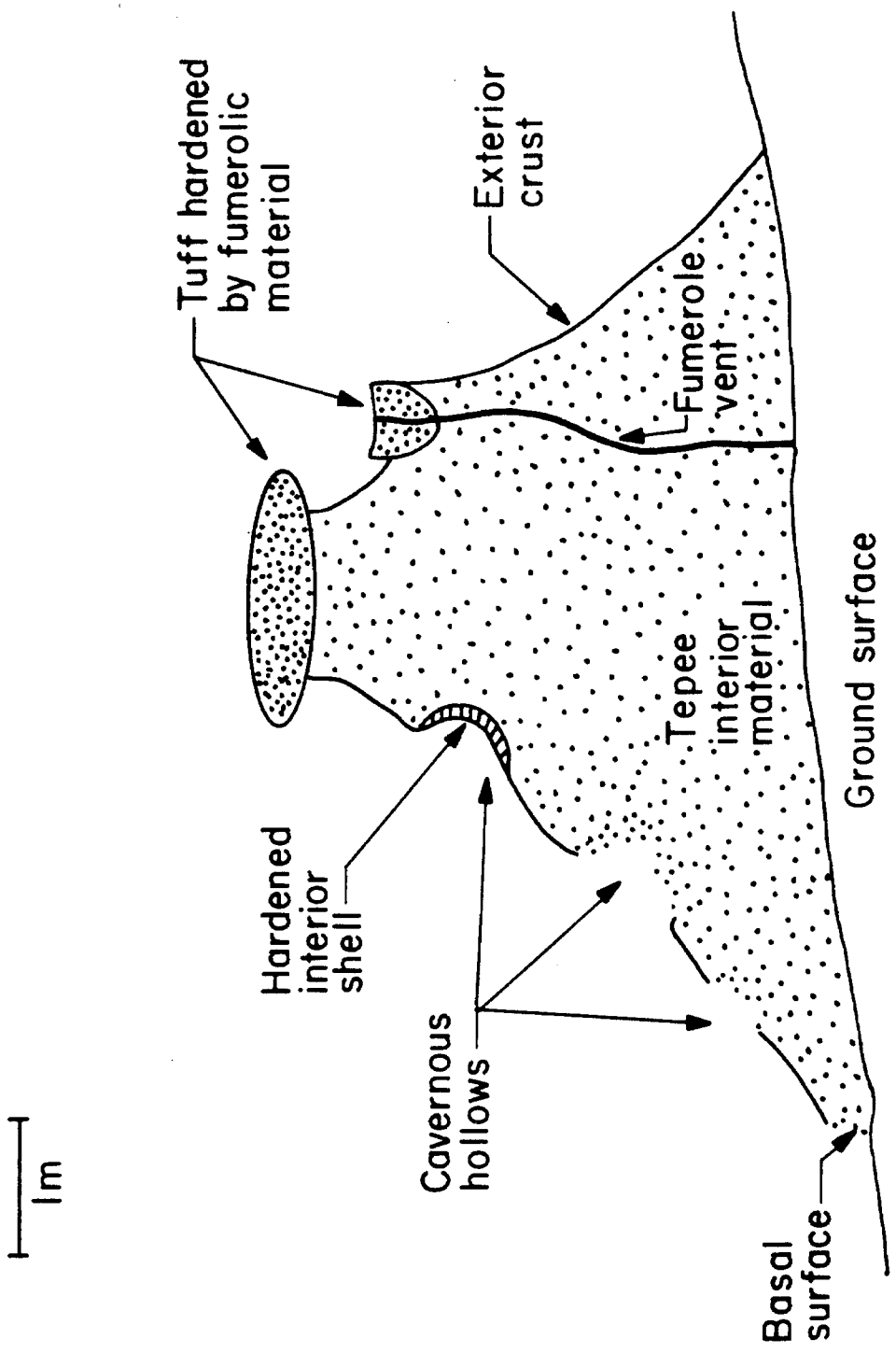
Tuff hardened by fumerolic material
Exterior crust
Fumerole vent
Tepee interior material
Ground surface
Hardened interior shell
Cavernous hollows
Basal surface
1m

FIGURE 41

TABLE 17

TOWEL CREEK TUFF

Rock Zone	Calcite Contents of Tuff Matrix (wt%)	Abrasion Resistance Hardness Values (10^5 N sec/m)	Coefficient of Relative Hardening
Hardened Fumerolic Material	28.8 ± .001	1.67 ± .15	2.1
Fumerole Vent Material	4.35 ± .001	0.79 ± .01	
Exterior Crust	0.012 ± .001	0.11 ± .03	2.8
Tepee Interior	< 0.001	0.04 ± .01	

hardness (Conca and Rossman, 1982). The interior rock does not have measurable amounts of calcite by CO_2 monometry, but the evolution of CO_2 was detected using a voltmeter in the vacuum chamber, placing the amount of calcite in the realm of a ten-thousandth of a percent by weight.

If calcite contents are plotted against hardness values, a definite relationship is observed between the two parameters (Figure 42). Since calcite content is the only chemical or petrological variation among the different materials, Figure 42 indicates that differences in calcite content are responsible for the variations in the physical properties among the different materials.

The presence of a calcite-cemented shell in the interiors of some of the hollows tends to stabilize those interiors against erosion. These shells are more common, but not restricted to, caverns higher up on the tepees. The formation of the interior shells at Cottonwood Basin is contrary to most hollow interiors studied elsewhere (Mustoe, 1982; Conca and Rossman, 1982) in which calcite either does not precipitate or precipitates as loose botryoidal aggregates or thin flakes that do not impart any observable hardness or resistance to the interior walls.

The fact that the tepees are small, isolated cones with calcite-cemented caprocks instead of the more usual massive outcrops may have a great influence on these relationships, especially on the movement of pore water during wetting and drying of the tepees. On two separate occasions, field observations were made in Cottonwood Basin on wetting (during a storm) and drying (for many days after a storm) of the tepees. During the first storm, all surfaces and underlying material appeared wet. After the second storm, almost all surfaces became air-dry after only a day of exposure to bright sun. However, the basal surfaces of the tepees (Figures 41 and 43) and the interior walls of the

Figure 42 Calcite contents of the matrix of the different materials plotted against their hardness values, illustrating a direct relationship between calcite content and hardness.

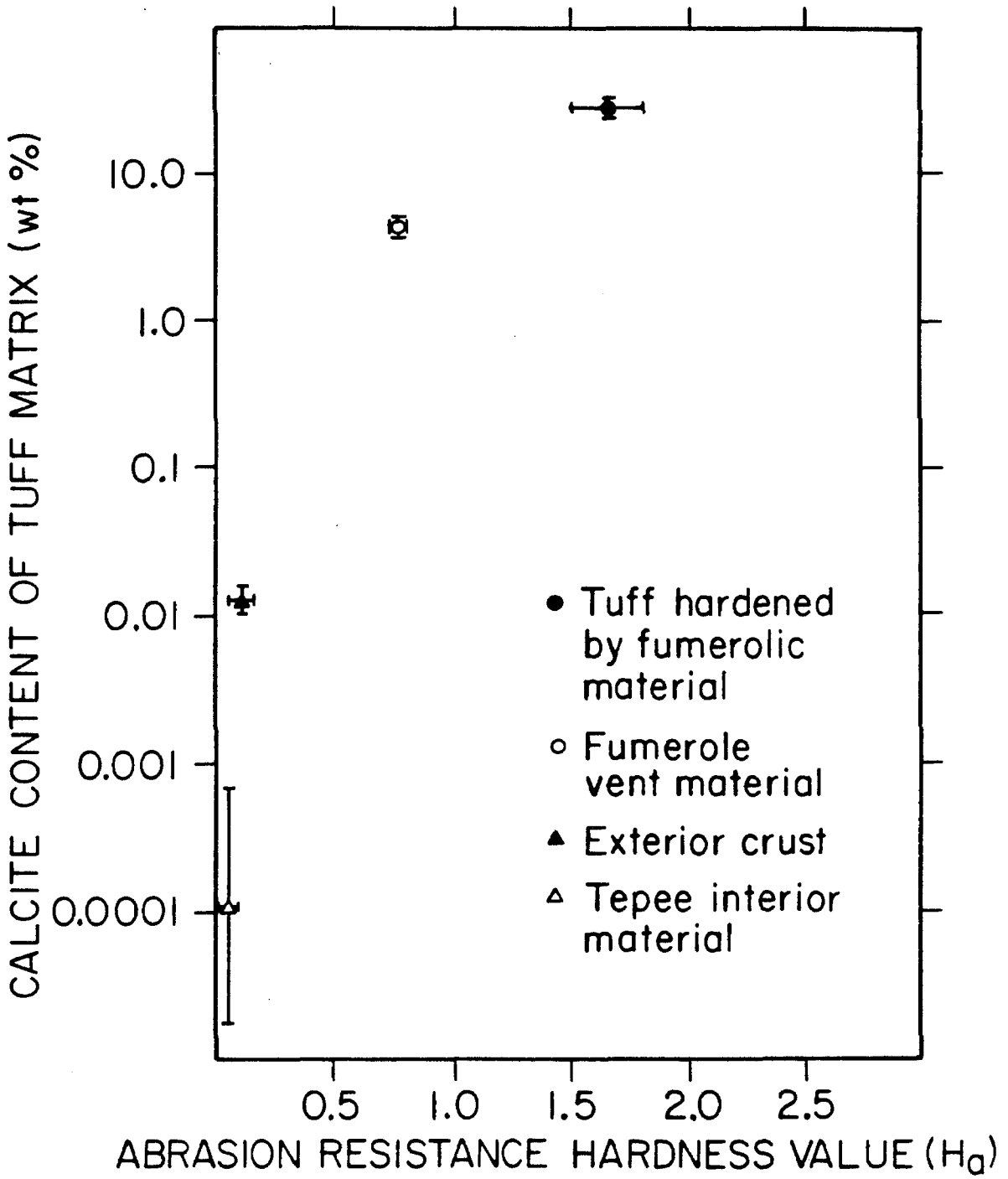
CALCITE CONTENT OF TUFF MATRIX (wt %)
10.0
1.0
0.1
0.01
0.001
0.0001
0.5
1.0
1.5
2.0
2.5
ABRASION RESISTANCE HARDNESS VALUE (Ha)
Tuff hardened by fumerolic material
Fumerole vent material
Exterior crust
Tepee interior material

FIGURE 42

lowest hollows (both large and small) remained wet for many days of exposure to bright sun whether shadowed or not. The interior walls of the hollows higher up on the tepees, both large and small, were dry after a few days. Material removed from the basal surfaces dried rapidly in the sun, indicating that for these surfaces to remain wet for any period of time, moisture must be constantly supplied from the interior. From these observations it can be seen that, after becoming wet during storms, the tepees dessicate primarily through the basal surfaces and lower hollows, and not through the exterior crust or upper hollows.

These observations have important implications for the development of the cavern and transport of dissolved materials, especially carbonate. It is at the basal surfaces that most of the physical erosion caused by fluvial processes occurs, and the exterior crust does not have a chance to develop. Therefore, greater erosion and greater moisture flux combine to make the basal surfaces the positions of greatest material weathering and removal, and the areas where caverns are most likely to originate (Figure 44). Basal surfaces do not homogeneously surround each tepee, but are concentrated in particular places as a result of the present fluvial erosion patterns. Thus, basal surfaces usually constitute less than a tenth of the circumference of a tepee or the base of an outcrop.

As the surrounding ground surface is lowered over time by erosion, the basal surfaces will be left elevated as an indentation that is both less resistant to weathering and an area of high moisture flux, as a result of having no exterior crust. It may then enlarge to form a cavernous hollow. As the ground surface lowers, the fluvial erosion pattern can and does change leading to a random development of hollows

Figure 43 Tepee showing a wet basal zone (dark) through which the tepee interior is dessicating. Flow through this basal surface accounts for almost all of the flux from the interior.

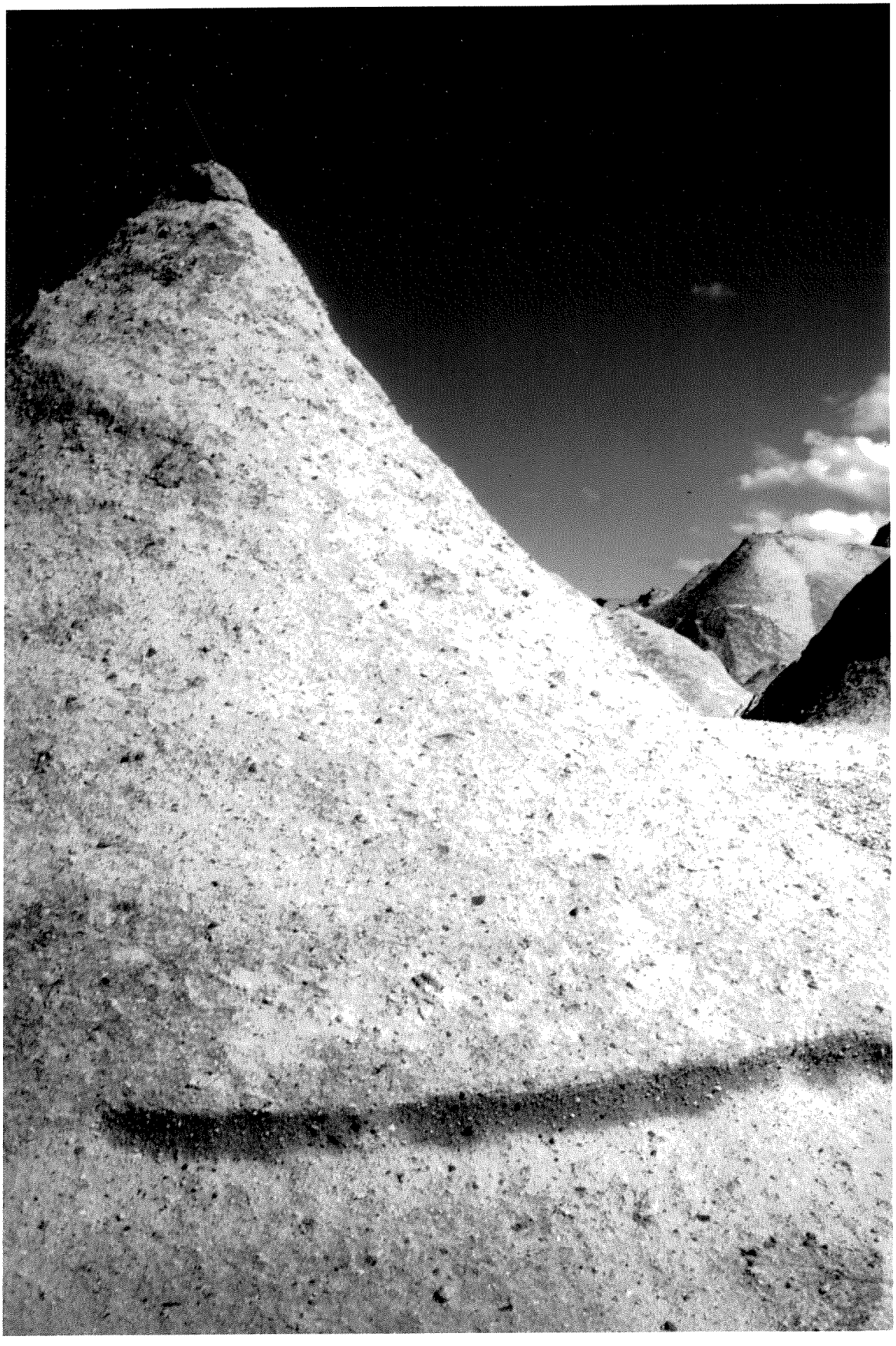

Figure 44 View of the basal surface of a tepee where exterior crusts are not able to form because of fluvial erosion. It appears as though cavernous hollows are initiated in this zone.

in the tepees, a pattern which is observed in most of the surfaces in Cottonwood Basin (Figure 40). However, in the cases where the fluvial erosion pattern does not change very much with time, a non-random array of cavernous hollows would be expected and is indeed observed in some instances (Figure 45).

The source of calcite for the crust and interior is the tuff hardened by fumerolic material. The variations in calcite contents between exterior and interior are determined by the aqueous chemistry of the carbonate, the peculiar geometry of the tepees, and their effect on transport of dissolved carbonate. Most importantly, carbonate dissolution, transport and precipitation at the exterior occur in a system open to the atmosphere with a fixed CO_2 partial pressure of $10^{-3.5}$ atm. However, the interior has a soil-like microclimate, porosity and biological activity. The CO_2 partial pressure will therefore be about $10^{-2.5}$ atm (Stumm and Morgan, 1981). Aqueous solutions in these two systems will behave differently. To illustrate this, consider the overall reactions:

$$H_2O = H^+ + OH^- \qquad pK_w = 14.0$$

$$CO_2 + H_2O = H_2CO_3^* \qquad pK_H = 1.5$$

$$H_2CO_3^* = H^+ + HCO_3^- \qquad pK_1 = 6.3$$

$$HCO_3^- = H^+ + CO_3^{2-} \qquad pK_2 = 10.3$$

$$CaCO_3(s) = Ca^{2+} + CO_3^{2-} \qquad pK_{sO} = 8.3$$

Figure 45 A tepee showing a non-random array of cavernous hollows, the floor of each hollow representing a paleo-basal surface. The two uppermost hollows have interior shells developed on their interior walls.

Because the ionic strength of the migrating solutions will be 10^{-3} M or less, species activities will be neglected. From these relationships the concentrations of each species can be expressed as a function of pH (Morel, 1983) and shown in graphical form as a log C-pH diagram (Figure 46). The solutions in each system will be saturated with respect to $CaCO_3$ when:

$$2(Ca^{2+}) \approx (HCO_3^-)$$

From Figure 46 it can be seen that this corresponds to $(Ca^{2+}) = 10^{-3.3}$ M for the exterior and $10^{-2.3}$ M for the interior, indicating that under equilibrium conditions the interior should have ten times the carbonate content of the exterior. However, the calcite content of the interior is two orders of magnitude less than the exterior.

Calcite dissolution and precipitation in the tuff is controlled by both equilibria and kinetics. For a system that does not reach equilibrium, a simple expression for the dissolution of calcite is given by Snoeyink and Jenkins (1980):

$$\frac{d(Ca^{2+})}{dt} = k\ S\ [(Ca^{2+})^* + (Ca^{2+})]$$

where $(Ca^{2+})^*$ = the aqueous saturation concentration (M), k is the rate constant (s^{-1} mg^{-1} M^{-1}) and S is the surface area (mg l^{-1} of a given particle size). As rainwater encounters the exterior, calcite will begin to dissolve. The characteristic time, i.e., the reciprocal of the kinetic rate constant, for the dissolution of calcite (for the micron-sized particles of the present case) is on the order of 10^3 sec (Morgan and Stone, 1984). Since the residence time for water at the exterior is

Figure 46 Log C-pH diagram for the aqueous carbonate species of the exterior solution of the tepees, having a P_{CO_2} of $10^{-3.5}$ atm. For the interior solutions, $P_{CO_2} = 10^{-2.5}$ atm and all equilibrium concentrations will be ten times that of the exterior.

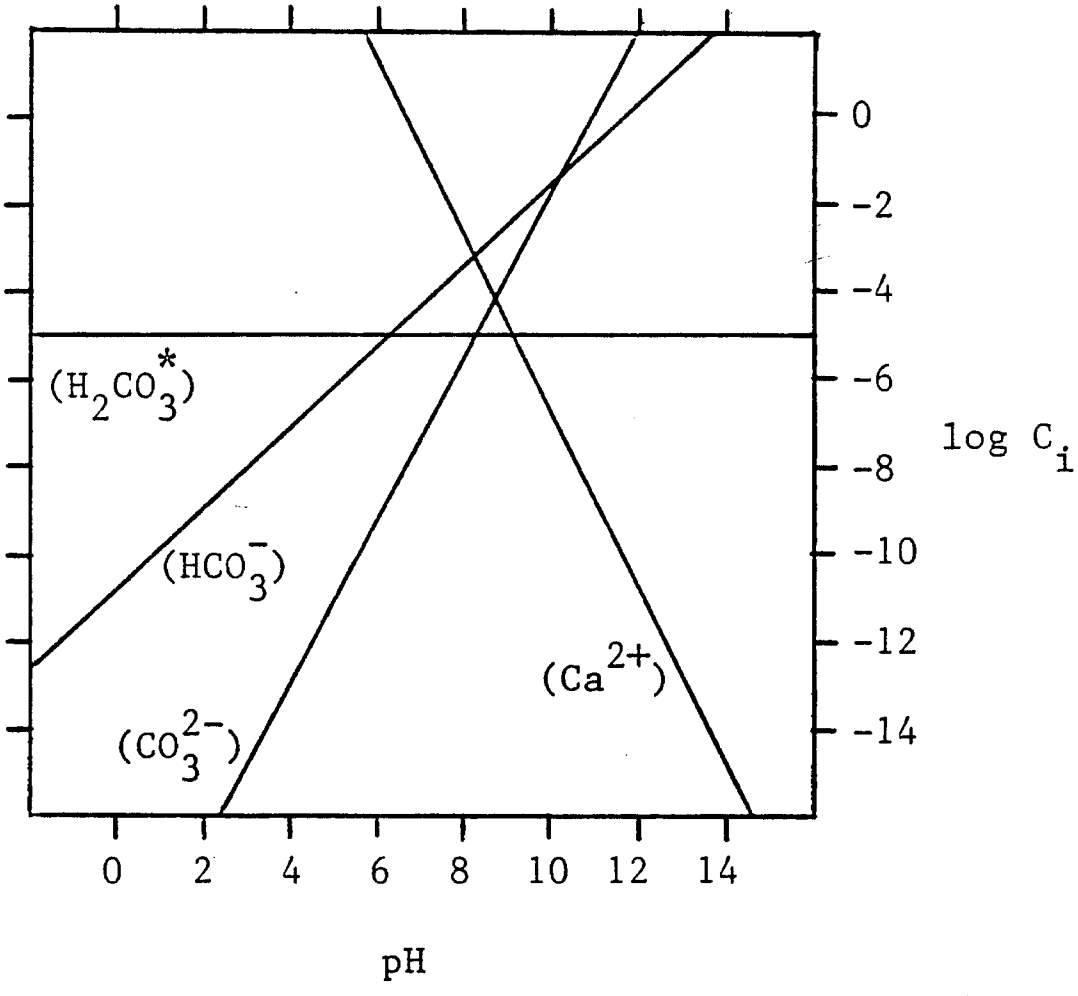

FIGURE 46

short, the dissolution is probably influenced by kinetics. At the same time, water flowing down from tuff hardened by fumerolic material will have already dissolved some carbonate, and its ability to dissolve more calcite may be much less than the initial rainwater. Also, as evaporation increases the concentration of dissolved solutes and the solution becomes saturated with respect to calcium carbonate, calcite will begin to precipitate at the surface.

As water enters the tepee interior, however, two effects become important. The increased P_{CO_2} of the interior means that no infiltrating solution from the exterior will be saturated with respect to calcite, but will be at least an order of magnitude undersaturated in Ca^{2+}. Thus, the solution will begin dissolving any calcite that is present. Secondly, the residence time of the water in the interior was observed in the field to be much longer than the characteristic time for dissolution, about 10^6 sec, so that equilibrium can be established.

The drying out of the Tepee can be separated into two stages (Hillel, 1971): (1) an early stage, during which the evaporation rate is determined by the external and surface conditions, such as atmospheric humidity and temperature, and (2) a falling-rate stage, during which the evaporation rate from the rock is lower and is determined by the material's hydraulic conductivity. During the initial stage, water moves outward in response to the evaporation-induced suction gradient at the surface. The rate can remain fairly constant as the increasing suction gradient owing to the decreasing water content tends to compensate for the decreasing hydraulic conductivity. This first stage was observed in the tepees to take about 10^6 sec. Eventually, the water content becomes so low that no more water is supplied to the surface, the suction gradient is at a maximum, and the surface becomes air-dry.

The second stage begins, and is accompanied by an inward-moving drying front. Movement of water from this front to the surface occurs by vapor diffusion. It is the carbonate content of the residual water at the beginning of the second stage that will precipitate as calcite in the interior as the tuff dries. The water content at this stage is uncertain, but will be in the range of 1 to 20% of the effective porosity. Choosing 10% for the tuff, and taking the interior calcite content as 10^{-4} wt%, we can determine the Ca^{2+} concentration in the residual pore solution required to precipitate 10^{-4} wt% calcite upon evaporation. The porosity of the tuff is 25% and its density is 2.0 g/cm^3. Therefore:

$$10(0.25)10^{-4}\,g/g \times 2.0\,g/cm^3 \times 10^3\,cm^3/1 \div 100\,g/mole = 5 \times 10^{-3}\,M\,(Ca^{2+})$$

which is exactly the equilibrium concentration calculated from Figure 46 for the interior. This indicates that the calcite content of the interior material is limited by the equilibrium chemistry of the infiltrating pore water, and should never increase above 10^{-4} wt% under present conditions.

CHAPTER 7

SUMMARY

Differential weathering effects are an intermediate step in a cause and effect relationship concerning the interaction of rock material with its environment. Certain information emerges from this study as facts about which processes and mechanisms operate in these diverse weathering situations. Speculations at a variety of confidence levels also result from this work, and, of course, many unsolved problems are left in its wake.

The only generalization which can be applied to differential weathering is that crystalline rocks tend to core-soften whereas clastic materials case-harden. This results from the overall differences in the intergranular bonding character between crystalline materials such as granite and clastic materials such as sandstone. Clastic materials will be affected by redistribution of secondary cements, and greater accumulation at an interface can result in case hardening. In clastic rock's, therefore, the hardness of different areas can either increase or decrease with time. On the other hand, a crystalline rock in a weathering environment will almost always have its intergranular and intragranular bonds disrupted by chemical alteration because these bonds are far out of equilibrium with the weathering environment. Spatial variations in disruption can result in core softening or case softening, but the hardness of all areas will decrease with time. Accumulation of secondary cements can often enhance differential effects in crystalline rocks by affecting the permeability of different areas but without case hardening the rock.

The two most important aspects of differential weathering systems

is the presence of an interface and the state of H_2O in the system. It is at the rock-atmosphere, rock-soil, and rock-water interfaces that many differential mechanisms occur because of the changes in composition, phase, temperature or pressure which frequently accompany movement of substances across that interface. Thus, a slowly migrating pore solution carrying dissolved solutes, drawn to a rock surface by an evaporation-induced pressure gradient, may saturate with respect to one or more phases as a result of vaporization of H_2O across the rock-atmosphere interface.

All of the mechanisms discussed in the previous chapters depend at some stage on the presence of liquid water, acting either as solvent, reactant or transport medium. Because of water's diverse role in weathering, spatial variations in water content, flux, dissolved solutes and dissolved gases will be important in the weathering history of geologic systems, and will be responsible in some way for any differential weathering effects observed.

The presence of water at a rock-atmosphere interface can result in large changes in the system, mostly changes in the solution's pH and Eh through changes in dissolved $CO_2(g)$ and $O_2(g)$, respectively, and by increasing the solution's ionic strength through evaporation or dilution. Similarly, at a rock-soil interface, the pH of a solution can decrease by dissolving more $CO_2(g)$ because of the usually higher P_{CO_2} of a soil environment, as well as redissolving soluble salts and raising its ionic strength, making that interface an area of higher reactivity in its ability to dissolve minerals.

These interfaces are seen as boundaries between two systems, such that the rock adjacent to the interface is considered to be in an open system that will not reach equilibrium because of the rapid rates of gas

phase reactions and transport compared to the slow rates of solid and aqueous silicate reactions. This explains why the caverns are initiated at and retreat from the rock-atmosphere interface. The direction and extent of this retreat may then be governed by variations in the pore water flux, as in the case of the Ferrar dolerite (Figure 31b), or by some other factor.

Table 18 is a summary of results from the field areas for which hardness data was obtained (see Chapter 2). The differential weathering effects of case hardening and core softening were caused by a variety of differential mechanisms.

Field observations and the experimental results from the Valley of Fire, Nevada, can be summarized as follows: (1) rocks of the Aztec formation within the Valley of Fire are extensively case-hardened; (2) case-hardening in the study area involves the presence of an induration crust (called the orange crust), usually between 0.5 and 5.0 mm thick, which has increased hardness and reduced friability over the interior of the rock, and differs from the interior in the amount of kaolinite (about a factor of five greater in the crust) and the presence of calcite (in concentrations between ≃ 0.001 and ≃ 5.0 wt%); (3) two out of thirteen outcrops sampled possesed a second yellow crust overlying the orange crust and which, even though much thinner than the orange crust (less than 0.5 mm), was significantly harder. Like the orange crust, the yellow crust contained more kaolinite than the interior but also contained colemanite, $CaB_3O_4(OH)_3 \cdot H_2O$; (4) the interior edge of the crusts are abrupt and the interior rock within the study area contains no calcite or colemanite above detection limits (≃ 0.001 wt%), and (5) thickness, physical properties, and calcite content of the case-hardened crusts within the study area show great local variations.

TABLE 18

Rock Type and Study Area	Differential Weathering Effect*	Proposed Differential Weathering Mechanisms
Aztec Sandstone Valley of Fire Nevada	case hardening C = 1.3	eolian deposition of constituents and recrystallization of calcite as a secondary cement at surface
Beacon Sandstone Farnell Valley Antarctica	case hardening C = 2.5	microclimatic influence on silica deposition as a secondary cement at the rock surface
Bishop Tuff Mono Basin California	case hardening C = 18.3	spatial variations in the devitrification of the glassy matrix
Towel Creek Tuff Cottonwood Basin Arizona	case hardening C = 2.8	microclimatic influence on calcite precipitation as secondary cement at the rock surface
tonalite Catavina Baja California	core softening C = 2.3	microclimatic influence on dissolution and alteration of primary minerals and precipitation of secondary minerals
Ferrar Dolerite Labyrinth Antarctica	core softening C = 3.7	microclimatic influence on silica deposition at rock exterior and variations in pore water flow
Vida Granite Taylor Valley Antarctica	core softening C = 2.0	silica deposition and eolian polishing of the rock exterior and variations in pore water flow

*The coefficient of relative hardening, C (defined as the ratio of the hardness values of the rock exterior to those of the rock interior), is given for a representative example from each study area.

The weathering effects on the tonalite at Catavina, Baja California can be summarized as follows: (1) kaolinite, quartz and hematite are the major weathering products formed, and calcite and gypsum have formed in trace amounts; (2) biotite has undergone loss of Fe^{2+} without major breakdown in structure and without the formation of measurable amounts of phases such as vermiculite or chlorite-saponite, but weathering has increased the water content of the biotite, (3) feldspar has weathered along cleavage surfaces and grain boundaries to supply Al and (along with minor dissolution of quartz) Si for the formation of kaolinite and secondary quartz (mixed layer illite/montmorillinite clays were not found in the weathered samples, but were found in the surrounding soils); (4) less kaolinite is present in the exterior than in the more friable interior, and the feldspars are not as highly fractured in the exterior as they are in the interior;(5) most of the hematite occurs towards the rock surfaces, and (6) the degree of relative hardening of the exterior (C) was equal to 2.26 ± 0.3. Abrasion resistance hardness values (H_a) inversely correlate with kaolinite contents.

These observations indicate that tonalite boulders at Catavina are core-softened as a result of greater kaolinization of the interior.

Model calculations for one-dimensional flow within a tonalite boulder indicate that core softening influences the flow of water by changing the hydraulic conductivities (water permeabilities) of different areas, thus increasing the flux of water through the cavern interior wall relative to the exterior.

The differential weathering between the interior and exterior is manifested as core softening in the dolerite and granitics of the Dry Valleys, and case hardening in the sandstones. The decreased hardness and increased permeability and porosity of the interior make it more

susceptible to weathering than the exterior, especially salt weathering.

In the Labyrinth, the exteriors of dolerite joint blocks become indurated with an iron oxide-contaminated silica coating to depths up to several centimeters, mostly by precipitation from surface runoff over exposed surfaces and along joint planes. This usually occurs before blocks are mass-wasted into talus piles, but can occur on already-weathered blocks. Initial weathering is dominated by hydration and dissolution of primary minerals and the formation of poorly crystalline kaolinite, vermiculite and quartz.

Infiltration of moisture into the blocks is primarily through the soil-rock interface. Although the silica coating reduces the chemical reactivity of the exterior, its most important effect is reduction of the permeability which diverts the flow of interstitial solutions away from this zone. The interior undergoes greater weathering and subsequent expansion can fragment the exterior zone into an array of polyhedra, the boundaries of which weather more rapidly than the rest of the polyhedra, causing them to spall off the block.

A fine eolian polish forms on rock surfaces in the Labyrinth troughs exposed to the austral winter winds, decreasing the exterior permeability. The polish decreases the exterior weathering but results only rarely in cavernous hollows.

Outside the Labyrinth the silica coating forms on the dolerite mostly on exposed surfaces which are at or near the soil level from precipitation at the rock-atmosphere interface. Subsequent deflation of the soil leaves these exteriors as higher standing resistant surfaces which can be undercut by weathering along their exposed vertical sides. The resulting morphology observed in the field is shown to follow the contours of the matric suction in a two-dimensional model of

saturated flow within a dolerite block.

The two volcanic tuffs investigated were both case-hardened but by different mechanisms. The differential weathering mechanism in the Bishop tuff was devitrification of the glassy matrix along joint planes to a depth of about a centimeter, whereas in the Towel Creek tuff dissolution of calcite from fossil fumerolic material and reprecipitation at the exterior surface of Tepees was the differential weathering mechanism.

From this study it can be seen that differential weathering depends upon many factors such as rock type, geologic history, exposure age, chemistry, pore water flow, environment and weathering processes. Each area must be investigated separately to determine the major factors responsible for the differential effects observed, and knowledge of the change in rock hardness with time is needed to distinguish between case hardening and core softening.

Figure 47 Cavernous weathering in the Mormon Rocks, San Bernadino, California, exhibiting extensive cavernous weathering. Scale is given by Mary Torregrossa (who stands 4' 11 $\frac{1}{2}$ " without boots).

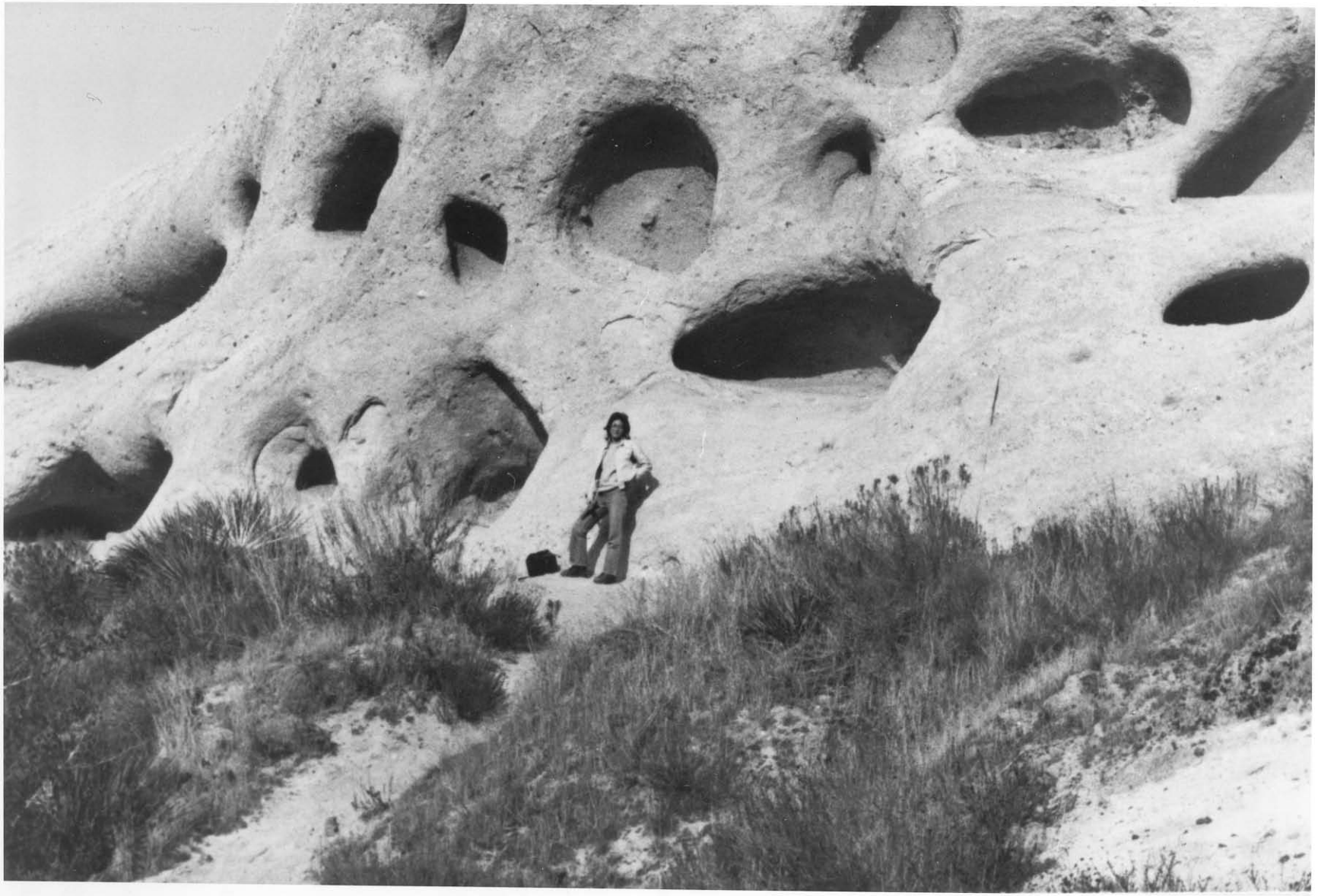

REFERENCES

1) Allen, A. D. (1962) "Formations of the Beacon Group in the Victoria Valley Region", N. Z. Jour. Geol. Geophys., vol. 5, p. 278 - 294.

2) Allen, A. D. and Gibson, G. W. (1962) "Outline of the Geology of the Victoria Valley Region", N. Z. Jour. Geol. Geophys., vol. 5, p. 234 - 242.

3) Anderson, A. L. (1931) "Geology and Mineral Resources of Eastern Cassia County", Idaho Bureau of Mines and Geology Bulletin, vol. 14, p. 56 - 61.

4) Antweiler, R. C. and Drever, J. I. (1983) "The Weathering of a Late Tertiary Volcanic Ash: importance of organic solutes", Geochim. Cosmochim. Acta, vol. 47, p. 623 - 629.

5) Archard, J. F. (1980) "Wear Theory and Mechanics",. Wear Control Handbook, Peterson and Winer (eds.), The American Society of Mechanical Engineers, New York, p. 35 - 80.

6) ASTM Standard D 1044-78. (1979) "Resistance of Transparent Plastics to Surface Abrasion", American Society for Testing and Materials. Philadelphia.

7) Augustithis, S. S. (1967) " On the Phenomenology and Geochemistry of Leaching and Element Agglutinates", Chemical Geology, vol. 2, p. 311 - 329.

8) van Autenboer, T. (1964) "The Geomorphology and Glacial Geology of the Sor-Rondone, Dronning Maud Land", Antarctic Geology, R. J. Adie, ed., North-Holland Pub. Co., Amsterdam, p. 81 - 103.

9) Avysuk, G. A., Markov, K. K., and Shumskiy, P. A. (1956) "Geographical observations on an Antarctic Oasis", National Commision International Geophysical Year 1957 - 58, Academy of Sciences, Antarctic Counsil, Moscow, U.S.S.R., 69 p.

10) Bailey, R. A., Dalrymple, G. B. and Lanphere, M. A. (1976) "Volcanism, Structure and Geochronology of Long Valley Caldera, Mono County, California", Jour. Geophys. Res., vol. 81, p. 725 - 744.

11) Berner, R. A. and Holdren, Jr., G. R. (1979) "Mechanism of Feldspar Weathering - II. Observations of feldspars from soils", Geochim. Cosmochim. Acta, vol. 43, p. 1173 - 1186.

12) Blackwelder, E. (1929) "Cavernous Rock Surfaces of the Desert", American Journal of Science, vol. 17, p. 393 - 399.

13) Boswell, C. R., Brooks, R. R. and Wilson, A. T. (1967) "Trace Element Content of Antarctic Lakes", Nature, vol. 213, p. 167 - 168.

14) Bowden, F. P. and Tabor, D. (1964) The Friction and Lubrication of Solids Part II. Oxford, 358 p.

15) Bradley, W. C., Hutton, J. T., and Twidale, C. R. (1978) "Role of Salts in development of granitic tafoni, South Australia", Journal of Geology, vol. 86, p. 647 - 654.

16) Bradley, W. C., Hutton, J. T., and Twidale, C. R. (1980) " Role of Salts in development of granitic tafoni, South Australia: A Reply", Journal of Geology, vol. 88, p. 121 - 122.

17) Brown, S. D. and Kistler, S. S. (1959) "Devitrification of High-SiO_2 Glasses of the System Al_2O_3-SiO_2", Jour. Amer. Ceramic Soc., vol. 42, p. 263 - 270.

18) Bryan, K. (1922) "Erosion and Sedimentation in Papago County, Arizona", United States Geological Survey Bulletin, vol. 730B, p. 19 - 90.

19) Bryan, K. (1923) "Pedestal Rocks in the Arid Southwest"' U.S. Geol. Surv. Bull. 760-A, p. 1 - 11.

20) Calkin, P. E. (1964) "Geomorphology and glacial geology of the Victoria Valley system, Southern Victoria Land, Antarctica", Ohio State Univ. Institute of Polar Studies Report, Number 10, 66 p.

21) Calkin, P. and Cailleux, A. (1962) "A quantitive study of cavernous weathering and its application to glacial chronology of Victoria Valley, Antarctica", Z. fer Geomorph., vol. 6, p. 317 - 324.

22) Cailleux, A. (1953) "Tafonis and alveolaire erosion", Cahiers Geologique Thoiry 16 - 17, p. 130 - 133.

23) Cailleux, A. and Calkin, P. (1963) "Orientation of Hollows in Cavernously Weathered Boulders in Antartica", Biuletyn Perglacjalny, nr 12. Lodz.

24) Charlesworth, L. J., Jr. (1959) "Case-hardening of the Hygiene Sandstone (Upper Cretaceous)", Compass, vol. 37, p. 19 - 28.

25) Claridge, G. G. C. (1965) "The Clay Mineralogy and Chemistry of Some Soils from the Ross Dependency, Antarctica", New Zealand J. Geol. Geophys. vol. 8, p. 186 - 220.

26) Claridge, G. G. C. and Campbell, I. B. (1968) "Origin of Nitrate Deposits", Nature, vol. 217, p. 428 - 430.

27) Claridge, G. G. C. and Campbell, I. B. (1977) "The Salts in Antarctic Soils, their Distribution and Relationship to Soil Processes", Soil Science, vol. 123, p. 377 - 384.

28) Conca, J. (1985) "Field and Laboratory Studies of Geologic Case Hardening", Antarctic Journal of the United States (in press).

29) Conca, J. and Cubba, R. (1985) "Abrasion Resistance Hardness Testing of Rock Material", submitted to the Internat. J. of Rock Mechanics and Mining Sciences.

30) Conca, J. and Rossman, G. R. (1982) "Case Hardening in Sandstone", Geology, vol 10, p. 520-523.

31) Conca, J. and Rossman, G. R. (1985) "Core Softening in Cavernously Weathered Tonalite", Jour. of Geology, vol. 93, p. 59 - 73.

32) Cooke, R. U. (1979) "Laboratory Simulation of Salt Weathering Processes in Arid Environments", Earth Surface Processes, vol. 4, p. 347 - 359.

33) Cooke, R. U. and Smalley, I. J. (1968) "Salt Weathering in Deserts", Nature, vol. 220, p. 1226 - 1227.

34) Cox, G. W. and Lawrence, W. T. (1983) "Cemented horizon in subarctic Alaskan sand dunes", Am. Jour. Sci., vol. 283, p. 369 - 373.

35) Dalrymple, (1980) "K-Ar Ages of Recent Rhyolites of the Mono and Inyo Craters, California", Earth and Planetary Science Letters, vol. 3, p. 289 - 298.

36) Day, M. J. and Goudie, A. S. (1977) "Field Assessment of Rock Hardness using the Schmidt Test Hammer", Brit. Geomorph. Res. Group Technical Bulletin, vol. 18, p. 19 - 29.

37) DeVore, G. W. (1958) "The surface chemistry of feldspars as an influence on their decomposition products", Proc. Nat. Conf. Clays and Clay Minerals, vol. 6, p. 26 - 41.

38) Dorn, R. I. and Oberlander, T. M. (1981) "Microbial Origin of Desert Varnish", Science, vol. 213, p. 1245 - 1247.

39) Dorn, R. I. and Oberlander, T. M. (1982) "Rock Varnish", Progress In Physical Geology, vol. 6, No. 3, p. 317 - 367.

40) Dragovich, D. J. (1967) "Flaking, a weathering process operating on cavernous rock surfaces", Geol. Soc. of Amer. Bull. 78, p. 801 - 804.

41) Dragovich, D. J. (1969) "The origin of cavernous surfaces (tafoni) in granitic rocks of southern South Australia", Z. Geomorph., vol. 13, p. 163 - 181.

42) Engel, C. G. and Sharp, R. p. (1958) "Chemical Data on Desert Varnish", Geological Society of America Bulletin, vol. 69, p. 487 -518.

43) Evans, A. G. and Marshall, D. B. (1980) "Wear Mechanics in Ceramics", Fundamentals of Friction and Wear of Materials, ASM, p. 439 - 452.

44) Evans, I. S. (1970) "Salt Crystallization and Rock Weathering: A Review", Revue de Geomorphologie Dynamique, vol. XIX, No. 4, p. 153 - 177.

45) Fahey, B. D. (1973) "An Analysis of Diurnal Freeze-thaw and Frost Heave Cycles in the Indian Peaks Region of the Colorado Front Range", Arctic and Alpine Research, vol. 5, p. 269 - 281.

46) Farmer, V. C. (1974) The Infrared Spectra of Minerals, Mineralogical Society Monograph 4, 539 p.

47) Farmer, V. C., Russel, J. D., McHardy, W. J., Newman, A. C. D., Alrichs, J. L. and Rimsaite, J. Y. H. (1971) "Evidence for loss of octahedral iron from oxidized biotites and vermiculites", Mineral. Magazine, vol. 38, p. 121 - 137.

48) Fischer, W. R. and Schwertmann, U. (1975) "The Formation of Hematite from Amorphous Iron(III)hydroxide", Clays and Clay Minerals, vol. 23, p. 33 - 37.

49) Friedman, I., Smith, R. L. and Long, W. D. (1966) "Hydration of Natural Glass and Formation of Perlite", Geol. Soc. Amer. Bull., vol. 77, p. 323 - 328.

50) Friedmann, E. I. (1982) "Endolithic Microorganisms in the Antarctic Cold Desert", Science, vol. 215, p. 1045 - 1053.

51) Furst M., Lowenstam, H. A. and Burnett D. S. (1976) "Radiographic study of the distribution of boron in recent mollusc shells", Geochimica et Cosmochimica Acta, vol. 40, p. 1381 - 1386.

52) Furst M. (1979) The Use of Boron Concentrations in Fossil Materials as a Paleosalinity Indicator, Ph D. Thesis, California Institute of Technology, Pasadena CA 91125, 187 p.

53) Fritz, S. J. and Ragland, P. C. (1980) "Weathering Rinds Developed on Plutonic Igneous Rocks in the North Carolina Piedmont", American Journal of Science, vol. 280, p. 546 - 559.

54) Gardner, W. R. (1959) "Solutions of the flow equation for the drying of soils and other porous media", Soil Sci. Soc. Amer. Proc., vol. 23,

p. 183 - 187.

55) Gardner, W. R. and Hillel, D. I. (1962) "The relation of external evaporative conditions to the drying of soils", J. Geophys. Res., vol. 67, p. 4319 - 4325.

56) Gastil, R. G., Phillips, R. P. and Allison, E. C. (1975) "Reconnaissance Geology of the State of Baja California", Geol. Soc. Am. Memoir 140, 170 p.

57) Gibson, G. W. (1962) "Evaporite Salts in the Victoria Valley Region", New Zealand J. Geol. Geophys., vol. 5, p. 361 - 374.

58) Gillespie, A. (1982) Quaternary Glaciation and Tectonism in the Southeastern Sierra Nevada, Inyo County, California (Chapter 3). PhD. thesis, California Institute of Technology, Pasadena, CA 91125, 695 p.

59) Glasby, G. P., McPherson, J. G., Kohn, B. P. Johnston, J. H., Keys, J. R., Freeman, A. G. and Tricker, M. J. (1981) "Desert Varnish in Southern Victoria Land, Antarctica", N. Z. Jour. geol. Geophys., vol. 24, p. 389 -397.

60) Goudie, A. (1974) "Further experimental investigation of rock weathering by salt and other mechanical processes", Z. Geomorph. N.F., Suppl. Bd 21, p. 1 - 12.

61) Grantz, A. (1976) "Sandstone caves (tafoni) in the central Santa Cruz Mountains, San Mateo County", California Geology, March, p. 51 - 54.

62) Green, W. H. and Ampt, G. A. (1911) "Studies on Soil Physics: I. Flow of air and water through soils", J. Agr. Sci., vol. 4, p. 1 - 24.

63) Grindley, G. W. and Warren , G. (1964) "Stratigraphic Nomencalture and Correlation in the Western Ross Sea Region", Antarctic Geology, SCAR Proceedings, Amsterdam, North-Holland Publishing Co., p. 314 - 333.

64) Haff, P. and Presti, D. (1982) "Barchan Dunes of the Salton Sea Region, California", (Preprint and personal communication).

65) Hildreth, W. (1979) "The Bishop Tuff: Evidence for the Origin of Compositional Zonation in Silicic Magma Chambers", Geol. Soc. Amer. Special Paper 180, pp. 43 - 75.

66) Hillel, D. (1971) Soil and Water Physical Principles and Properties, Academic Press, New York, 288 p.

67) Ireland, P. (1979) "Geomorphological variations of 'case-hardening' in Puerto Rico", Z. Geomorph. Suppl,-Bd., vol. 32, p. 9 - 20.

68) Jennings, J. N. (1968) "Tafoni", The Encyclopedia of Geomorphology, R. W. Fairbridge, ed., Reinhold Book Corp., vol. III, p. 1103 - 1104.

69) Johnston, J. H. (1972) "Salt Weathering Processes in the McMurdo Dry Valley Regions of South Victoria Land, Antarctica", New Zealand J. Geol. Geophys., vol. 16, p. 221 - 224.

70) Keller, W. D. (1957) The Principles of Chemical Weathering, 2nd ed., Lucas Bros., Columbia, Missouri, 111 p.

71) Kelly, W. C. and Zumberge, J. H. (1961) "Weathering of a quartz diorite at Marble Point, McMurdo Sound, Antarctica", Journal of Geology, vol. 69, p. 433 - 446.

72) Kiersch, G. A. (1950) "Navajo Sandstone, San Rafael Swell, Utah", AAPG Bull., vol. 34, p. 923 - 942.

73) King H. G. R. (1969) The Antarctic, Blandford Press, London, 276 p.

74) Kistler, R. (1966) "Structure and Metamorphism in the Mono Craters quadrangle, Sierra Nevada, California", S. S. Geological Survey Bull. 1221-E, 53 p.

75) Klute, A. (1965) "Laboratory Measurements of Hydraulic Conductivity of Saturated Soil", Methods of Soil Analysis, Amer. Soc. Agron., Monograph 9, p. 210 - 221.

76) Kny, E and Nauer, G. (1978) "On the Possibility of Devitrification of Ancient Glass", Jour. Non-Crystalline Solids, vol. 29, p. 207 - 214.

77) Lambe, T. W. and Whitman, R. V. (1969) Soil Mechanics, Wiley, New York, 553 p.

78) Langmuir, D. (1971) "Particle Size Effect on the Reaction Geothite = Hematite + Water", American Journal of Science, vol. 271, p. 147 - 156.

79) Lattman, L. H. (1973) "Calcium Carbonate Cementation of Alluvial Fans in Southern Nevada", Geological Society of America Bulletin, vol. 84, p. 3013 - 3028.

80) Lewis, R. E. (1983) Geology of the Hackberry Mt. Volcanic Center, Yavapai County, Arizona, PhD. Thesis, California Institute of Technology, Pasadena, CA 91125, 297 p.

81) Linkletter, G. O. (1970) "Weathering and Soil Formation in the Dry Valleys of Southern Victoria Land: a Possible Origin for the Salts in the Soils", in International Symposium on Antarctic Geology and Geophysics, Oslo, R. J. Adie (ed), Series B, no. 1, p. 441 - 446.

82) Longwell, C. R., Pampeyan, E. H., Bowyer, B., and Roberts, R. J. (1965) "Geology and Mineral Deposits of Clark County, Nevada", Nevada Bureau of Mines Bulletin 62, 210 p.

83) Loughnan, F. C. (1969) Chemical Weathering of the Silicate Minerals, American Elsevier Publishing Co., New York, 154 p.

84) Malin, M. (1974) "Salt Weathering on Mars", Jour. of Geophys. Res., vol. 79, p. 3888 - 3894.

85) Marchand, D. E. (1974) "Chemical weathering, soil development, and geochemical fractionation in a part of the White Mountains, Mono and Inyo Counties, California", U.S.G.S. Prof. Paper 352-J, p. 379 - 424.

86) Martini, I. P. (1978) "Tafoni weathering, with examples from Tuscany, Italy", z. geomorph. N. F., vol. 22, p. 44 - 67.

87) Matalon, R. and Packter, A. (1955) "The Liesegang Phenomenon. I." Journal of Colloid Science, vol. 10, p. 46 - 62.

88) McCraw, J. D. (1967) "Soils of Taylor Dry Valley, Victoria Land, Antarctica, with notes on soils from other localities in Victoria Land", N. Z. Jour. Geol. Geophys., vol. 10, p. 498 - 539.

89) McDonald, G. A. (1972) Volcanoes, Prentice Hall, Inc., Englewood Cliffs, N. J., 510 p.

90) McGinnies, W. C., Goldman, B. J., and Paylore, P. (eds), (1968) "Deserts of the World, an appraisal of research into their physical and biological environments", University of Arizona Press, Tuscon, 788 p.

91) McKelvey, B. C. and Webb, P. N. (1962) "Geologic Investigations in Southern Victoria Land, Antarctica", New Zealand J. Geol. Geophys., vol. 5, p. 143 - 162.

92) Mehrotra, P. K. (1983) "Mechanisms of Wear in Ceramic Materials",. Wear of Materials, ASME, p. 194 - 201.

93) Morel, F. M. M. (1983) Principles of Aquatic Chemistry, John Wiley and Sons, New York, 446 p.

94) Morgan, J. J. and Stone, A. (1984) "Kinetics of Chemical Processes of Importance in Lacustrine Environments", in Chemical Processes in Lakes, W. Stumm (ed.), Wiley Interscience.

95) Mukherjee, S. P., Zarzycki, J., Badie, J. M. and Traverse, J. P. (1976) "Influence of Hydroxyl Groups on the Crystallization of Lanthanum Silicate Glass", Jour. Non-Crystalline Solids, vol. 20, p. 455 - 458.

96) Mustoe, G. E. (1982) "The Origin of Honeycomb Weathering", Geol. Soc. of Am. Bull., vol. 93, p. 108 - 115.

97) Nahon, D., Janot, C., Karpoff, A. M. Paquet, H. and Tardy, Y. (1977) "Mineralogy, Petrography and Structures of Iron Crusts (Ferricretes) Developed on Sandstones in the Western Part of Senegal", Geoderma, vol. 19, p. 263 - 277.

98) Neall, V. E. and Smith, I. E. (1967) "The Mcmurdo Oasis", Tuatara, 15 (3),

p. 117 - 128.

99) Norton, D. and Knapp, R. (1977) "Transport Phenomena in Hydrothermal Systems: the nature of porosity" Amer. J. Sci., vol. 277, p. 913 - 936.

100) Ollier, C. D. and Tuddenham, W. G. (1962) "Inselbergs of Central Australia", Z. Geomorph., vol. 5, p. 257 - 276.

101) Packter, A. (1956a) "The Liesegang Penomenon. II," Journal of Colloid Science, vol. 11, p. 96 - 106.

102) Packter, A. (1956b) "The Liesegang Phenomenon. III," Journal of colloid Science, vol. 11, p. 150 - 157.

103) Pewe, T. L. (1960) "Multiple Glaciation in the McMurdo Sound Region, Antarctica - A Progress Report", Journal of Geology, vol. 68, p. 498 - 514.

104) Pewe, T. L. (1974) "Geomorphic Processes in Polar Deserts", Polar Deserts and Modern Man, Smiley and Zumberge, eds. University of Arizona Press, Tuscon, p. 33 - 52.

105) Potter, R. M. and Rossman, G. R. (1977) "Desert Varnish: the importance of clay minerals", Science, vol. 196, p. 1446 - 1448.

106) Potter, R. M. (1979) The Tetravalent Manganese Oxides: clarification of their structural variations and relationships, and characterizations of their occurrence in the terrestrial weathering environment as desert varnish and other manganese oxide concentrations, Ph. D. Thesis. California Institute of Technology, Pasadena, CA 91125, 245 p.

107) Prebble, M. M. (1967) "Cavernous weathering in Taylor Dry Valley, Victoria Land, Antarctica", Nature, vol. 216, p. 1194 - 1195.

108) Putnam, W. C. (1949) "Quaternary Geology of the June Lake District, California", Geol. Soc. Amer. Bull., vol. 60, p. 1281 - 1302.

109) Rabinowicz, E. (1965) Friction and Wear of Materials. John Wiley and Sons, New York, 244 p.

110) Reiche, P. (1950) "A survey of weathering processes and products", Univ. New Mexico Publ. in Geology, vol. 3.

111) Rice, A. (1976) "Insolation Warmed Over", Geology, vol. 4, p. 61 -62.

112) Roth, E. S. (1964) "Temperature and Water Content as Factors in Desert Weathering", Jour. of Geology, vol. 73, p. 454 - 468.

113) Sekyra, J. (1972) "Forms of Mechanical Weathering and their Significance in the Stratigraphy of the Quaternary in Antarctica", Antarctic Geology and Geophysics, R. J. Adie, ed., Universitets-forlaget, Oslo, p. 669 - 674.

114) Selby, M. J. (1971) "Salt Weathering of Landforms and an Antarctic Example", Proc. Sixth Geography Conf., New Zealand Geographical Society (Inc.), Christchurch, p. 30 - 35.

115) Selby, M. J. (1972) "Antarctic Tors", Z. Geomorph. Suppl. Band 13, p. 73 - 86.

116) Selby, M. J. (1977) "On the origin of sheeting and laminae in granitic rocks: evidence from Antarctica, the Namib Desert and the central Sahara", Madoqua, vol. 10, No. 3, p. 171 - 179.

117) Selby, M. J. and Wilson, A. T. (1971) "The Origin of the Labyrinth, Wright Valley, Antarctica", Geol. Soc. Amer. Bull., vol. 82, p. 471 - 476.

118) Sheridan, M. (1965) The Mineralogy and Petrology of the Bishop Tuff, Ph.D. Thesis, Stanford University, 165 p.

119) Shvartzev, S. L. and Bazhenov, V. A. (1978) "Geochemical conditions for the formation of Illite in weathering-crust products", Geochemistry International, vol. 15, No. 2, p. 49 - 56.

120) Smith, B. J. (1978) "The origin and geomorphic implications of cliff foot recesses and tafoni on limestone hamalas in the northwest Sahara", Z. Geomorph, N. F., vol. 22, p. 21 - 43.

121) Snoeyink, V. L. and Jenkins, D (1980) Water Chemistry, John Wiley and Sons, New York, 463 p.

122) Stumm, W. and Morgan, J. J. (1981) Aquatic Chemistry, John Wiley and Sons, New York, 780 p.

123) Swartzendruber, D. (1969) "The Flow of Water in Unsaturated Soils", In Flow Through Porous Media, R. J. M. DeWiest (ed), Academic Press, New York, p. 215 - 287.

124) Twidale, C. R. and Bourne, J. A. (1976) "The Shaping and Interpretation of Large Residual Granite Boulders", Journal of the Geol. Soc. of Australia, vol. 23, part 4, p. 371 - 381.

125) Van de Kamp, P. C. (1973) "Holocene continental sedimentation in the Salton Basin, California: A reconnaissance." GSA Bull., vol. 84, p. 827 - 848.

126) Wagstaff, F. E., Brown, S. D. and Cutler, I. B. (1964) "The Influence of H_2O and O_2 Atmospheres on the Crystallization of Vitreous Silica", Phys. Chem Glasses, vol. 5, p. 76 - 81.

127) Walker, T. (1967) "Formation of Red Beds in Modern and Ancient Deserts", Geological Society of Am. Bull., vol. 78, p. 353 - 368.

128) Walker, T., Waugh, B. and Grone, A. J. (1978) "Diagenesis in first-cycle desert alluvium of Cenozoic age, southwestern United States and northwestern Mexico", Geological Society of Am. Bull., vol. 89, p. 19 - 32.

129) Wellman, H. W. and Wilson, A. T. (1965) "Salt weathering, A Neglected Geological Erosive Agent in Coastal and Arid Environments", Nature, vol. 205, p. 1097 - 1098.

130) Weyl, P. K. (1959) "Pressure Solution and the Force of Crystallization", J. Geophys. Res., vol. 64, p. 2001 - 2025.

131) Whalley, W. W. B and McGreevy, J. P. (1983) "Weathering", Progress in Physical Geography, vol. 7, p. 559 - 586.

132) Whipple, E. R. (1974) "A Study of Wilson's Determination of Ferrous Iron in Silicates", Chemical Geology, vol. 14, p. 223 - 238.

133) White, W. A. (1944) "Geomorphic Effects of Indurated Veneers on Granites in the Southeastern States", Journal of Geology, vol. 52, p. 33 - 341.

134) White, S. E. (1976) "Is Frost Action Really Only Hydration Shattering? A Review", Arctic and Alpine Research, vol. 8, p. 1 - 6.

135) Whitney, M. I. (1978) "The role of vorticity in developing lineation by wind erosion", Geological Society of Am. Bull., vol. 89, p. 1 - 18.

136) Wilhelmy, H. (1964) "Cavernous rock surfaces in semi-arid and arid climates", Pakistan Geogr. Rev., vol. 19, p. 8 - 13.

137) Wilson, M. J. and Farmer, V. C. (1970) "Study of Weathering in a Soil Derived from a Biotite-Hornblende Rock", Clay Minerals, vol. 8, p. 435 - 444.

138) Wilson, M. J. and Jones, D. (1983) "Lichen Weathering of Minerals: implications for pedogenesis", in Residual Deposits: Surface Related Weathering Processes and Materials, R. C. L. Wilson (ed.), Blackwell Scientific Publications, Oxford, p. 5 - 12.

139) Winkler, E. M. (1980) "Role of Salts in Development of Granitic Tafoni, South Australia: A Discussion", Journal of Geology, vol. 88, p. 119 - 120.

140) Yariv, S. and Cross, H. (1979) Geochemistry of Colloid Systems, Springer-Verlag, New York, 450 p.

APPENDICES

APPENDIX 1

INFRARED SPECTROSCOPY OF FOUR HYDRATED BORATES

James L. Conca

May 25, 1981

INTRODUCTION

Infrared absorption spectra of four hydrated borates (two calcium borates and two sodium borates) were obtained in the 4000 - 400 cm^{-1} range. Table 1 lists the chemistry and structure of each hydrated borate. The purpose of this study is to determine if there is an effect on the IR absorption due to polymerization of isolated polyanions into chains of polyanions. Polymerization and the resulting loss of H_2O are the only difference in chemistry between members of each chemical group, i.e., between Colemanite and Meyerhofferite and between Kernite and Tincalconite.

0.50 mg of each mineral was incorporated into a KBr pellet and spectra were taken with a Perkin - Elmer Model 180 Infrared double - beam spectrophotometer. Use of the same sample concentrations for each mineral allows direct comparison of peak heights in the spectra.

BORATE ABSORPTIONS AND SYMMETRY

The hydrated borates studied are composed of ring polyanion groups consisting of BO_3 triangles and BO_4 tetrahedra sharing corners to form the ring. The expected vibrational modes from each type of boron polyhedra will be different. Ideally, BO_3 triangles have D_{3h} symmetry, while BO_4 tetrahedra have T_d symmetry. Within the crystal structure the geometries are distorted to the point where the polyhedra have actual symmetry of C_1. However, the distortions are not so great that the predicted absorption bands cannot be roughly assigned, although detailed Group Theoretical analysis is beyond the scope of this study. It is suggested by the spectra that the degree of deviation from ideal symmetry is

reflected in the band position and intensity.

The fundamental modes of vibration for the BO_3 triangle are as follows:

Representation	Symbol	Vibration	approximate position for the ideal case
A_1'	ν_1	symmetric stretch	950 cm^{-1}
A_2''	ν_2	out-of-plane bend	750 cm^{-1}
E'	ν_3	asymmetric stretch	1250 cm^{-1}
E'	ν_4	in-plane bend	600 cm^{-1}

The following fundamental modes of vibration for the BO_4 tetrahedra have not been well determined:

Representation	Symbol	Vibration	approximate position for the ideal case
A_1	ν_1	symmetric stretch	below 950 cm^{-1}
E	ν_2	bend	below 600 cm^{-1}
F_2	ν_3	asymmetric stretch	$\approx$ 1000 cm^{-1}
F_2	ν_4	bend	$\approx$ 600 cm^{-1}

HYDRATED CALCIUM BORATES

The polyanion in Meyerhofferite consists of one BO_3 triangle and two BO_4 tetrahedra cornersharing in a 6-membered ring (Christ et al., 1958). All oxygens not part of the ring strucure itself are actually hydroxyl groups. The large polyanions are linked through calcium-oxygen bonds to form zigzagging strings along (001). The calcium is in an extremely distorted octahedra with an additional oxygen and hydroxyl coordinating at larger distances. Adjacent strings are linked only through hydrogen bonds.

In Colemanite, the same polyanions are linked by corner-sharing between a BO_3 triangle of one polyanion and a BO_4 tetrahedra of the next polyanion forming infinite chains along (001). Adjacent chains are linked by hydrogen bonding.

Table 2 and Figures 1 through 4 show the infrared absorption spectra for both calcium borates. (Note the different absorbance scales for different spectra). The spectra are complex and band-for-band correlations are difficult. However, gross features may be correlated. The large absorptions in the region from 1300 - 1400 cm^{-1} are due primarily to the BO_3 asymmetric stretch (ν_3). The large absorptions in the region from 900 - 1000 cm^{-1} are due to the tetrahedral BO_4 ν_3 and the ν_1 of both polyhedra. From 1000 - 1150 cm^{-1}, OH in-plane bending is the major absorber.

The overall shifting toward lower energies of the ν_3 bands for both polyhedra in Colemanite may be due to the loss of hydroxyl groups upon polymerization and coupling of the anions (Weir, 1966). A more direct effect of the loss of hydroxyl groups on the infrared spectra due to polymerization may be the decrease in the absorptions over the range 1050 - 1150 cm^{-1} when going from Meyerhofferite to Colemanite. All OH bonded to trigonal boron in Meyerhofferite is completely gone in the polymerized chains of Colemanite, as well as half of the OH bonded to one of the tetrahedral borons. However, the number of hydroxyls bonded to the other type of tetrahedral boron is unaffected by polymerization. If we look at the region from 1000 - 1150 cm^{-1} pertaining to the OH in-plane bending, we see in Meyerhofferite three prominent absorptions at 1120 cm^{-1}, 1085 cm_{-1}, and 1020 cm^{-1}. Polymerization into Colemanite results in a dramatic decrease in the absorption at 1120 cm^{-1}, a significant decrease in the band at 1085 cm^{-1} with a slight shift to 1070 cm^{-1}, while the band at 1020 cm^{-1}

shows hardly any change in peak height but is slightly shifted to 1040 cm^{-1}. This is consistent with (but not proof of) the idea that the absorption at 1120 cm^{-1} corresponds to the trigonal boron OH in-plane bending, the absorption at 1085 cm^{-1} corresponds to the OH in-plane bending in the tetrahedral boron that is involved in polymerization (with loss of half its OH groups), and the absorption at 1020 cm^{-1} corresponds to the OH in-plane bending of the tetrahedral boron that is not involved in polymerization.

A related phenomenon can be seen in the region from 3400 - 3600 cm^{-1}. In the Meyerhofferite spectra three absorption bands corresponding to three different OH stretching occur at 3440 cm^{-1}, 3490 cm^{-1}, and 3600 cm^{-1}. Polymerization in Colemanite has resulted in the elimination of the band at 3440 cm^{-1}, dramatic decrease in the band at 3490 cm^{-1} and shifting to 3520 cm^{-1}, and little effect on the band at 3600 cm^{-1}. These observations mirror the effects at the lower energies.

Another effect of polymerization is the restriction and removal of certain out-of-plane OH bending, which may account for the noticeable absence of absorption peaks for Colemanite in the region from 500 - 800 cm^{-1}.

One of the most notable differences between the two spectra is that in Colemanite the region from 1300 - 1400 cm^{-1} has sharper absorptions, higher absorption peaks, and less splitting than in Meyerhofferite. Also the band positions are shifted to lower energies in Colemanite. This is in disagreement with Weir, 1966, who observed broader and more complex absorptions for Colemanite in the region. However, this same sharpening and increase in peak height is seen going from Tincalconite to the polymerized Kernite (Figures 7 and 8) in the present study.

Polymerization of the borate polyanions in the case of the calcium borates in this study results in a more symmetric BO_3 triangle than in Meyerhofferite. Because the oxygens in the B-O bonds in the BO_3 triangles in Colemanite are all bonded to boron in other BO_4 tetrahedra, the B-O bond lengths for the three B-O bonds in BO_3 are all closer to the mean bond length (within 0.015 Å) than in Meyerhofferite. In the latter, two of the three oxygens in the B-O bonds of the BO_3 triangles are bonded to boron in BO_4 tetrahedra. The other oxygen is bonded to H which is hydrogen-bonded to H_2O and to an oxygen on another polyanion. This results in a slightly wider range in the triangular B-O bond lengths (within 0.030 Å of the mean value) and a greater asymmetry to the polyhedra.

The closer approach of the BO_3 in Colemanite to the D_{3h} symmetry over that in Meyerhofferite may account for two differences in their spectra. Normally, in the ideal case, ν_3 of the BO_3 triangle is doubly degenerate (as is ν_4). The distortions in the crystal environment has removed the degeneracy and produced the two major absorptions in the region. However, the "higher" symmetry situation in Colemanite has resulted in less splitting of the ν_3 mode for BO_3 in this region. The band position for ν_3 in Colemanite (1335, 1367 cm^{-1}) is closer to the ideal BO_3 position of 1250 cm^{-1} than is the case for Meyerhofferite (1360, 1400 cm^{-1})

HYDRATED SODIUM BORATES

Kernite and Tincalconite show many of the same features and effects of polymerization as for the calcium borates (Figures 7 through 10). However, even more complexities arise in the structure and spectra of the sodium borates, and this study will not discuss them further than to include their spectra for comparison with the calcium borates.

REFERENCES

1) Christ, C.L., et al., 1958, Acta Cryst., 11, 761.

2) Christ, C.L. and Clark, J.R., 1960, Z. Krist., 114, 321.

3) Christ, C.L. and Clark, J.R., 1977, Phys. Chem. Minerals, 2, 59.

4) Cooper, W.F., et al., 1973, Am. Min., 58, 21.

5) Farmer, V.C., 1974, The Infrared Spectra of Minerals, Mineralogical Society Monograph 4, 205.

6) Giacovazzo, C., et al., 1973, Am. Min., 58, 523.

7) Hornig, D.F., and Plumb, R.C., 1957, J. Chem. Phys., 26, 637.

8) Weir, C.E., 1966, J. of Research N.B.S. A, 70A, 153.

TABLE 1 Description of Samples

Mineral	Formula	Structure*	Locality
Colemanite	$Ca[B_3O_4(OH)_3] \cdot H_2O$	3: Δ +2T chains	Thompson Mine Death Valley, CA
Meyerhofferite	$Ca[B_3O_3(OH)_5] \cdot H_2O$	3: Δ +2T isolated	20-Mule Team Canyon Death Valley, CA
Kernite	$Na_2[B_4O_6(OH)_2] \cdot 3H_2O$	4:2 Δ +2T chains	Open Pit Mine Boron, CA
Tincalconite	$Na_2[B_4O_5(OH)_4] \cdot 3H_2O$	4:2 Δ +2T isolated	Searles Lake, CA

*according to Christ and Clark, 1977.

TABLE 2 Infrared Absorption Spectra of Four Hydrated Borates

Colemanite(cm^{-1})	Meyerhofferite(cm^{-1})	Kernite(cm^{-1})	Tincalconite(cm^{-1})
3600 s	3600 s	3545 s	
3520 mb		3400 sb	3460 msh
	3490 m	3350 svb	3330 sb
	3440 vs		
3250 svb	3310 svb		
		1470 msh	1475 s
1455 wsh		1420 wsh	1425 m
1430 wsh	1440 msh		1400 m
1367 vs	1400 s		1385 m
	1385 m	1365 vs	1350 s
1335 vs	1360 vs	1335 msh	
1320 vwsh	1335 vwsh		1280 m
1275 msh	1270 msh		1255 m
1230 m	1225 msh		1220 wsh
1155 msh	1150 wsh		1160 vwsh
1120 m	1120 s	1155 msh	
			1130 s
1070 msh	1085 s	1130 w	
	1040 wsh		1075 m
1040 s	1020 s	1065 ssh	1025 ssh
1025 wsh		1015 vs	1000 vs
950 msh		970 vs	
940 vs		950 ssh	
	970 s		945 s
	945 msh	875 m	880 w
900 vs	905 s	825 m	830 s
865 vwsh	845 wsh		775 w
815 w	810 m	765 wb	
790 wsh		740 w	
760 s	760 m	725 w	
730 m	727 m		710 m
695 w	680 m	690 m	
670 w	665 vwsh	650 wb	
625 vw	615 w		650 wvb
605 vw	605 vwsh	615 w	
580 m	580 m		605 w
550 w	550 vw	570 vw	
	530 vw	550 m	
515 w			520 vwb
495 vw	495 vw	495 wb	
	470 w	455 w	460 m
430 wb	430 wb		

s=strong m=medium w=weak b=broad sh=shoulder v=very

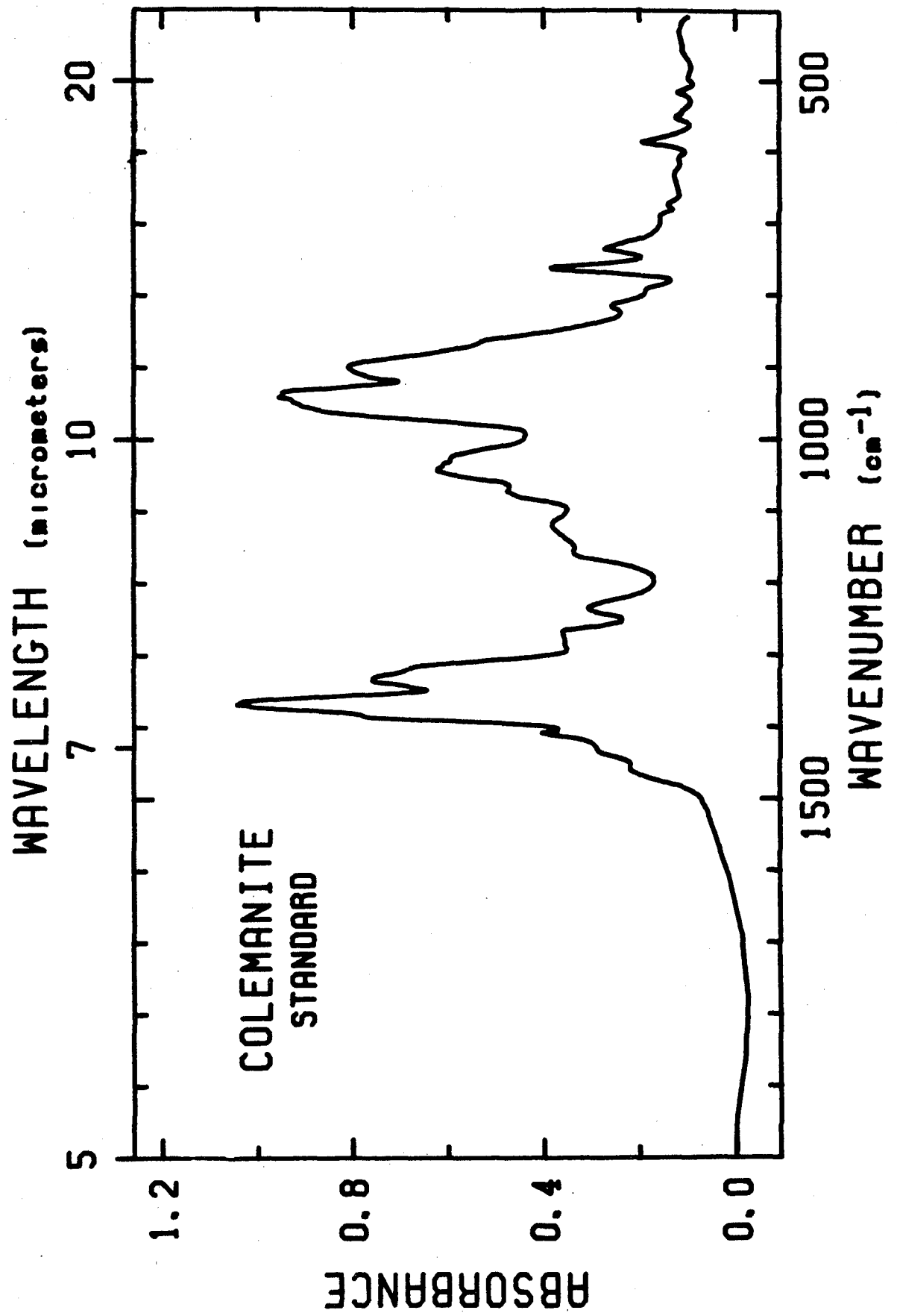
ABSORBANCE
1.2
0.8
0.4
0.0
WAVELENGTH (micrometers)
5
7
10
20
WAVENUMBER (cm-1)
1500
1000
500
COLEMANITE
STANDARD

FIGURE 1

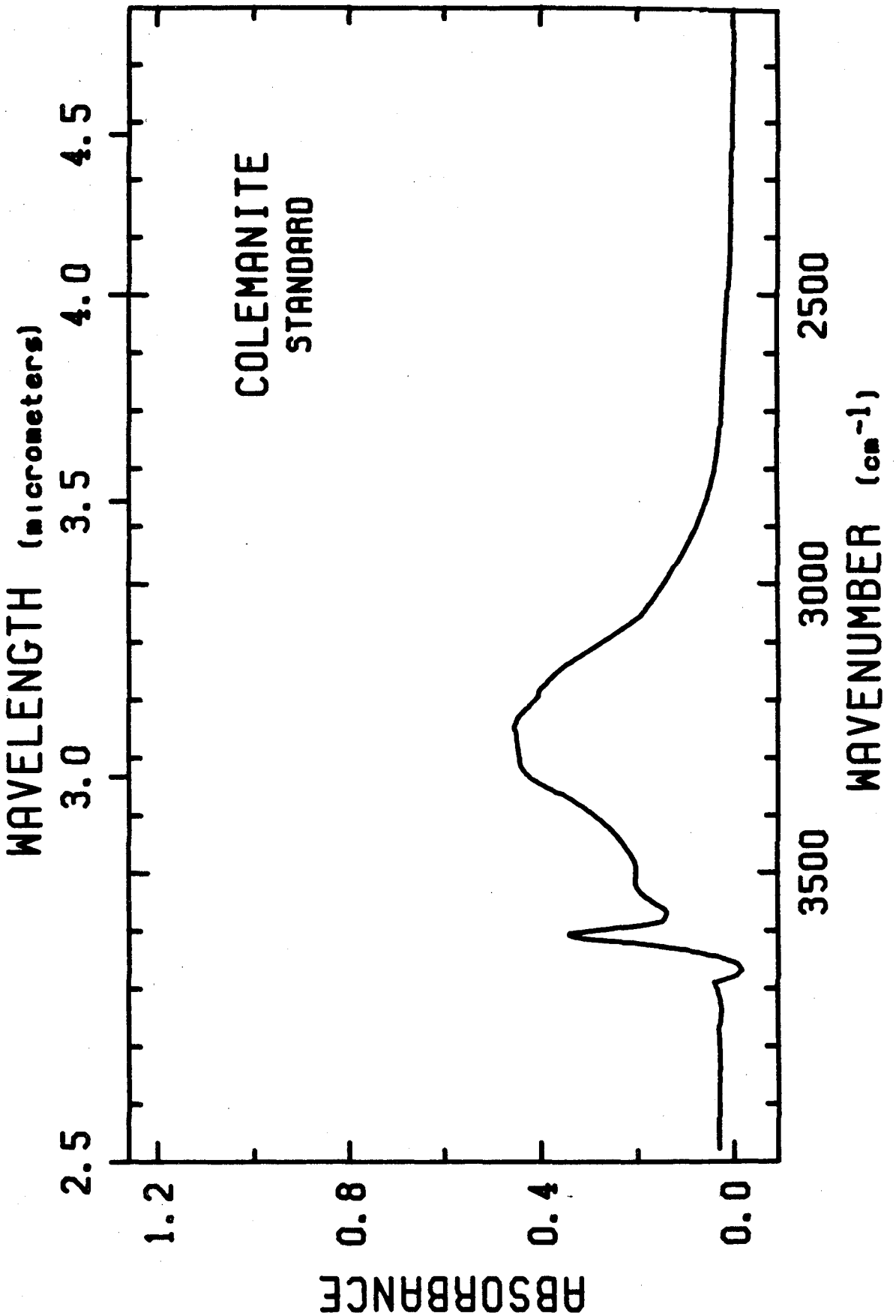
COLEMANITE
STANDARD
WAVELENGTH (micrometers)
2.5
3.0
3.5
4.0
4.5
WAVENUMBER (cm⁻¹)
3500
3000
2500
ABSORBANCE
0.0
0.4
0.8
1.2

FIGURE 2

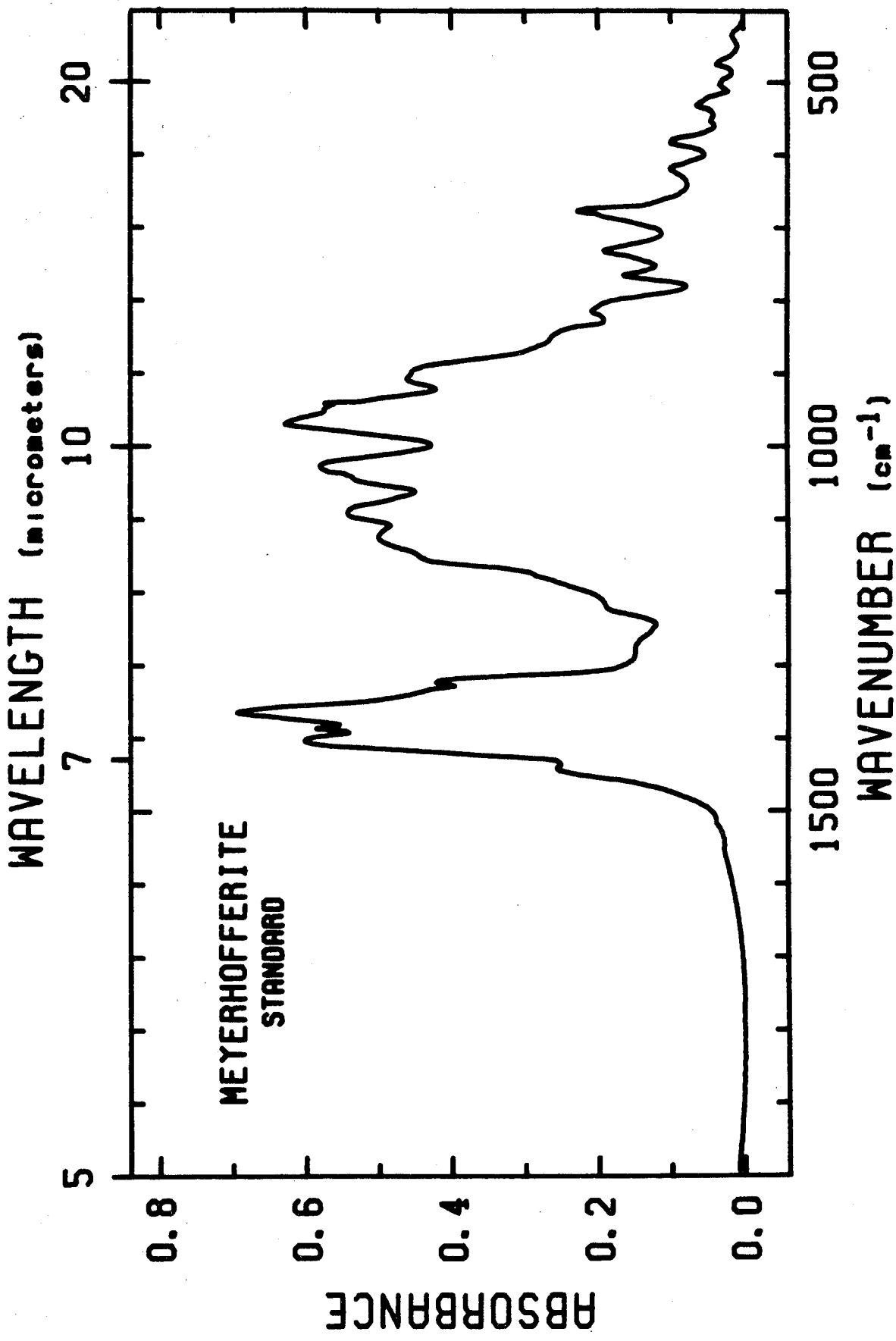
ABSORBANCE
0.0
0.2
0.4
0.6
0.8
WAVELENGTH (micrometers)
5
7
10
20
WAVENUMBER (cm⁻¹)
1500
1000
500
MEYERHOFFERITE
STANDARD

FIGURE 3

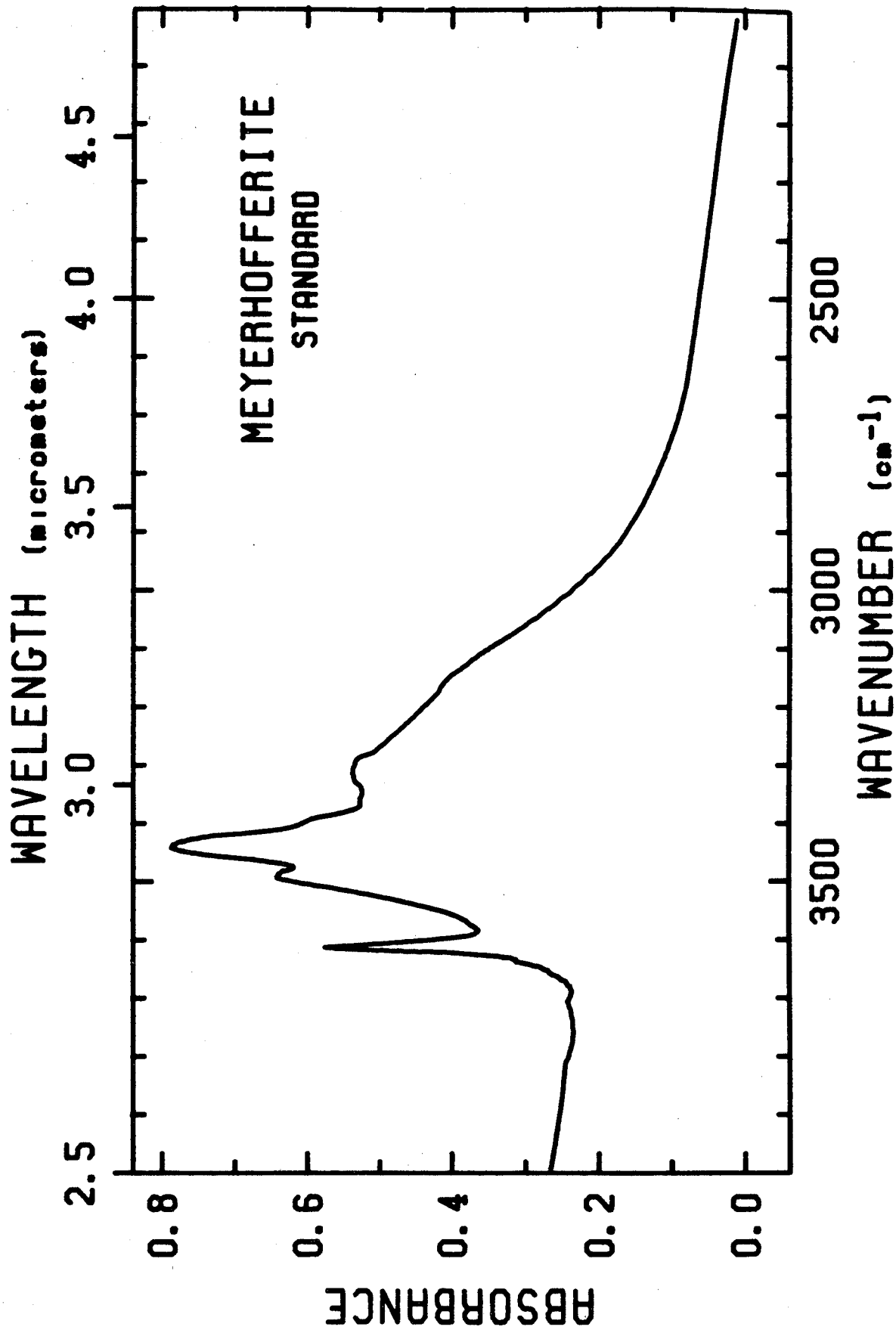
MEYERHOFFERITE
STANDARD
WAVELENGTH (micrometers)
2.5
3.0
3.5
4.0
4.5
WAVENUMBER (cm⁻¹)
3500
3000
2500
ABSORBANCE
0.0
0.2
0.4
0.6
0.8

FIGURE 4

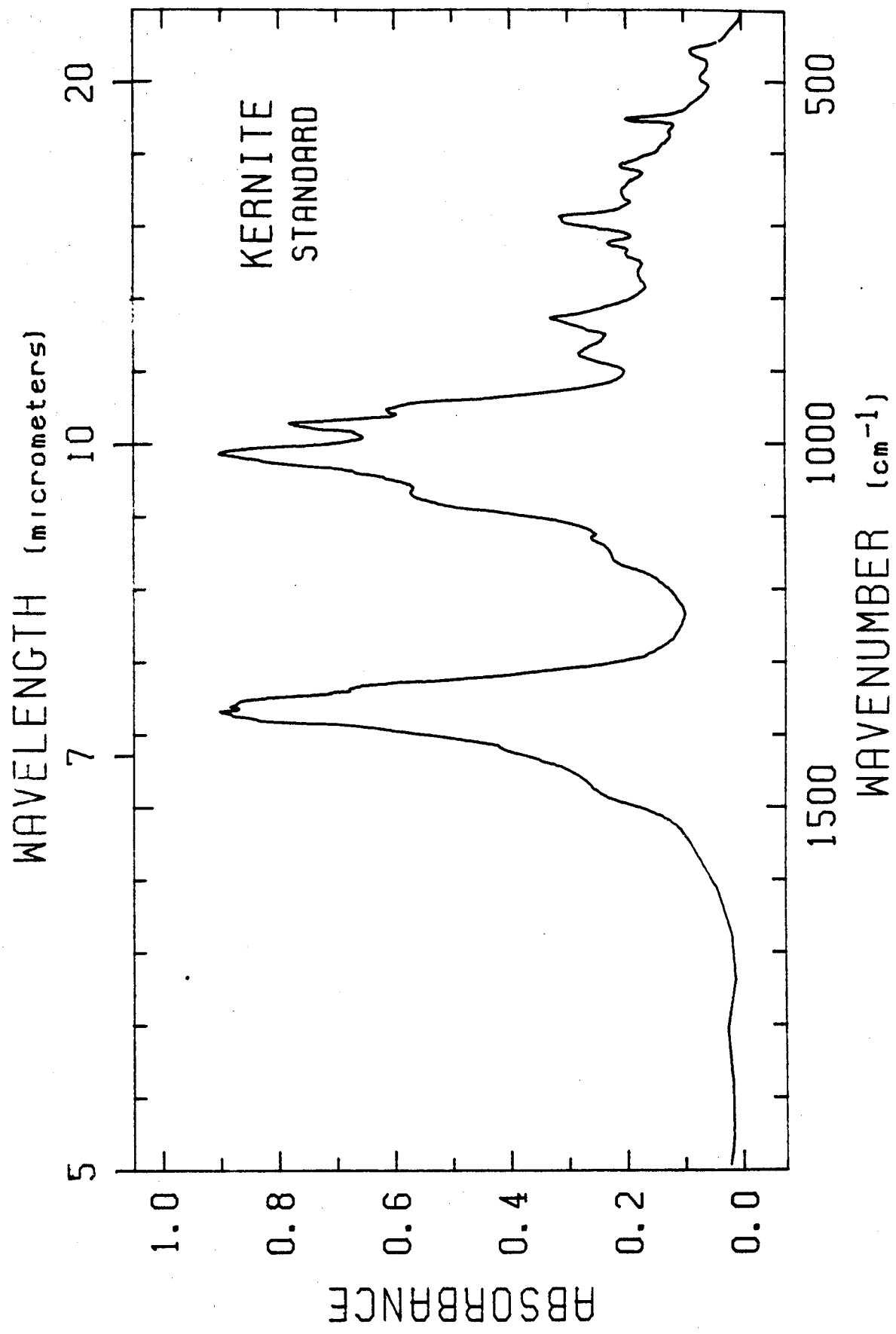
KERNITE
STANDARD
WAVELENGTH (micrometers)
5
7
10
20
WAVENUMBER (cm⁻¹)
1500
1000
500
ABSORBANCE
0.0
0.2
0.4
0.6
0.8
1.0

FIGURE 5

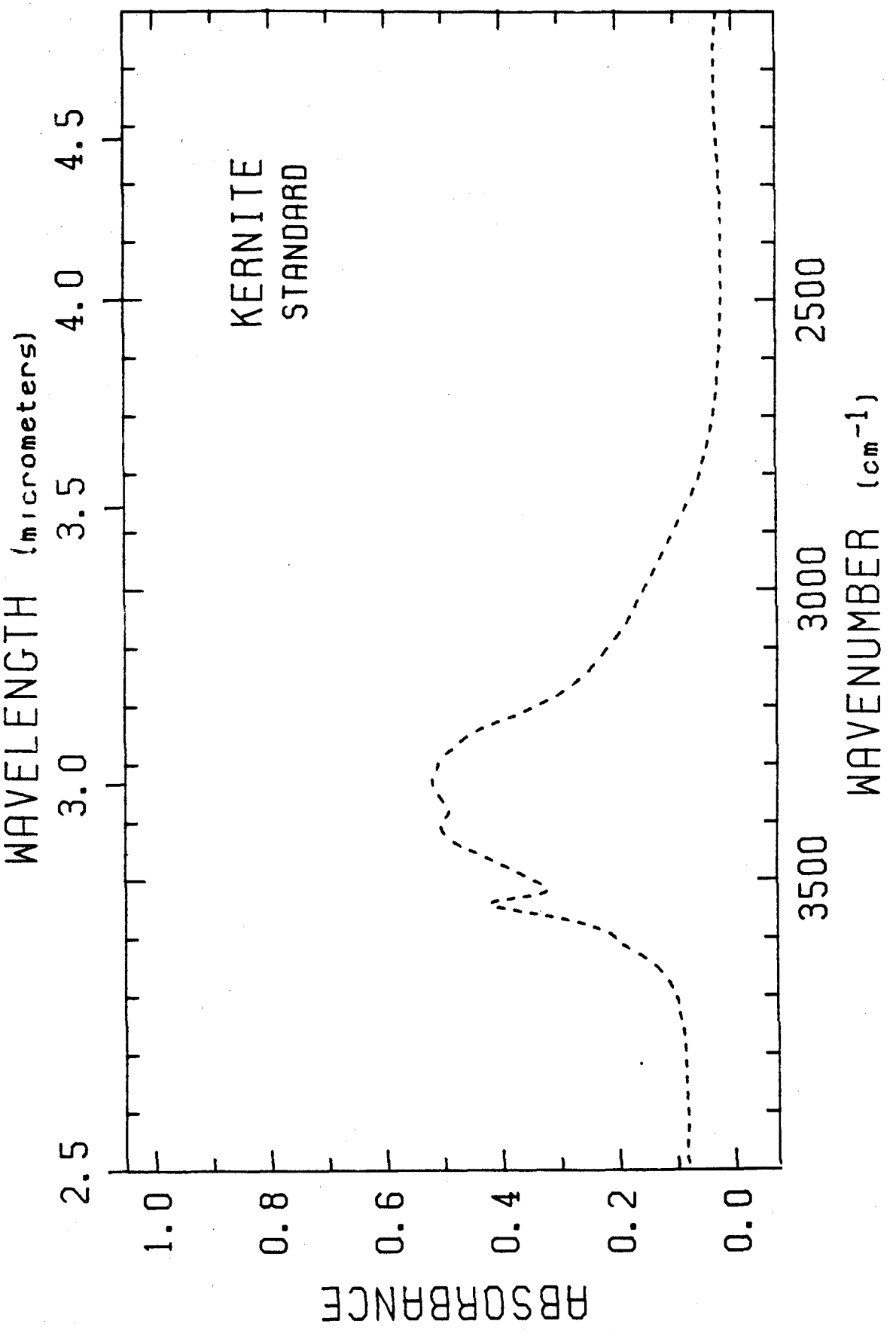
KERNITE
STANDARD
WAVELENGTH (micrometers)
2.5
3.0
3.5
4.0
4.5
WAVENUMBER (cm⁻¹)
3500
3000
2500
ABSORBANCE
0.0
0.2
0.4
0.6
0.8
1.0

FIGURE 6

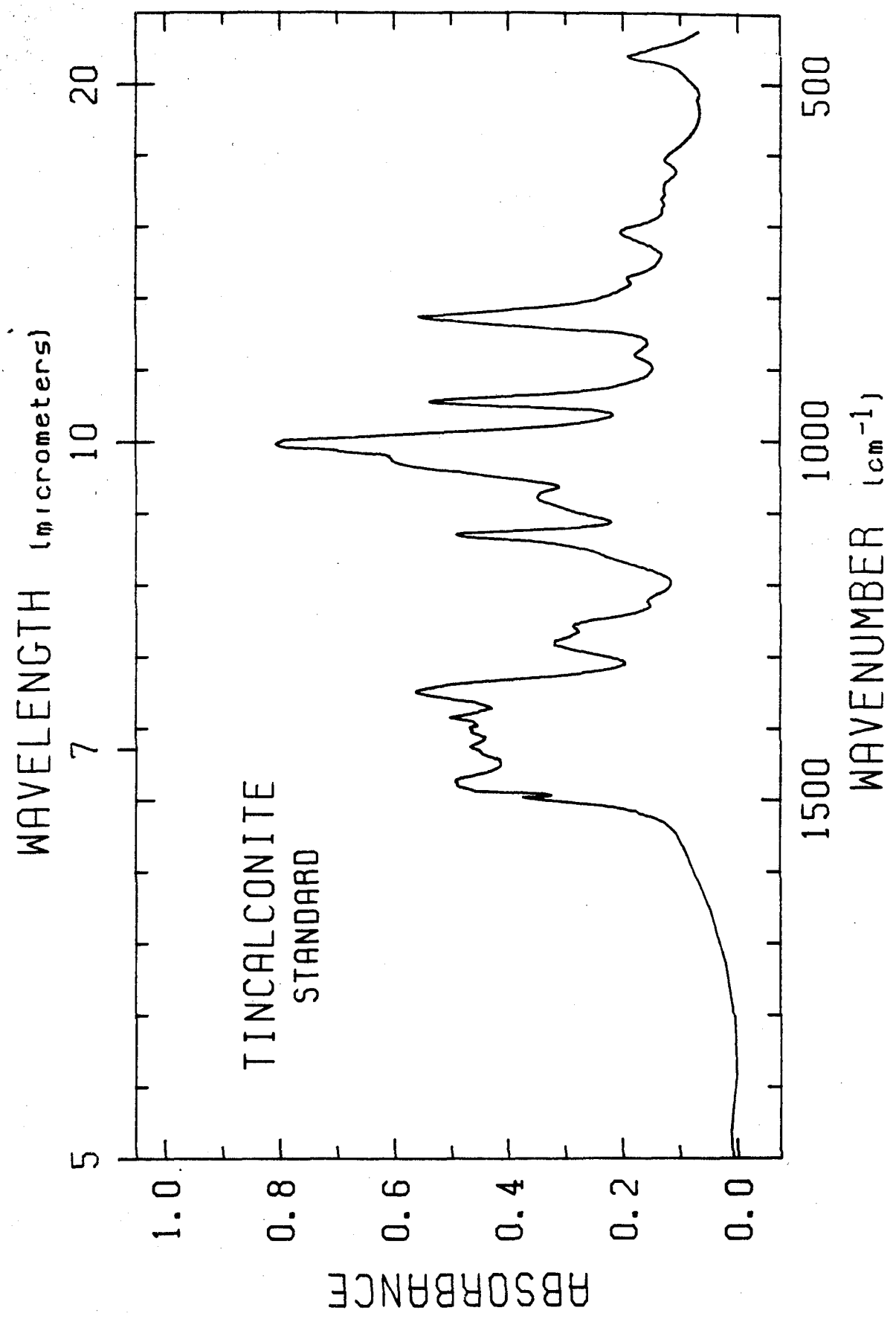
WAVELENGTH (micrometers)
5
7
10
20
WAVENUMBER (cm^{-1})
1500
1000
500
ABSORBANCE
0.0
0.2
0.4
0.6
0.8
1.0
TINCALCONITE
STANDARD

FIGURE 7

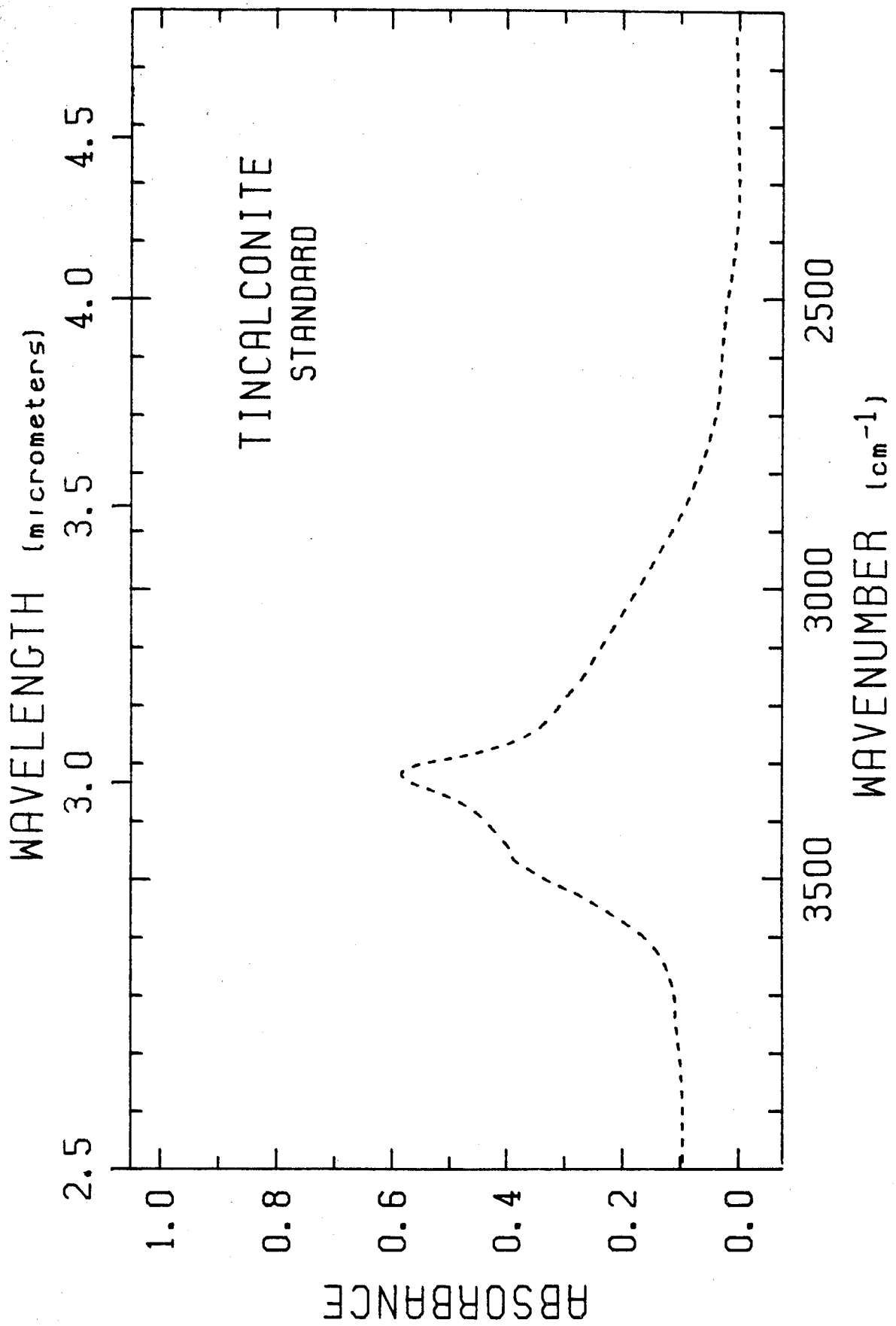
TINCALCONITE
STANDARD
WAVELENGTH (micrometers)
2.5
3.0
3.5
4.0
4.5
WAVENUMBER (cm^{-1})
3500
3000
2500
ABSORBANCE
0.0
0.2
0.4
0.6
0.8
1.0

FIGURE 8

APPENDIX 2

SOLUTION TO THE LAPLACIAN FOR THE

LABYRINTH BOUNDARY CONDITIONS

James L. Conca

January 1985

The Labyrinth boundary conditions are given in Figure 1, for saturated, steady-state flow of water through a dolerite boulder. For the condition that $\nabla^2\psi = 0$ let:

$$\psi(x,z) = Az^2 + \phi(x,z) \qquad \text{so that} \qquad \nabla\phi^2 = -2A$$

The boundary conditions for the top and bottom surfaces of the boulder are then:

$$\frac{\partial\psi}{\partial z}(x,0) = \frac{\partial\phi}{\partial z}(x,0) = 0$$

$$q = q_o = -K\frac{\partial\psi}{\partial z}(x,-h) = -K\left[\, 2A(-h) + \frac{\partial\phi}{\partial z}(x,-h)\,\right]$$

Choosing $A = q_o/2Kh$ gives $\partial\phi/\partial z(x,-h) = 0$.

The side surfaces have a step function as the boundary condition:

$$-K\frac{\partial\psi}{\partial x}(\pm\frac{L}{2},\, z) = -K\frac{\partial\phi}{\partial x}(\pm\frac{L}{2},\, z) = f(z)$$

where $f(z) = 0$ at $-h \leq z \leq -h'$, and $f(z) = E = q_oL/2h'$ at $-h \leq z \leq 0$.

Using separation of variables to solve this problem, let

$$\phi(x,z) = g_n(x)\;Z(z) \qquad \text{where} \qquad Z(z) = C\cos(kz) + D\cos(kz)$$

and $g_n(x)$ is symmetrical about $x = 0$. Evaluating the derivative at the top surface gives:

$$\frac{\partial \phi}{\partial z}(x,0) = 0 = - kC \sin(k0) + kD \cos(k0)$$

Therefore, D = 0 and Z(z) = C cos(kz). Evaluating the derivative at the bottom surface gives:

$$\frac{\partial \phi}{\partial z}(x,-h) = - kC \sin(-kh) = 0 \quad \text{or} \quad k = k_n = \frac{n\pi}{h} \quad (n = 0, 1, 2, \ldots)$$

Absorbing all constants into one gives the form:

$$\phi(x,z) = \sum_n^{\infty} g_n(x) \cos(k_n z) \quad \text{where} \quad n = 0, 1, 2, \ldots$$

Differentiating gives:

$$\nabla^2 \phi = \sum_n^{\infty} \left[\frac{d^2 g_n}{dx^2} - k_n^2 g_n(x) \right] \cos(k_n z) = - 2A$$

which is in the form of a Fourier series:

$$f(z) = \sum_n a_n \cos(k_n z) \quad \text{where} \quad a_n = \frac{d^2 g_n}{dx^2} - k_n^2 g_n(x)$$

for $n \geq 1$ $\quad a_n = 0$ $\quad$ which gives $\quad g_n(x) = \alpha_n \cosh(k_n x)$ $\quad n \geq 1$

for $n = 0$ $\quad \frac{d^2 g_o}{dx^2} = - 2A$ $\quad$ giving $\quad g_o(x) = - Ax^2 + Bx + C$

letting $B = C = 0$ gives $\quad g_o(x) = - Ax^2 = - \frac{q_o x^2}{2Kh}$

Plugging back in to the side boundary conditions gives:

$$-K\frac{\partial\phi}{\partial x}(\pm\tfrac{L}{2},z) = f(z) = -K\sum_{n}^{\infty}\frac{\partial g_n}{\partial x}(\pm\tfrac{L}{2},z)\cos(k_n z)$$

or $$f(z) = -K\left[\,AL + \sum_{n=1}^{\infty} k_n\alpha_n \sinh(k_n\tfrac{L}{2})\cos(k_n z)\,\right]$$

if we let $$f(z) = f_o + \sum_{n=1}^{\infty} f_n \cos(k_n z)$$

then $$f_o = ALK \quad \text{and} \quad \underset{n\geq 1}{\alpha_n} = -\frac{f_n}{k_n K \sinh(k_n\frac{L}{2})}$$

so $$\underset{n\geq 1}{g_n(x)} = -\frac{f_n}{k_n K \sinh(k_n\frac{L}{2})}\cosh(k_n x)$$

which gives the final form of the solution as:

$$\psi(x,z) = (z^2 - x^2)\frac{q_o}{2Kh} - \sum_{n=1}^{\infty}\frac{f_n}{k_n K \sinh(k_n\frac{L}{2})}\cosh(k_n x)\cos(k_n z)$$

To determine f_n we must solve $f(z) = f_o + \sum_{n=1}^{\infty} f_n \cos(\frac{n\pi z}{h})$

Let $w(z) = f(z) - f_o$ where $w(z) = \sum_{n=1}^{\infty} f_n \cos(\frac{n\pi z}{h})$

Then $$\int_0^h w(z)\cos(\tfrac{m\pi z}{h})\,dz = \sum_{n=1}^{\infty} f_n \int_0^h \cos(\tfrac{m\pi z}{h})\cos(\tfrac{n\pi z}{h})\,dz$$

Letting $z' = \frac{\pi z}{h}$ and $dz' = \frac{\pi}{h} dz$ transforms the integral to:

$\frac{h}{\pi} \int_0^{\pi} \cos(mz') \cos(nz') dz'$ which is zero for $m \neq n$, but for $m = n$ becomes

$$\frac{h}{\pi} \int_0^{\pi} \cos^2(mz') dz' = \frac{h}{\pi} \int_0^{\pi} \frac{1}{2} [1 + \cos(2mz')] dz' = \frac{h}{\pi} (\frac{\pi}{2}) = \frac{h}{2}$$

This is a Kroenecker delta where $\delta_{mn} = 1$ for $m = n$
$\delta_{mn} = 0$ for $m \neq n$

Substituting gives $$\int_0^h w(z) \cos(\frac{m\pi z}{h}) dz = \sum_{m=1}^{\infty} f_m \frac{h}{2} \delta_{mn}$$

or $$\frac{2}{h} \int_0^h w(z) \cos(\frac{m\pi z}{h}) dz = f_m = \frac{2}{h} \int_0^h [f(z) - f_o] \cos(\frac{m\pi z}{h}) dz$$

This becomes $$f_m = \frac{2}{h} \int_0^{h'} (E - ALK) \cos(\frac{m\pi z}{h}) dz - \frac{2}{h} \int_{h'}^h ALK \cos(\frac{m\pi z}{h}) dz$$

Evaluating this expression gives $f_m = f_n = \frac{2E}{n\pi} \sin(\frac{n\pi h'}{h})$ when $m = n$

Because $f(z)$ is an even step function and $E = q_o L/2h'$, the final solution in the domain $-L/2 \leq x \leq L/2$, $-h \leq z \leq 0$, is given by:

$$\psi(x,z) = (z^2 - x^2) \frac{q_o}{2Kh} - \sum_{n=1}^{\infty} [\frac{q_o Lh \sin(\frac{n\pi h'}{h})}{n^2\pi^2 h'K \sinh(\frac{n\pi L}{h2})}] \cosh(\frac{n\pi x}{h}) \cos(\frac{n\pi z}{h})$$

Figure 48 Scene of the first field testing of ARHT in the San Gabriel Mountains. Scale is given by Andrew Astor's mustache which stands 8 cm X 2 cm at 1 atm and 25° C.